Master of Science Thesis

Fatigue life prediction of carbon fibre-reinforced epoxy laminates using a single S-N curve

A.A.R. Broer

Faculty of Aerospace Engineering · Delft University of Technology

Delft University of Technology

Fatigue life prediction of carbon fibre-reinforced epoxy laminates using a single S-N curve

Master of Science Thesis

For obtaining the degree of Master of Science in Aerospace Engineering at Delft University of Technology

A.A.R. Broer

23 May 2018

Faculty of Aerospace Engineering · Delft University of Technology

Delft University of Technology
Faculty of Aerospace Engineering
Department of Aerospace Structures and Materials

GRADUATION COMMITTEE

Dated: 23 May 2018

Chair holder: Prof.dr.ir. R. Benedictus

Committee members: Dr. D. Zarouchas

Dr. C.D. Rans

Dr.ir. W.J.C. Verhagen

Abstract

Fatigue life prediction is key in design and analysis of cyclic loaded structures such as wind turbines or aircraft. For this purpose, prediction models have been developed that require experimental data in order to interpolate or extrapolate fatigue behaviour to different loading conditions. Multiple Stress-Life (S-N) curves are often required as input to the fatigue life prediction models. Moreover, due to the anisotropic nature of Fibre-Reinforced Plastic (FRP) laminates, several complex damage mechanisms occur during fatigue loading, resulting in large scatter. Therefore, multiple fatigue tests are required to eliminate the influences of scatter and to obtain a representative S-N curve. Hence, fatigue life prediction is expensive in terms of cost and time. In this work, a method is presented for the fatigue life prediction of carbon fibre-reinforced epoxy laminates, subjected to T-T or T-C constant amplitude loading. Predictions are based solely on static strength data and fatigue life data corresponding to one conventional stress ratio (i.e., either R = 0.1 or R = -1). Thereby, experimental efforts related to fatigue life prediction are reduced and, due to the simplicity of the model, fatigue life predictions are easily obtained.

The presented approach consists of two models that, when combined, allow for the prediction of any carbon-epoxy lay-up. One model is applicable to laminates characterised by a static strength larger than the absolute compressive strength (i.e., UTS>|UCS|) while the other is applicable to laminates showing the opposite (i.e., |UCS|>UTS). The Constant Life Diagram (CLD) models were derived from the anisomorphic CLD model and also show a dependency on the critical stress ratio. However, no longer experimental data is required at this uncommonly used stress ratio.

Each of the two proposed CLD models was evaluated by looking at its predictive accuracy for several carbon-epoxy laminates. For the first model, applicable to laminates characterised by UTS>|UCS|, three laminates from literature were evaluated with lay-ups $[45/90/\text{-}45/0]_{2S}$, $[0/60/\text{-}60]_{2S}$, and $[0/90]_{3S}$. In addition, an experimental campaign

was conducted on a carbon-epoxy (AS4/8552) laminate with lay-up $[90/0/90]_{2S}$. It was found that, in general, the predicted fatigue lives were located in similar fatigue life scales as the experimental validation data. For the second model, applicable to laminates characterised by |UCS|>UTS, similar conclusions were drawn for laminates with a lay-up of $[\pm 60]_{3S}$ and $[45]_{16}$ found in literature: the model-based predictions were in vicinity of the experimental data. For both models, the size of the input dataset showed large influence on the final fatigue life predictions.

In addition, a comparison was made with the two-, three-, and four-segment anisomorphic model. It was seen that a similar or improved predictive performance can be obtained as that of the anisomorphic model, even with datasets of limited size. Compared to the two-segment anisomorphic model, this allows for the use of fatigue life data at a more conventional stress ratio while maintaining a similar sized input dataset and similar accuracy in the fatigue life predictions of carbon-epoxy laminates characterised by UTS>|UCS|. For fatigue life predictions of carbon-epoxy laminates showing |UCS|>UTS, not only a more conventional stress ratio is employed, also less input data is required for fatigue life predictions of a similar accuracy. Hence, reductions in experimental efforts are obtained when employing the presented model while providing fatigue life predictions in similar scales as the experimental validation data.

Contents

List of Figures

List of Tables

List of Abbreviations

ε-N	Strain-Life
ABD	Anti-Buckling Device
ASTM	American Society for Testing and Materials
C-C	Compression-Compression
CA	Constant Amplitude
CFRP	Carbon-Fibre Reinforced Plastic
CLC	Combined Loading Compression
CLD	Constant Life Diagram
CLL	Constant Life Line
DOF	Degrees Of Freedom
FRP	Fibre-Reinforced Plastic
GFRP	Glass-Fibre Reinforced Plastic
HCF	High-Cycle Fatigue
ISO	International Organization for Standardization
LCF	Low-Cycle Fatigue

LS	Least Squares
LSPR	Least Squares Percentage Regression
MAPE	Mean Average Percentage Error
MNB	Mean Normalised Bias
P-S-N	Probabilistic S-N
R-ratio	Stress Ratio
RMSPE	Root Mean Squared Percentage Error
S-N	Stress-Life
SSE	Sum of Squared Errors of Prediction
T-C	Tension-Compression
T-T	Tension-Tension
UCS	Ultimate Compressive Strength
UD	Unidirectional
UTS	Ultimate Tensile Strength
VA	Variable Amplitude

List of Symbols

Symbol	Description	Unit
Greek		
χ	Critical stress ratio	[-]
χ_L	Left auxiliary stress ratio	[-]
χ_R	Right auxiliary stress ratio	[-]
χ_S	Sub-critical stress ratio	[-]
$\Delta\sigma$	Stress range	[MPa]
ϵ	Strain	[-]
μ	Mean of the normal distribution	[-]
ψ	Fatigue strength ratio	[-]
ψ_χ	Critical fatigue strength ratio	[-]
ψ_χ^L	Fatigue strength ratio describing the fatigue limit	[-]
ψ_{χ_L}	Fatigue strength ratio related to χ_L	[-]
ψ_{χ_R}	Fatigue strength ratio related to χ_R	[-]
σ	Stress	[MPa]
$\sigma_a^{(i)}$	Amplitude stress at R-ratio equal to (i)	[MPa]
σ_a^I	Amplitude stress datapoint from the input dataset	[MPa]
σ_B	Extrapolated maximum applied stress at a fatigue cycle of	[MPa]
σ_m	Mean applied stress	[MPa]

$\sigma_m^{(i)}$	Mean applied stress at R-ratio equal to (i)	[MPa]
σ_0	Model fitting parameter	[-]
σ^2	Variance of the normal distribution	[-]
$\sigma_{\max}$	Maximum applied stress	[MPa]
σ_a	Amplitude stress	[MPa]
σ_m^I	Mean stress datapoints from the input dataset	[MPa]
$\sigma_{\min}$	Minimum applied stress	[MPa]
$\sigma_{\min}^{(i)}$	Minimum stress at R-ratio equal to (i)	[MPa]

Roman

A	Model fitting parameter	[-]
a	Model fitting parameter	[-]
B	Model fitting parameter	[-]
b	Model fitting parameter	[-]
C	Model fitting parameter	[-]
$(n-p)$	Degrees of freedom of a model	[-]
E	Error/deviation	[-]
e	Log-normal error	[-]
f	Frequency	[Hz]
I	Relative improvement	[-]
i	Integer	[-]
k	Model fitting parameter	[-]
k_C	Constant life line exponent	[-]
k_T	Constant life line exponent	[-]
K_χ	Model fitting parameter	[-]
L	Likelihood	[-]
l	Log-likelihood	[-]
M	Integer	[-]
m	Model fitting parameter	[-]
M_i	Model (predicted) value of datapoint	[-]
N	Number of fatigue cycles	[-]
n	Model fitting parameter	[-]
$\bar{N}$	Average number of fatigue cycles to failure	[-]

N_f	Number of fatigue cycles to failure	[-]
P	Probability of failure	[-]
R	Stress ratio	[-]
r	Residual	[-]
S	Stress	[MPa]
s	Standard normalised error	[-]
s^2	Bias-corrected estimator of σ^2	[-]
T	Temperature	[°]
T_i	True value of datapoint	[-]
y_i	Value y for the i$^{\text{th}}$ datapoint	[-]
z	Constant life line exponent	[-]

Preface

Dear reader,

The work that lies in front of you is the final work in achieving the MSc degree in Aerospace Engineering at Delft University of Technology. For the past months, I have put all my time, efforts, and struggles into this project. This was not possible alone and therefore I would like to take the time to thank the following people.

I would like to start with expressing my gratitude to my supervisor Dimitrios Zarouchas for his guidance and feedback throughout the graduation process. With his support and the challenges that he provided me with, I was able to reach much more than I had ever expected. Thank you Dimitrios, working together with you has been a pleasure.

Special thanks go out to the students and staff of the Structural Integrity and Composites department at TU Delft, as well as the DASML technicians for their support in the thesis work. Their jokes are always able to brighten up my day.

I also want to thank my parents and family, not only here in the Netherlands but also in the Americas. You have always had an endless belief in me, even when I didn't. Thank you for your support, I have reached my goal!

My dear friends, you always put a big smile on my face. You have been an important part of my journey in Delft and I hope to share many more new memories with you all.

Lastly, I would like to thank Ricki, without whom I wouldn't have made it this far. Thank you for your endless support, love, and latino jokes: siempre negativo, nunca positivo!

I hope you enjoy the reading,

Agnes Broer
Delft, 14 May 2018

“It’s not the will to win that matters... Everyone has that. It’s the will to prepare to win that matters.”

— *Bear Bryant*

Chapter 1

Introduction

Structures such as wind turbines or aircraft are continuously subjected to cyclic loading. This results in a deterioration of the structure's properties and, eventually, to failure. Therefore, it is key to predict the fatigue life of these structures during both their design and usage. The focus of this thesis lies on fatigue life prediction models that rely on experimental tests, namely static strength tests, as well as fatigue life tests in which a constant amplitude load is applied to a specimen and the number of cycles to failure is measured. These experimental results are then used for interpolation or extrapolation to different loading conditions related to T-T or T-C constant amplitude loading. Most models require several S-N curves as input which results in the need for conducting large numbers of experimental tests. However, fatigue life tests are both time-consuming and costly. Therefore, it is of interest to minimise the number of tests required as input to these models and thereby allow for faster and easier, yet accurate, fatigue life predictions.

Several authors have developed approaches minimising the required size of the input dataset while providing an acceptable predictive accuracy, such as Sendeckyj (1981) and Kawai and Koizumi (2007). Others rely on an entirely different approach, such as Kassapoglou (2007), who determines the fatigue life curve based on only static strength test data. The most simple version of the anisomorphic model by Kawai and Koizumi (2007) requires only one S-N curve as input while providing fatigue life predictions for carbon fibre-reinforced epoxy laminates in similar fatigue life scales as experimentally obtained results. The employed S-N curve is related to an unconventional stress ratio, namely the critical stress ratio. Employing the critical stress ratio allows for influence of both the tensile and compressive damage mechanisms. However, testing under this critical stress ratio is rare, and thus, when employing this approach for predicting fatigue behaviour, new fatigue life tests are often required. Moreover, for some carbon fibre-reinforced epoxy laminates, additional S-N curves (two and three for the three- and four-segment anisomorphic model by Kawai and Murata (2010) and Kawai and Itoh (2014), respectively) are required as input, leading to increased experimental efforts.

In this work, two CLD models are presented that are adapted from the anisomorphic model. Each model is applicable to a different lay-up for a carbon fibre-reinforced epoxy laminate, for which distinctions are made based on the values of the tensile and compressive static strength. Namely, one model is applicable to laminates characterised by UTS>|UCS| while the other is applicable to those showing |UCS|>UTS. Both models only employ fatigue life data related to one S-N curve that corresponds to a more conventional stress ratio R: either R = 0.1 or R = -1. These two stress ratios are more frequently used than the critical stress ratio, thereby allowing for a wider applicability and easier use of the model.

Two main research questions will be answered in this work, which are defined as:

> How to adapt the anisomorphic fatigue life prediction model such that a different input dataset can be used to minimise the number of required S-N curves and allow for a more conventional stress ratio?
>
> What is the relative predictive performance of the proposed models with respect to the anisomorphic fatigue life model when comparing similar laminates tested in constant amplitude loading at different stress ratios (T-T and T-C)?

This thesis commences with a general introduction into fatigue loading in Chapter 2. Focus lies on the used definitions, an explanation of both S-N curves and CLDs, as well as the challenges seen in fatigue life testing. Chapter 3 covers the basics of the anisomorphic model, from which the models proposed in this work are derived. Chapter 4 and 5 present a fatigue life prediction model for carbon-epoxy laminates characterised by UTS>|UCS| and |UCS|>UTS, respectively. In addition, the predictive accuracy of the models is assessed by means of fatigue datasets found in literature and an experimental campaign. Finally, Chapter 6 and 7 provide the conclusions and recommendations of this work.

Chapter 2

Basics of Fatigue Loading

In this chapter the basics of fatigue loading are covered. The chapter commences with a description of fatigue loading, including the main definitions employed in the remainder of this report. Section 2.2 illustrates the use of S-N curves while Section 2.3 introduces the CLD concept. Lastly, in Section 2.4, focus lies on challenges and considerations regarding experimental testing and their implication on the obtained test results.

2.1 Fatigue Loading Definitions

Fatigue of a material can occur when a repetitive or cyclic load, with stress values below Ultimate Tensile Strength (UTS) and Ultimate Compressive Strength (UCS), is applied to a structure. Fatigue is a damage mechanism causing a permanent deterioration of the material with an increasing number of load cycles, leading to a reduction in load bearing capabilities. The stress values during cyclic loading directly impact the lifetime of the structure: lower stresses lead to a longer lifetime, i.e. more load cycles that can be applied until the structure fails. On the other hand, higher stresses in the load cycle that are close to UTS or UCS lead to fatigue failure after only a small number of cycles, as shown in Figure 2.1. The relation between the applied stress level during Constant Amplitude (CA) loading and the number of fatigue cycles until failure is often presented using S-N curves, which are discussed in more detail in Section 2.2.

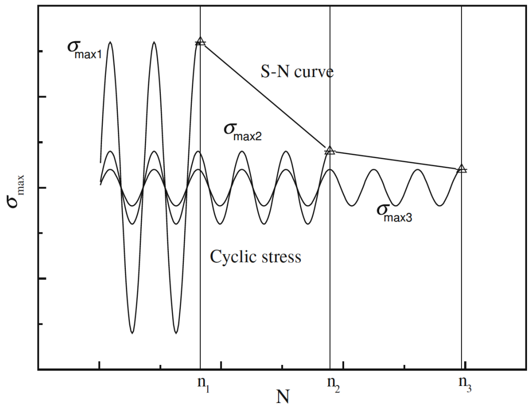

Figure 2.1: S-N curve showing the effects of different cyclic loading stresses on the lifetime, reprinted from Vassilopoulos and Keller (2011).

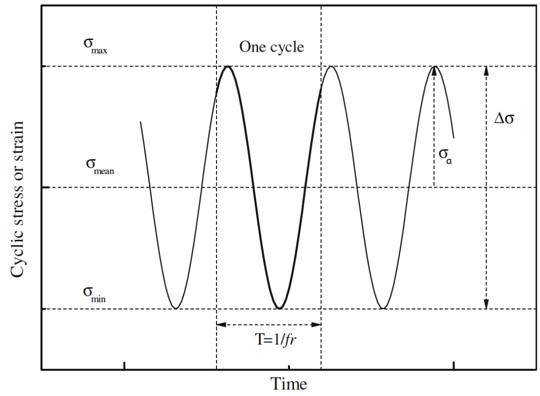

Figure 2.2: Cyclic constant amplitude (CA) loading including standard terms, reprinted from Vassilopoulos and Keller (2011).

CA loading is a repetitive cyclic loading in which the amplitude and mean stress remain constant, as shown in Figure 2.2. The figure shows a sinusoidal load often used in fatigue testing. Several terms can be identified for each stress cycle, which are shortly summarised next.

- $\boldsymbol{\sigma_{\min}}$ **[MPa]** The minimum stress $\sigma_{\min}$ is the lowest stress value reached during the loading cycle.
- $\boldsymbol{\sigma_{\max}}$ **[MPa]** The maximum stress $\sigma_{\max}$ is the highest stress value reached during the loading cycle.
- $\boldsymbol{\sigma_a}$ **[MPa]** The amplitude stress σ_a is defined as $\sigma_a = \frac{\sigma_{\max} - \sigma_{\min}}{2}$.
- $\boldsymbol{\sigma_m}$ **[MPa]** The mean stress σ_m is defined as $\sigma_m = \frac{\sigma_{\max} + \sigma_{\min}}{2}$.
- $\boldsymbol{\Delta\sigma}$ **[MPa]** The stress range $\Delta\sigma$ is defined as the difference between the maximum and minimum applied stresses: $\Delta\sigma = \sigma_{\max} - \sigma_{\min}$.
- $\boldsymbol{R}$ **[-]** The stress ratio R is defined as the ratio of the minimum to the maximum applied stress: $R = \frac{\sigma_{\min}}{\sigma_{\max}}$.
- $\boldsymbol{f}$ **[Hz]** The frequency f defines the number of repeated cycles occurring per unit time: $f = \frac{1}{T}$.

Three cyclic loading types can be identified based on the minimum and maximum stress, as shown in Figure 2.3, which are defined as

- Tension-Tension (T-T) loading,
- Tension-Compression (T-C) loading,
- Compression-Compression (C-C) loading.

T-C loading with a positive mean stress is also called tension-dominated loading, whereas a negative mean stress is called compression-dominated loading. The boundary between the two is defined by reversed loading where R = -1 (i.e., $\sigma_{\max} = \sigma_{\min}$).

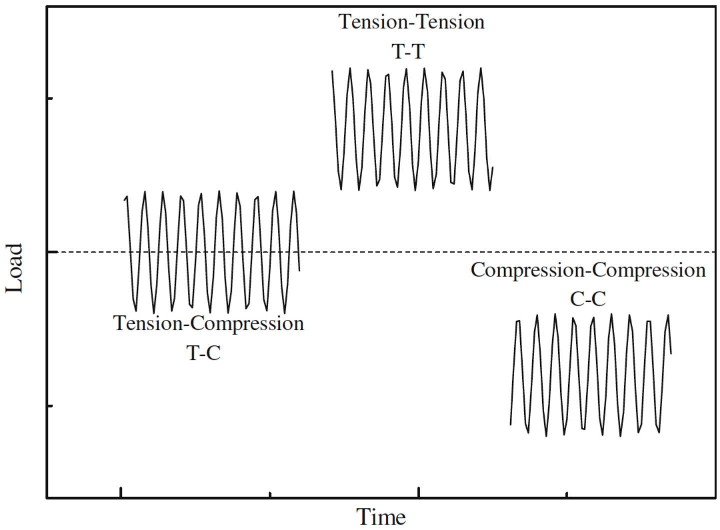

Figure 2.3: Cyclic loading types, reprinted from Vassilopoulos and Keller (2011).

The previously considered loading cycles are uni-axial CA loads. However, uni-axial CA loading is uncommon when a structure is in-service. Instead, multi-axial Variable Amplitude (VA) loading and spectrum loading are more typical. Fatigue life prediction models are different for CA and VA loading, as well as those for uni-axial and multi-axial loading, and those combining multi-axial and VA loading are often most complex. However, models predicting the effects of multi-axial VA loading are frequently based or derived from models proposed for uni-axial CA loading. Therefore, the focus in this report will merely lie on the prediction of uni-axial CA loading cases and possible adaptations for other loading types are provided in the recommendations.

2.2 Graphical Representation of Fatigue Life: S-N curve

The stress-life (S-N) curve visually presents fatigue life data and can be used as an aid in the design and analysis of FRPs. A wide range of S-N curve models exist, of which some merely describe experimental fatigue life data and interpolate between datapoints, while others, the so-called Master S-N curves, also extrapolate fatigue behaviour to other loading conditions (e.g., different Stress Ratio (R-ratio) or loading frequency). Besides the S-N curve, some authors employ a Strain-Life (ε-N) curve (e.g., Kensche (1995) and Ronold and Echtermeyer (1996)). However, this requires additional testing equipment to measure strains. Therefore, the focus of this work remains on S-N curves rather than ε-N curves.

An S-N curve, sometimes also called Wöhler curve, depicts the applied stress S versus the number of fatigue cycles N until failure for a constant R-ratio. The applied stress is often given as the amplitude or peak stress of the CA loading cycle. An example of an S-N curve, with the amplitude stress on the y-axis, is provided in Figure 2.4. Even though the stress amplitude is plotted on the y-axis, it is the independent variable and the number of cycles to failure is the dependent variable. In order to construct an S-N curve, only fatigue life data consisting of the applied fatigue loads and measured fatigue life is needed. However, fatigue life data is required at several stress levels in order to allow for interpolation between datapoints. Moreover, due to potential presence of scatter, especially for FRPs, multiple datapoints are often required per stress level to eliminate the influence of outliers.

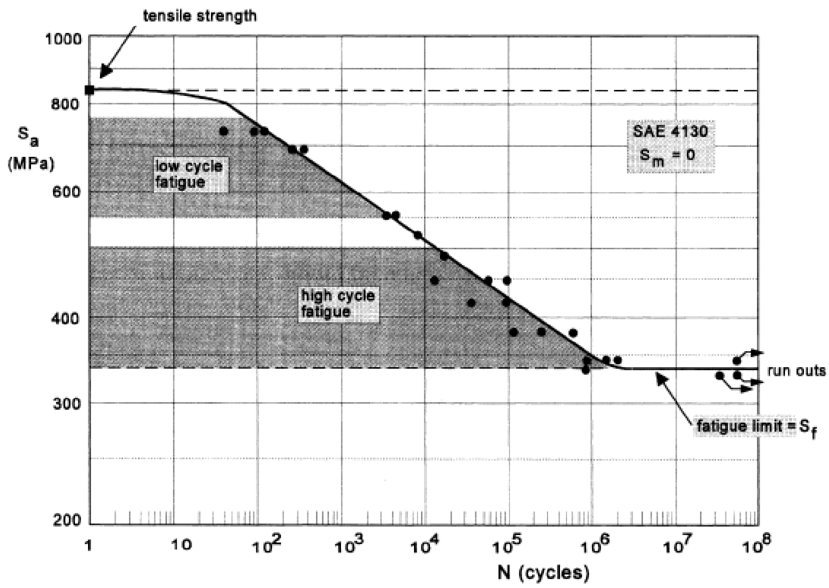

Figure 2.4: Example of an S-N curve including the low-cycle plateau, fatigue limit, and run-outs, reprinted from Schijve (2009).

The S-N curve depicted in Figure 2.4 is for a constant R-ratio, a constant loading frequency, similar specimens, and comparable testing conditions. Only the amplitude and mean stress are varied per specimen in order to obtain the fatigue life at different CA loading cycles. Two or three regions can be identified in the S-N curve. For this work, these regions are defined as:

1. Low-Cycle Fatigue (LCF): $N < 10^3$
2. Intermediate cycle range: $10^3 < N < 10^6$
3. High-Cycle Fatigue (HCF): $10^6 < N$

Occasionally, the intermediate cycle range is discarded or very small, and only LCF and HCF regimes are defined, as shown by Schijve (2009). Whereas the first two regions are often distinguishable, the fatigue or endurance limit, associated with HCF, is usually not clearly observable for continuous FRP laminates (Kawai, 2010). This implies the need for many fatigue life tests to provide accurate estimations of HCF. However, HCF tests consume more time compared to the other two regions since cycles above $N > 10^6$ are reached. Therefore, in case HCF is not of particular importance for the application, often only conservative predictions are made based on the fatigue lives of higher stress levels. In this work, the main focus is on the intermediate cycle range, where $10^3 < N < 10^6$.

2.2.1 Including Static Strength Data in S-N Curve Estimation

S-N curves are used to describe changes in fatigue life for different CA loads at constant R-ratios. A fatigue cycle of $N = 1$ equals quasi-static loading. However, the inclusion of static strength data in S-N curves can be disputed. Foremost, different failure modes are seen in quasi-static and fatigue loading. Therefore, proposing one predictive curve for different failure and loading mechanisms seems illogical. Yet, as shown by Nijssen (2006), including static strength data can significantly improve fatigue life predictions in the low-cycle regime. Hence, its inclusion should be considered when LCF is of interest.

Besides different failure modes, another difference exists between static strength and fatigue life data. Namely, static strength data is often obtained at lower strain rates. It was shown by a number of authors (e.g., Naito (2014), Nijssen (2005), Taniguchi et al. (2007), Xia et al. (2007)) that when a tensile static strength test is conducted at higher strain rates, similar to those in fatigue loading, the static strength of a laminate can significantly increase. However, it is difficult to select an appropriate strain rate for the static strength loading because the strain rate varies during fatigue loading; a constant strain rate implies a varying test frequency during fatigue loading (Vassilopoulos, 2010).

Another reason to debate the inclusion of static strength data in S-N curves is its effect on other cycle regions. Static strength data can influence S-N curve estimations significantly as shown by, for example, Nijssen et al. (2004) and Nijssen (2005, 2006). Often, all regions of the S-N curve are affected when static strength data is included. For example, HCF predictions can differ due to a change in slope of the S-N curve (Nijssen et al., 2004). Only in methods consisting of a separated LCF prediction approach or methods that have been constructed as such to include static strength data, the slope is unaffected. However, many curve fitting methods, e.g. linear regression methods, show different results when including static strength data and it is difficult to describe both LCF and HCF using a single curve (Nijssen, 2006). For that reason, Nijssen et al. (2004) recommends to only include static strength data when LCF is of importance for the application and to exclude it where possible for improved predictions of other S-N curve regimes. In this work, the static strength will be included in the S-N curve due to the nature of the employed curve fitting function (Chapter 4), which minimises the influence on fatigue life predictions of other S-N curve regions.

2.2.2 Effects on Fatigue Life

Multiple aspects can affect the fatigue life of an FRP, which are summarised next. In addition, changes in fatigue life are related to the change in shape and location of the S-N curve.

- **R-ratio:** The R-ratio affects the fatigue life and thereby the form of the S-N curve. It was shown by Kawai and Yano (2016b) that, for a Carbon-Fibre Reinforced Plastic (CFRP) laminate, T-T ($0 < R < 1$) and T-C ($R < 0$) loads lead to steeper S-N curve slopes than C-C loads ($R > 1$). Thus, dependent on the loading type, the fatigue sensitivity of a CFRP laminate changes.

- **Loading Frequency:** Fatigue loading can lead to energy dissipation in the laminate causing heating of the laminate. When the loading frequency is sufficiently high such that the laminate does not have time to cool down and temperatures reach the glass transition temperature T_g, the fatigue performance can be affected negatively, leading to lower fatigue lives (Vassilopoulos, 2010). Moreover, at lower frequencies, hysteresis effects can influence the fatigue life significantly because they can lead to localised stress redistribution processes. Thereby, the matrix crack propagation rate os reduced and the fatigue life is increased, as shown by Reifsnider et al. (1977) and Barron et al. (2001).

- **Testing temperature:** When increasing the testing temperature, a similar effect on the fatigue life is seen. Kawai and Matsuda (2012) and Kawai et al. (2012) show that elevated testing temperatures lead to a downward shifted S-N curve, i.e. a reduction in fatigue life for similar stresses. In this work, the influence of testing temperature on the final results is not considered.

- **Water absorption:** Kawai et al. (2013) explored the influence of water absorption on the fatigue life. A similar reduction of the fatigue life occurred due to water absorption as was seen for high load frequencies and temperatures: the fatigue life reduces and the S-N curve shifts downward with an increasing level of water absorption. In this work, the influence of water absorption and humidity on the final results is not considered.

- **Materials:** A different material will affect the fatigue life and thereby lead to a different S-N curve. For example, a material that is more sensitive to fatigue loading will have a steeper fatigue curve. In other words, for the same loading conditions, the material will have a lower fatigue life than a material with a lower fatigue sensitivity.
- **Interrupted loading:** Loading that is not continuously applied can be beneficial for the fatigue life. An interrupted load cycle is common when structures are in-service, for example for aircraft and wind turbines. It was shown by Vassilopoulos and Keller (2011) that an interrupted fatigue cycle can cause an increase in fatigue life of up to 41%. In this work, only continuous applied CA loads are considered.

2.2.3 S-N Curve Models

Several S-N curve models can be identified that differ in, for example, their description of the fatigue life curve or predictive capabilities under different loading conditions. The S-N curve models can be classified into two categories. Firstly, the empirical fitted S-N curves merely describe the relation of the experimental data variables. These cannot be used for extrapolation of fatigue performance predictions to other loading conditions or laminates. Secondly, the so-called master S-N curves are capable of extrapolating predicted fatigue behaviour to other loading conditions. These extrapolations are often related to different R-ratios or loading frequencies. Both model categories require experimental static strength data and/or fatigue life data as input. Examples of these model categories are shown in Figure 2.5 and each category is shortly discussed next.

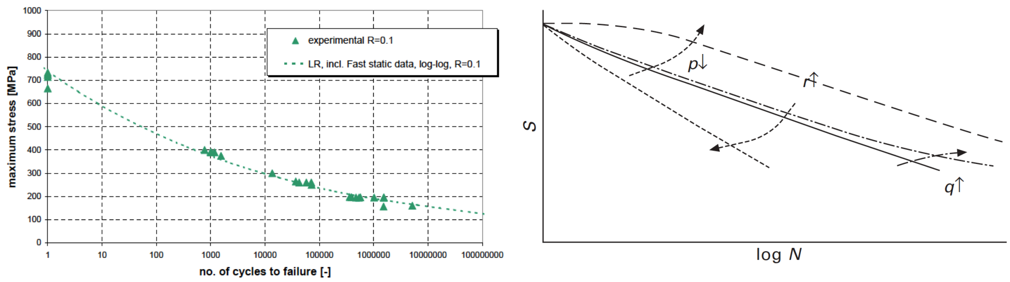

(a) Example of curve-fitting using linear regression on experimental fatigue life data, reprinted from Nijssen et al. (2004).

(b) Example of the concept of the Master S-N curve methods, reprinted from Nijssen (2010).

Figure 2.5: Examples of S-N curve models.

Empirical Fitted S-N curves

Empirical fitted S-N curves are merely descriptive functions used to describe experimental fatigue life data, specifically, the relation between applied stress and fatigue life. The methods in this category are relatively simple because they do not involve any extrapolation and can be seen as curve-fitting methods. Several curve expressions have been suggested, most commonly the power-law and exponential formulation. These are discussed in more detail in Appendix A. More elaborated functions have also been proposed, for example, by Jarosch and Stepan (1970) who include the possibility to describe the fatigue limit. Kohout and Věchet (2001) identify three fatigue life regions (low-cycle, mid-range, and the high-cycle region) and propose three inter-dependable functions to describe a complete S-N curve. All S-N curve functions employ model fitting parameters that are estimated based on experimental input data using regression analysis techniques such as Least Squares (LS).

Master S-N curves

Master S-N curves are a type of fatigue life prediction models that extrapolate fatigue behaviour to other loading conditions than those of the input data. Most commonly, an S-N curve at a different R-ratio is predicted. For example, Mandell (Bach, 1992) proposes a function for the S-N curve that depends on the R-ratio. For a changing R-ratio, the slope of the curve changes accordingly. Epaarachchi and Clausen (2003) adapted the master S-N curve model by Caprino and D'Amore (1998) to include, besides the R-ratio dependency, the fibre direction and loading frequency. This results in an extended equation in which two fitting parameters are present that are based on experimental static strength and fatigue life data corresponding to one S-N curve.

Some of the models in this category only employ static strength data and no experimental fatigue life data, such as the model proposed by Kassapoglou (2007). When only static strength data is employed as input, all S-N curves are de facto extrapolations. On the other hand, when also fatigue life data is included as input, one S-N curve forms the base from which other S-N curves are extrapolated.

Applicability to this Study

None of the methods from the first model class, the empirical fitted S-N curves, are of interest in this research. Primarily because no predictive capabilities are present, thereby requiring new experimental fatigue life data for each considered S-N curve. On the other hand, the master S-N curves do provide predictions. Moreover, they do this based on limited numbers of experimental data. However, some of the models have only been validated for Glass-Fibre Reinforced Plastic (GFRP)s (e.g., that of Epaarachchi and Clausen (2003)) or, as shown by Vassilopoulos et al. (2010a) for the model of Kassapoglou (2007), the accuracy diminishes in most evaluated cases due to the simplicity of the model. Therefore, the master S-N curves are also not be further considered in this study. Instead, the focus will lie on CLDs, which are discussed in Section 2.3.

2.3 Graphical Representation of Fatigue Life: Constant Life Diagram

Constant life diagrams (CLD) are frequently used in fatigue life predictions of FRPs for R-ratios different than those evaluated during experimental testing. CLDs allow for interpolation between fatigue life data obtained at different R-ratios and thereby for a straightforward prediction of S-N curves for a wide range of R-ratios. Several CLD models are available, varying in amount of experimental data required, as well as shape of the Constant Life Line (CLL) and validity to different materials. This section begins with a basic definition of a CLD, followed by an overview of different CLD models.

2.3.1 Definition of Constant Life Diagram

The CLD is a two-dimensional graph showing, in its most common form, the amplitude stress σ_a versus the mean stress σ_m. An example of a CLD is shown in Figure 2.6. Each curve (called CLL) relates to a different constant fatigue life: closer to the origin means a longer fatigue life due to the lower applied stresses while the fatigue life reduces when moving away from the origin.

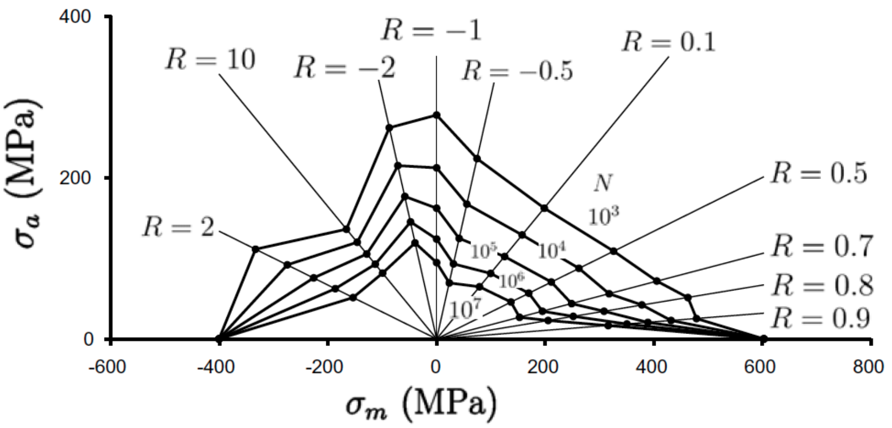

Figure 2.6: CLD example showing constant life curves for different values of fatigue life for an E-Glass ortho-polyester laminate, reprinted from Post and Case (2008).

Radial (linear) lines arising in the origin and moving outward correspond to constant R-ratios. The radial lines can be used to derive S-N curves at these different R-ratios. In order to retrieve an S-N curve for a constant R-ratio, use must be made of fatigue life data located on one radial: different combinations of amplitude and mean stress lead to different values of the fatigue life. The procedure involved in deriving the S-N curve predictions is discussed in more detail in Chapter 3.

The CLD can be split into four regions based on the value of R, as seen in Figure 2.7:

1. Compression-compression (C-C) region: $R > 1$
2. Compression-dominated (T-C) region: $R < -1$
3. Tension-dominated (T-C) region: $-1 < R < 0$
4. Tension-tension (T-T) region: $0 < R < 1$

Correspondingly, the scale of the applied mean stress changes for each region. Note that a singularity is present when moving from the compression-dominated T-C region to the C-C region: a jump occurs from R = -∞ to $R = \infty$.

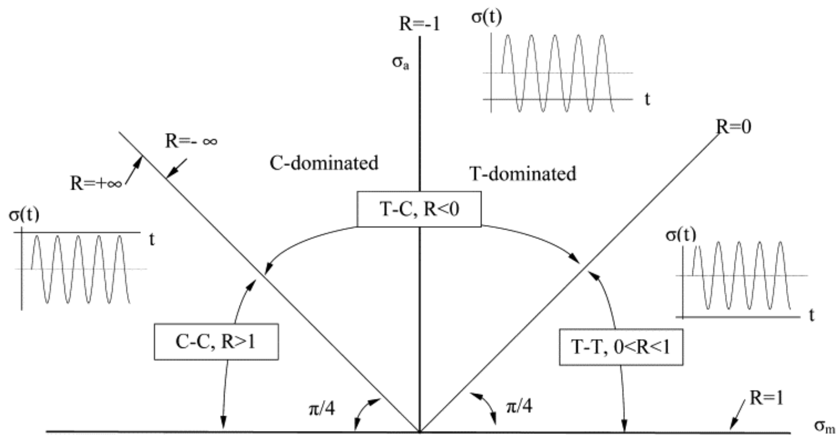

Figure 2.7: CLD example visualising the four different loading regions, reprinted from Philippidis and Vassilopoulos (2002).

The boundaries of the CLD are given by the CLL corresponding to $N = 1$, i.e. static strength, which is described by two linear lines intersecting the x- and y-axis in the UTS or UCS value. The design space is given inside the triangle, whereas the considered structure will fail outside the design space before reaching the maximum absolute stress value in the fatigue cycle (i.e., before reaching either $\sigma_{\max}$ or $\sigma_{\min}$).

The x-axis, where $\sigma_a = 0$, relates to $R = 1$ ($\sigma_{\min} = \sigma_{\max}$), whereas the y-axis, where $\sigma_m = 0$, relates to R = -1 ($\sigma_{\min}$ = -$\sigma_{\max}$). For most CLD models, CLLs converge to the UTS or UCS value on the x-axis. However, some CLD models differ from this assumption such as the parallel Goodman CLD, where CLLs do not converge. Furthermore, some authors (e.g., Nijssen (2006) and Vassilopoulos et al. (2010a)) state that CLLs should not converge to the UTS or UCS value because $R = 1$ does not correspond to static strength but instead to creep (static fatigue). For example, Andersons and Paramonov (2011) adhere to the view that CLLs should converge to creep rupture strength rather than UTS or UCS, where the time to rupture equals fatigue life (Owen, 1970). Note that this discussion is similar to that for the S-N curve on whether static data, LCF or creep must be considered in fatigue analyses.

In this work, the assumption is made that the CLLs converge to the UTS or UCS value on the x-axis and $R = 1$ is not considered in the fatigue life predictions. The cause of this assumption is found in the employed CLD method. The CLD model on which this study is based, as will be seen in Chapter 3, makes a similar assumption for convergence to UTS and UCS, leading to acceptable fatigue life results for $R \neq 1$. Moreover, it neither covers the description or prediction of creep. In addition, if it is assumed that the CLLs converge to, for example, creep rupture strength, creep tests must be conducted. These tests, which require more experimental efforts than static strength tests, must be performed even when creep is not of interest. For these reasons, it is assumed that the CLLs converge to UTS and UCS and the prediction of $R = 1$ is not considered.

2.3.2 Constant Life Diagram Models

Several CLD models have been proposed in literature, yet all methods require static strength and fatigue life data as input. However, they differ in CLL shape, the location of intersection with the x- and y-axis, and the required size of the input dataset. Several methods are introduced in the following paragraphs. For details regarding each approach, the reader is referred to the corresponding literature. Examples of the presented CLD models are shown in Figure 2.8.

Goodman Diagrams
The Goodman CLDs[1] are linear diagrams constructed using static strength data and either one or multiple S-N curves. Several variations from the classic Goodman diagram exist that vary in, for example, shape of the CLD (symmetry versus asymmetry), location of the stress amplitude peaks, or convergence of the CLLs on the x-axis. However, each model is consistent in the use of linear-defined CLLs. Kawai (2010) has identified five variants of the Goodman diagram, classified as:

1. Classic symmetric Goodman,
2. Classic asymmetric Goodman,
3. Shifted Goodman,
4. Inclined Goodman,
5. Parallel Goodman.

[1] Note that CLDs are often referred to as Goodman or Gerber diagrams. However, as clarified by Sendeckyj (2001), accreditation issues have originated in the past 150 years. In this work, the Goodman and Gerber diagrams and their variants will be treated as a type of CLD rather than used as a synonym for CLD.

Piecewise Linear CLD
The piecewise linear CLD is constructed using static strength data and several S-N curves. Subsequently, between datapoints corresponding to a similar fatigue life, lines are constructed to obtain linear CLLs. The number of employed S-N curves can be varied. Increasing the number of S-N curves results in more accurate fatigue predictions than the previously discussed Goodman diagrams. However, the latter is a disadvantage of this method because it increases the required experimental efforts.

Gerber Diagrams
The Gerber CLDs are non-linear diagrams constructed using static strength data and either one or multiple S-N curves. They are similar to the Goodman diagrams but assume a parabolic function rather than a linear function for the CLLs. Again, several variations of this CLD exist, each varying a different aspect (e.g., size of the input dataset or (a)symmetry). Kawai (2010) has classified the models into four categories as:

1. Symmetric Gerber,
2. Asymmetric Gerber,
3. Shifted Gerber,
4. Inclined Gerber.

Piecewise Non-Linear CLD
The piecewise non-linear CLD has been proposed by Vassilopoulos et al. (2010b) and is constructed using static strength data and either two or three S-N curves (R = -1, R = 10 and/or R = 0.1). The CLLs converge to the values of UTS and UCS on the x-axis and have a non-linear shape. The model parameters in the CLL functions can be obtained directly from fatigue life data, thereby no optimisation process is required. Another advantage of the piecewise non-linear model is its high accuracy and good performance with respect to other CLD models, as shown by Vassilopoulos et al. (2010b).

Harris' Bell-Shaped CLD
The bell-shaped CLD has been proposed by Harris and his colleagues (Beheshty and Harris, 1998, Beheshty et al., 1999, Gathercole et al., 1994, Harris, 2003, Harris et al., 1997) and is based on static strength and fatigue life data consisting of at least 20 test results. The CLLs are constructed using three model parameters to optimise the curves. These model parameters are either derived using fatigue test data or empirical values from similar materials. However, the latter will negatively impact the predictive accuracy. The bell-shaped CLD is computationally inexpensive due to the lack of optimisation procedures required. Overall, the model is capable of providing reliable and relatively accurate predictions for both CFRP and GFRP laminates while not requiring large computational efforts, though it requires a relative large fatigue dataset as input.

Kawai's Anisomorphic CLD

Kawai and Koizumi (2007) have proposed the anisomorphic CLD for carbon-epoxy laminates, which is a non-linear CLD constructed using only static strength data and one experimental S-N curve. The employed S-N curve is related to the critical R-ratio, which is defined as the ratio of the static compressive strength (UCS) to the static tensile strength (UTS). By requiring little experimental input data, the method is limiting time-consuming and expensive testing procedures. Moreover, the proposed method is computationally inexpensive. Kawai and Murata (2010) and Kawai and Itoh (2014) have proposed expansions of the original two-segment CLD, namely the three- and four-segment anisomorphic model, respectively, to predict the fatigue life of carbon-epoxy laminates with a lay-up characterised by |UCS|>UTS. The latter two models require additional input data with respect to the two-segment model by employing two and three S-N curves as input, respectively. Thereby, the accuracy of the fatigue life predictions is improved but the involved experimental efforts are increased.

Boerstra's Multislope CLD

Boerstra (2007) has proposed the multislope CLD to predict the fatigue life of E-glass laminates. A notable distinction with the previously introduced CLD models is the use of sparse fatigue life data besides static strength data. No longer one or multiple complete S-N curves are required as input but any fatigue life data can be employed. The multislope model employs five model parameters that are determined using a LS method based on the input data. On the one hand, this makes the model more computationally expensive. On the other hand, it reduces the standard deviation compared to the Goodman diagram, as shown by Boerstra (2007).

Applicability to this Study

In the previous paragraphs, several CLD models were presented of which one must be selected as a basis for further adaptation in this study. The purpose of this work is to minimise the size of the experimental input data dataset while providing an acceptable predictive accuracy in fatigue life for a carbon fibre-reinforced epoxy laminates, as discussed in Chapter 1. The fatigue life predictions must be in the same order as the experimentally obtained results. Based on these requirements, a comparison can be made between all CLD models. For this purpose, an overview of the three most important aspects of each model is provided in Table 2.1.

Immediately, the Goodman, Gerber, and piecewise linear CLDs can be discarded. These models are either not accurate due to their simplicity or require large amounts of experimental data. For the latter reason, Harris' bell-shaped CLD is also not relevant to this study. Boerstra's multislope CLD contains a rather complex prediction model with respect to the other models by employing five model parameters. Moreover, it is only validated for GFRPs while CFRPs are considered in this work. Therefore, Boerstra's multislope model cannot be selected for further adaptation. This leaves two remaining models for consideration: Kawai's anisomorphic CLD and the piecewise non-linear CLD.

Table 2.1: Aspects of different CLD models.

CLD model	Accuracy	Amount of required fatigue life data required	Validated for CFRPs
Goodman	Variant-dependent	Variant-dependent	Yes
Piecewise Linear	Same scale order	Large fatigue life dataset	Yes
Gerber	Variant-dependent	Variant-dependent	Yes
Piecewise Non-Linear	Same scale order	2 or 3 S-N curves	Only GFRP
Bell-Shaped	Same scale order	Large fatigue life dataset	Yes
Anisomorphic	Same scale order	1, 2 or 3 S-N curves	Yes
Multislope	Same scale order	Sparse fatigue life data	Only GFRP

The piecewise non-linear CLD requires a minimum of two S-N curves as input while the most simple version of the anisomorphic CLD (i.e., two-segment) only requires one S-N curve. Moreover, the anisomorphic model has been validated for CFRPs while the piecewise non-linear model was proposed for GFRPs. In terms of accuracy, the models were compared by Vassilopoulos and Keller (2011) for three GFRP laminates. In general, the piecewise non-linear model showed a higher accuracy. However, the input to the anisomorphic model was different than the critical R-ratio and the evaluation was performed for GFRPs rather than CFRPs. Based on the previous aspects, the anisomorphic model is of most interest in this study. Yet, they have one major disadvantage; the use of the critical R-ratio. Testing at this critical R-ratio is rare and when employing this approach, often new fatigue life tests must be conducted. Therefore, it is of interest to use the anisomorphic model as a basis to develop a method that also only uses one S-N curve but instead corresponds to a more conventional R-ratio (e.g., R = 0.1 or R = -1). In this work, two adapted models are proposed (Chapter 4 and 5) that have been derived from the anisomorphic model. For this purpose, an in-depth description of Kawai's anisomorphic model is provided in Chapter 3.

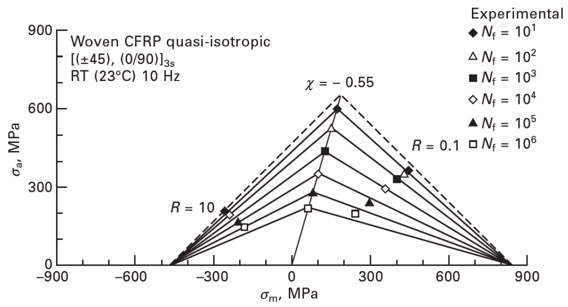

(a) Goodman diagram (inclined), reprinted from Kawai (2010).

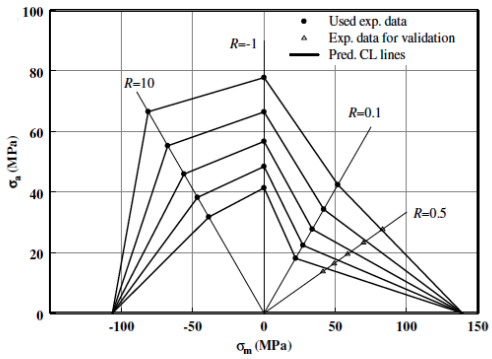

(b) Piecewise linear CLD, reprinted from Vassilopoulos et al. (2010a).

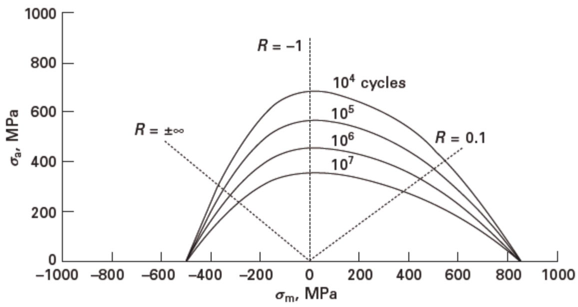

(c) Gerber diagram (asymmetric), reprinted from Kawai (2010).

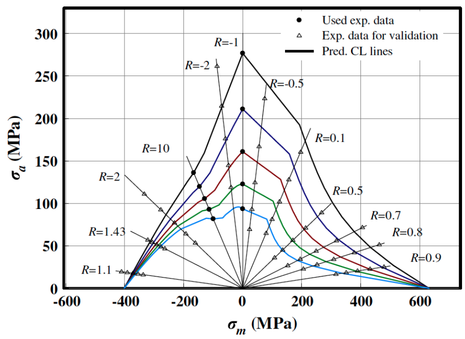

(d) Piecewise non-linear CLD, reprinted from Vassilopoulos et al. (2010b).

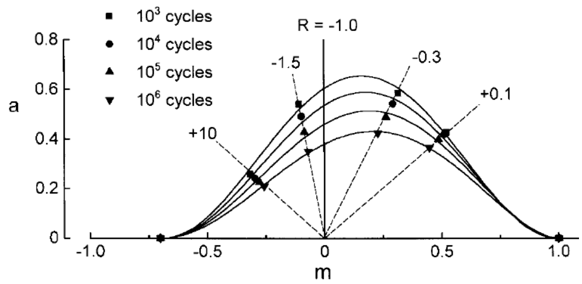

(e) Harris' bell-shaped CLD, reprinted from Beheshty and Harris (1998).

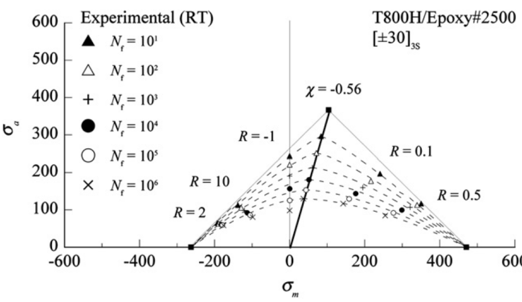

(f) Kawai's anisomorphic CLD, reprinted from Kawai and Murata (2010).

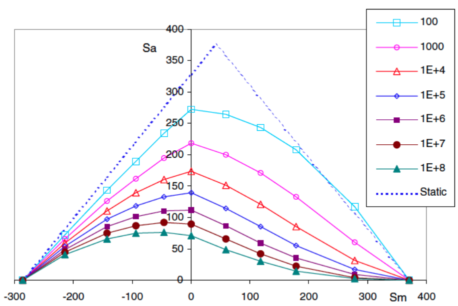

(g) Boerstra's multislope CLD, reprinted from Boerstra (2007).

Figure 2.8: Examples of CLD models.

2.4 Experimental Testing

Experimental testing is key for predicting and analysing fatigue behaviour of composites and the results are used as input to the predictive models. The anisomorphism of composite laminates and the complex damage mechanisms under cyclic loading lead to large variety in performance under fatigue loading and difficulty in prediction of fatigue life. Large scatter is seen for similar CFRPs consisting of the same material and lay-up, and manufactured under similar conditions, and its variability can be up to two decades for fatigue life (Nijssen, 2010). Small variations in test conditions and set-up can aggravate these differences, thus, in order to construct fatigue life prediction models, it is of importance to minimise any changes between tests. Several test standards have been defined, of which the standards by the International Organization for Standardization (ISO) and the American Society for Testing and Materials (ASTM) are most known. These standards will not be discussed in detail, instead the focus in this section lies on three main aspects involved the design of fatigue experiments.

Firstly, the number of fatigue life tests required for construction of one S-N curve will be established. A minimum number of fatigue life tests is required to take into account the variability of fatigue life data. Secondly, censoring of data and run-outs are shortly discussed. Lastly, different types of fatigue life tests and their individual considerations are covered. For information regarding other testing aspects, the reader is referred to the information provided by Nijssen (2010). Note that only small-scale coupon testing, with no initial damages or open holes, is considered, used either as input to predictive models or for verification and validation purposes.

2.4.1 Number of Fatigue Tests

Due to the large scatter seen in fatigue life test results for CFRP laminates, it is of importance that a representative dataset is obtained that describes the fatigue life behaviour. It is very well possible that an acceptable test result is obtained that, if the same test is repeated several times under the same conditions, turns to be an outlier located in the lower or upper tail of a probability distribution. If, for example, only three fatigue life tests are conducted to construct an S-N curve, of which two datapoints are outliers, a non-representative sample of the mean fatigue life behaviour for the considered laminate will be obtained. Therefore, it is of importance that a sufficient number of fatigue life tests are performed.

ASTM (1980 (2015)) have provided recommendations on the minimum number of fatigue life tests for S-N curve establishment based on its purpose. For preliminary and exploratory research or research and development testing of specimens, a minimum number of 6 to 12 specimens should be tested to construct an S-N curve. For design allowables or reliability data, a larger number of specimens should be tested, namely a minimum of 12 to 24 specimens. Furthermore, it is of importance that these fatigue life tests are spread over several stress levels to describe all fatigue life scales. These recommendations have been made based on those given by Little and Jebe (1975). They have stated that when the shape of the S-N curve is unknown, data at six stress levels is required to describe a potential curve consisting of a LCF plateau, straight middle region, and a fatigue limit. Once the S-N curve shape is established, additional testing should only be focused on replication. Note that the provided recommendations are general and have not been tailored to CFRP laminates. Hence, a larger number of tests might be required to obtain a representative sample.

2.4.2 Run-outs and Censoring of Data

Run-outs are tests that are stopped before reaching final failure. Stopping of a fatigue life test might be done after reaching a set number of fatigue cycles (e.g., 1,000,000 cycles). The results from these tests should not always be discarded because they contain information on the fatigue behaviour at lower stress levels. Their inclusion in and effect on the S-N curve depend on the remainder of the dataset.

In some cases, test results have to be censored from the dataset because they are invalid. For example, if failure inside clamping of the specimen occurs (i.e. tab failure), causing the test to be unrepresentative of the fatigue behaviour. Furthermore, slipping of the specimen in the clamp might occur, also leading to censoring of the test result. Other potential cases for censoring are misalignment of the test set-up causing, for example, twisting of the specimen, or an interrupted loading of the specimen. The latter might enhance the obtained fatigue life until failure, as discussed in Section 2.1 on aspects affecting the fatigue life. The previously mentioned aspects are only examples but should be kept in mind because each will influence the obtained test result and thereby the estimated S-N curve.

2.4.3 Type of Fatigue Tests

Three types of fatigue tests can be identified based on their applied loading, i.e. 1) T-T, 2) T-C, and 3) C-C tests. Of these three tests, T-T loading is most straightforward and has the least amount of considerations. For the latter two types of tests, the main aspect to consider is the occurrence of buckling during compression-loading. Buckling must be avoided because it will influence final results and can lead to premature failure. Two options are available to minimise the risk of buckling. Firstly, one can minimise the gauge length (distance between clamped areas) to reduce the risk of buckling and premature failure. For example, ASTM (2001) recommends a gauge length of 12 mm for determining compressive properties using a Combined Loading Compression (CLC) test fixture. A second option is to employ an Anti-Buckling Device (ABD) during (partial) compressive tests. An ABD limits out-of-plane deformations of the specimen. However, these are imminent when matrix failure occurs. By preventing these type of deformations, fatigue life test results might be altered. For example, this can result in the specimen being capable of sustaining higher absolute compressive stresses during fatigue life when an

ABD is used than the UCS value obtained without an ABD. Consequently, this can result in an S-N curve showing increasing stresses for longer lives. Therefore, it is not recommended to include ABDs in the test set-up if not required. Because the use of an ABD can influence the obtained test results considerably and it is not always indicated whether or not an ABD was included during testing, this work will only consider fatigue life prediction of T-T and T-C loading, and no C-C loading, without the use of an ABD in the T-C loading type.

Chapter 3

Anisomorphic Constant Fatigue Life Diagrams

The anisomorphic CLD for carbon fibre-reinforced epoxy laminates, first proposed by Kawai and Koizumi (2007), is a non-linear model capable of constructing a CLD based on a limited amount of experimental fatigue life data. The most simple version of the anisomorphic model requires only tensile and compressive static strength values and a so-called critical S-N curve as input. This critical S-N curve describes the fatigue life under the critical R-ratio χ: the static compressive over the static tensile strength. The method is limiting time-consuming and expensive testing procedures normally required for predicting fatigue lives by reducing the input size. This section commences with an explanation of the general concept of the anisomorphic CLD and an overview of the different model versions. The subsequent sections cover the two-, three-, and four-segment versions of the anisomorphic CLD. Lastly, a discussion on the different models is provided, including a consideration of their limitations and possible improvements.

3.1 General concept of the anisomorphic CLD

An overview of the different models is provided in Table 3.1. The table presents an overview of the lay-ups for which each model has been validated and the corresponding paper in which the model was first introduced. Generally, the two-segment CLD is applicable to laminates showing UTS>|UCS| while the more elaborated three- and four-segment CLDs are also applicable to laminates showing |UCS|>UTS. The latter laminates require a more extensive prediction model due to large distortions seen in the CLD, especially in the T-C and C-C region left of the $R = \chi$ radial. In order to describe these distortions, additional input data is required by the anisomorphic models, as shown in Table 3.1. On the one hand, the two-segment anisomorphic model is the most simple anisomorphic model, employing only static strength data (UTS and UCS) and fatigue life data at $R = \chi$. On the other hand, the three- and four-segment anisomorphic model require additional input fatigue life data at the so-called sub-critical R-ratio χ_S or the left and right auxiliary R-ratio χ_L and χ_R, respectively. Accordingly, the three- and four-segment anisomorphic model require two and three S-N curves as input, respectively. Note that the three- and four-segment CLDs counteract the simplification initially offered by the two-segment anisomorphic CLD (i.e., fewer input data required with respect to other available prediction methods while keeping an acceptable predictive accuracy). Nonetheless, the increase in complexity is compensated by the improved accuracy in fatigue life predictions.

Table 3.1: Overview of the different anisomorphic CLD models.

Anisomorphic model	Initially proposed by	Input data	Considered lay-ups
Two-segment CLD	Kawai and Koizumi (2007)	UTS, UCS, S-N curve under $R = \chi$	$[45/90/\text{-}45/0]_{2s}$ $[0/60/\text{-}60]_{2s}$, $[0/90]_{3S}$
Three-segment CLD	Kawai and Murata (2010)	UTS, UCS, S-N curve under $R = \chi$ and χ_S	$[\pm 30]_{3S}$, $[\pm 45]_{3S}$ $[\pm 60]_{3S}$
Four-segment CLD	Kawai and Itoh (2014)	UTS, UCS, S-N curve under $R = \chi$, χ_L, χ_R	$[0]_{16}$, $[10]_{16}$ $[15]_{16}$, $[30]_{16}$ $[45]_{16}$, $[90]_{16}$

All three models (partially) base the predicted CLD on the so-called critical R-ratio χ, which is defined as (Kawai and Koizumi, 2007)

$$\chi = \frac{UCS}{UTS}, \tag{3.1}$$

where χ obtains a value in the range $-\infty<\chi<0$. For CFRP laminates, it was shown by Kawai and Koizumi (2007) that the sensitivity to fatigue loading is largest at, or in the vicinity of, $R = \chi$. For lay-ups characterised by UTS>|UCS|, this results not only in an S-N curve with the steepest slope of all R-ratios but also in CLL peaks near the $R = \chi$ radial. In T-C loading, fatigue behaviour of both T-T and C-C loading is combined since the failure modes and damage mechanisms differ in these loading types (Rotem and Nelson, 1989). Kawai and Koizumi (2007) assume that under $R = \chi$ loading, the laminate is equally influenced by both tension and compression fatigue behaviour, and thereby that the probability of occurrence of either type of failure mode is equal. For T-C loads related to $R < \chi$, the fatigue behaviour and failure modes are more similar to C-C fatigue loading. For T-C loads related to $R > \chi$, the fatigue behaviour and failure modes are similar to those seen in T-T type loading. Therefore, it was assumed by Kawai and Koizumi (2007) that a transition of the dominant failure mode occurs at $R = \chi$. Note that for lay-ups characterised by |UCS|>UTS, the assumption of largest fatigue sensitivity near $R = \chi$ still seems to be valid (Kawai and Itoh, 2014). However, it no longer results in CLL peaks at $R = \chi$, as shown in Section 3.3 and 3.4.

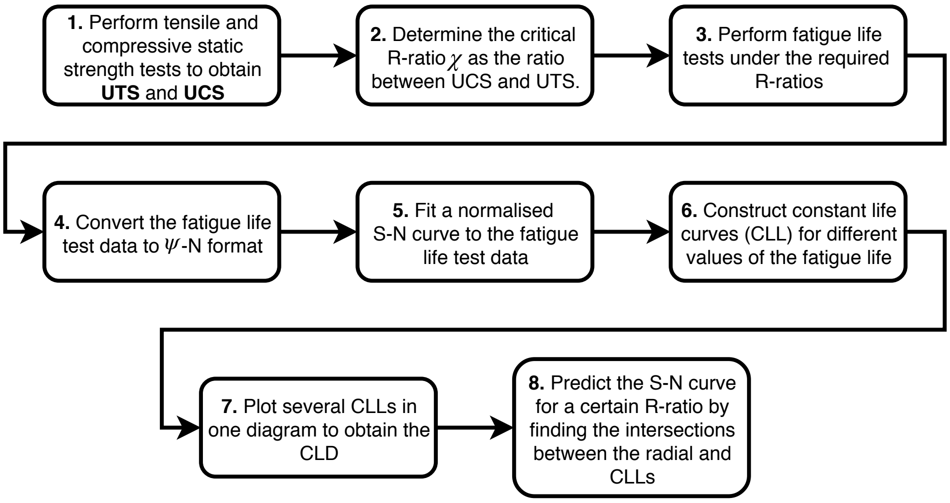

Figure 3.1: Flowchart depicting the general approach used by all anisomorphic models.

General method

The anisomorphic models follow a general procedure in constructing the CLD and predicting S-N curves using static strength and fatigue life input data. A flowchart depicting this general method is included in Figure 3.1 and the different steps are shortly explained next. Each model version applies changes to the the general method by, for example, including additional input data or adapting the CLL functions. The details of each model are discussed in the corresponding sections.

1. Static strength test data, in the form of UTS and UCS, is required as input to the model.

2. The critical R-ratio χ can be calculated as the ratio between UCS and UTS (Equation 3.1).

3. CA fatigue life tests are performed at $R = \chi$. For the three- and four-segment CLDs, additional fatigue life tests at $R = \chi_S$ or $R = \chi_L$ and $R = \chi_R$ are required, respectively.

4. Fatigue life data is converted from $(\sigma_{\max}, N_f)$ to (ψ, N_f), where ψ is defined as $\psi = \sigma_{\max}/\sigma_B$ (Kawai and Koizumi, 2007) and σ_B is the extrapolated stress value at $N_f = 1$.

5. A normalised curve $\psi = f^{-1}(2N_f)$ is fitted to fatigue life test data in order to describe an S-N curve.

6. CLLs for different values of fatigue life N_f can be constructed using the fitted normalised S-N curve.

7. The CLD is obtained by depicting several CLLs in the same diagram.
8. An S-N curve at a different R-ratio than the input R-ratio can be predicted by determining intersections of the CLLs with the radial corresponding to the R-ratio of interest.

3.2 Two-Segment Anisomorphic CLD

The two-segment anisomorphic CLD proposed by Kawai and Koizumi (2007) is an adapted version of the inclined Goodman diagram, where the CLL expressions have been slightly altered to include an exponent. The CLLs peak at the radial corresponding to $R = \chi$, thereby essentially dividing the CLD into two segments. CLLs in each segment are described using a different expression that merge on the radial. An example of the two-segment anisomorphic CLD is presented in Figure 3.2 for a carbon-epoxy laminate with lay-up $[45/90/\text{-}45/0]_{2S}$.

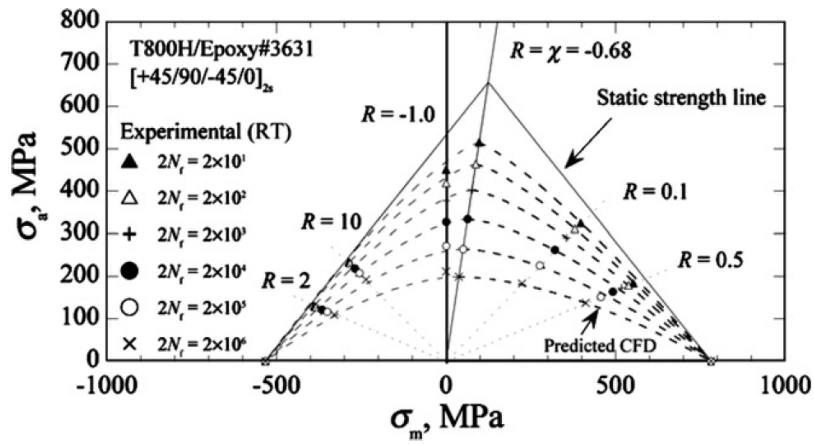

Figure 3.2: Two-segment anisomorphic CLD for a carbon-epoxy laminate with lay-up $[45/90/\text{-}45/0]_{2S}$ showing constant life curves for different values of the fatigue life cycles, as well as radial lines corresponding to a constant R-ratio, reprinted from Kawai and Koizumi (2007).

The two-segment model is based on three main assumptions:

1. The fatigue behaviour of carbon-epoxy laminates under CA loading at any R-ratio can be predicted based on the behaviour under fatigue loading at $R = \chi$.
2. Amplitude stress peaks of the CLL for a constant value of the fatigue life are located at the radial related to $R = \chi$.
3. The shape of CLLs gradually changes from a straight line to a parabola for an increasing fatigue life.

The procedure of constructing a CLD and predicting S-N curves for different R-ratios using the two-segment anisomorphic model is presented next.

Step 1-3
Firstly, the static tensile and compressive strength of the laminate are required as input to the model. Based on the static tensile and compressive strength, the value of χ can be determined using Equation 3.1. Next, an S-N curve for this critical R-ratio is constructed by performing fatigue life tests at $R = \chi$.

Step 4
On the fatigue life test datapoints for $R = \chi$, a normalised S-N curve expression is fitted defined by the fatigue strength ratio ψ_χ, where ψ_χ is defined as (Kawai and Koizumi, 2007)

$$\psi_\chi = \frac{\sigma_{\max}^{\chi}}{\sigma_B}, \tag{3.2}$$

which is the ratio between the maximum applied stress $\sigma_{\max}^{\chi}$ (at $R = \chi$) and strength σ_B. σ_B is obtained by extrapolating the S-N curve for $R = \chi$ to $N_f = 1$ (static strength point) and evaluating which stress value fits the extrapolated curve. Its value often corresponds to either UTS or UCS. Consequently, this implies that fatigue life data, often in the form of ($\sigma_{\max}$, N_f), must be transformed to (ψ_χ, N_f). Then, the value of ψ_χ ranges between $0 \leq \psi_\chi \leq 1$.

Step 5
To the transformed fatigue life data, a curve can be fitted and the function parameters can be obtained. Different normalised S-N fitting curves are available, each employing different function parameters. However, all curves suggested by Kawai and his colleagues fit the fatigue life data to a function in the form of (Kawai, 2010)

$$2N_f = f\left(\psi_\chi\right). \tag{3.3}$$

For the two-segment CLD, Kawai and Koizumi (2007) suggested an equation given as

$$2N_f = \frac{2}{K_\chi} \frac{(1-\psi)^a}{\psi^n}, \tag{3.4}$$

where K_χ, a, and n are fitting parameters (laminate-specific constants). A discussion on the manner of fitting is provided in more detail in Appendix A.

Step 6
Next, the fitted critical S-N curve can be used to determine corresponding stress amplitude peaks in the CLD. Note that all peaks lie on the radial related to $R = \chi$, defined as fatigue life stress combinations in the form of (N_f, σ_m^χ, σ_a^χ). The $R = \chi$ radial is also the radial dividing the CLD in two segments. The general formulation for a CLD radial is given as

$$\frac{\sigma_a}{\sigma_m} = \frac{1-R}{1+R}, \tag{3.5}$$

where σ_a and σ_m are the amplitude and mean stress, respectively. Once the peaks of the CLD are defined, other stress combinations (σ_m, σ_a) on the CLL for the same fatigue life N_f can be calculated using the equations given as (Kawai and Koizumi, 2007)

$$-\frac{\sigma_a - \sigma_a^{\chi}}{\sigma_a^{\chi}} = \left(\frac{\sigma_m - \sigma_m^{\chi}}{UTS - \sigma_m^{\chi}}\right)^{2-\psi_{\chi}} \quad \text{if} \quad \sigma_m^{\chi} \leq \sigma_m \leq UTS, \tag{3.6}$$

$$-\frac{\sigma_a - \sigma_a^{\chi}}{\sigma_a^{\chi}} = \left(\frac{\sigma_m - \sigma_m^{\chi}}{UCS - \sigma_m^{\chi}}\right)^{2-\psi_{\chi}} \quad \text{if} \quad UCS \leq \sigma_m < \sigma_m^{\chi}. \tag{3.7}$$

These CLL expressions are modified equations of the CLLs used in the inclined Goodman diagram by including an exponent in the form of $(2 - \psi_{\chi})$, where the value of ψ_{χ} falls in the range $0 \leq \psi_{\chi} \leq 1$. For $\psi_{\chi} = 1$, the inclined Goodman diagram with linear-shaped CLLs is obtained while for smaller values of ψ_{χ} (i.e., an increasing fatigue life), the CLLs are parabolas.

Step 7
A CLD can be established by evaluating Equations 3.6 and 3.7 for different values of the fatigue life N_f and plotting the obtained curves in the same diagram. An example of a CLD established using the two-segment anisomorphic model was previously presented in Figure 3.2 for a carbon-epoxy laminate with lay-up $[45/90/\text{-}45/0]_{2S}$.

Step 8
Once a CLD has been obtained, it can be used to predict S-N curves for different R-ratios. It is known that all stress combinations of one S-N curve lie on one radial corresponding to the R-ratio of interest. Therefore, in order to derive an S-N curve prediction from the CLD, it is required to find intersections of the radial with different CLLs because each CLL corresponds to a constant value of N_f. To find the (σ_m, σ_a)-combination at which a radial and CLL intersect, it is required to solve a set of equations composed of Equation 3.5 and Equations 3.6 and 3.7. In this set of equations, the location of the stress peak (σ_m^{χ}, σ_a^{χ}) for a specified N_f is known from the curve fitted to the input fatigue life data. Moreover, the value ψ_{χ} is a function of these peak stresses ($\psi_{\chi} = f(\sigma_{\max})$) and UTS and UCS are required as input to the anisomorphic model. Solving the set of equations results in values for σ_m and σ_a where the radial and CLL intersect. Repeating this procedure for different values of N_f and combining the found intersections, results in a predicted S-N curve for the R-ratio of interest.

Applicability
The two-segment anisomorphic CLD was validated by Kawai and Koizumi (2007) by applying it to three different carbon-epoxy (T800H/3631 and T800H/2500) laminates. The lay-ups of the considered laminates are $[45/90/\text{-}45/0]_{2s}$, $[0/60/\text{-}60]_{2s}$, and $[0/90]_{3s}$. Kawai and Koizumi (2007) provide a comparison between test results and the predicted CLD and S-N curves. The error of the predictions was not quantified and results were only compared qualitatively. Furthermore, the size of the datasets used for validation is

limited with small amounts of test results. Therefore, some predictions were extrapolated beyond the available test data. Due to a lack of sufficient amounts of test data, the predictions in these regions cannot be assessed. Moreover, any obtained conclusions must be seen as preliminary until more evaluations with additional test results are performed.

Kawai and Koizumi (2007) concluded that a “good agreement” is seen for the considered laminates between the predictions and test results for both the CLD and S-N curves and that results were acceptable for all loading regimes (T-T, T-C, C-C). Even though Kawai and Koizumi (2007) report a “good agreement” between predictions and the validation dataset, some comments can be made when evaluating the presented diagrams. From most diagrams presented by Kawai and Koizumi (2007), it can be concluded that the predictions seem to be in agreement with experimental data for T-T and T-C loading. However, for C-C loading with $R = 2$ and $R = 10$, predictions seem to be less reliable with larger differences and a different S-N curve slope than test results indicate. These inaccurate predictions can be caused by a variety of sources. For example, an inaccurate assumption on the CLL function in the left segment for T-C loading at $R < \chi$ and C-C loading. Another source can be the large scatter naturally present in C-C fatigue life data. Large variability in fatigue life is also seen in the datasets evaluated by Kawai and Koizumi (2007). However, due to the limited amount of performed tests, it cannot be assessed whether the employed test datapoints are outliers or whether indeed large variability is present in the results. Additional validation, also of other laminates, is required to evaluate the applicability of the model and the sources of these inaccuracies.

In addition to the previously mentioned laminates, the two-segment CLD was also applied to angle-ply carbon-epoxy (T800H/2500) laminates with lay-ups $[\pm 30]_{3S}$ and $[\pm 45]_{3S}$ by Kawai and Murata (2010). They describe the agreement between the predicted CLD and test data for the laminates as “good” while the S-N curve agreements are evaluated as “reasonably good”. The predictions for $R = 10$ again show a lower accuracy. Furthermore, the datasets used for validation are again limited in their size and thus only preliminary conclusions can be drawn. It is recommended to perform additional evaluations of these laminates with more fatigue life data to evaluate the predictions. Besides these two lay-ups, the two-segment model was also applied to a carbon-epoxy (T800H/2500) laminate with lay-up $[\pm 60]_{3s}$ (Kawai and Murata, 2010) and off-axis Unidirectional (UD) carbon-epoxy (T700S/2592) laminates (Kawai and Itoh, 2014). However, the predictions for these laminates were less accurate and sometimes even “poor” (Kawai and Murata, 2010). Therefore, an altered version of the CLD model is required to describe these laminates. The adapted versions of the anisomorphic model (three- and four-segment CLD) are presented in the next sections (Section 3.3 and 3.4).

3.3 Three-Segment Anisomorphic CLD

The three-segment anisomorphic CLD, proposed by Kawai and Murata (2010), is derived from the two-segment anisomorphic CLD and an example is shown in Figure 3.3 for a carbon-epoxy laminate with lay-up $[\pm 60]_{3S}$. The CLD is defined by three segments bounded by the critical R-ratio χ and the sub-critical R-ratio χ_S. The model was composed based on the evaluation of three angle-ply carbon-epoxy (T800H/2500) laminates with lay-ups of $[\pm 30]_{3S}$, $[\pm 45]_{3S}$, and $[\pm 60]_{3S}$. It was found that the $[\pm 60]_{3S}$-laminate, in contrast to the $[\pm 30]_{3S}$- and $[\pm 45]_{3S}$-laminates, shows a distortion in the CLD left of the $R = \chi$ radial and that the peaks of the CLD are no longer located on or in the vicinity of $R = \chi$ but instead are located at lower R-ratios. The two-segment CLD model cannot accompany this change in CLL shape. For this reason, a sub-critical R-ratio χ_S was introduced by Kawai and Murata (2010), resulting in a CLD consisting of three segments. Consequently, no longer only static strength data and fatigue life data at $R = \chi$ is required but also fatigue life data at $R = \chi_S$ is needed. The manner of constructing a CLD and derivation of an S-N curve using the three-segment anisomorphic model will be discussed in this section.

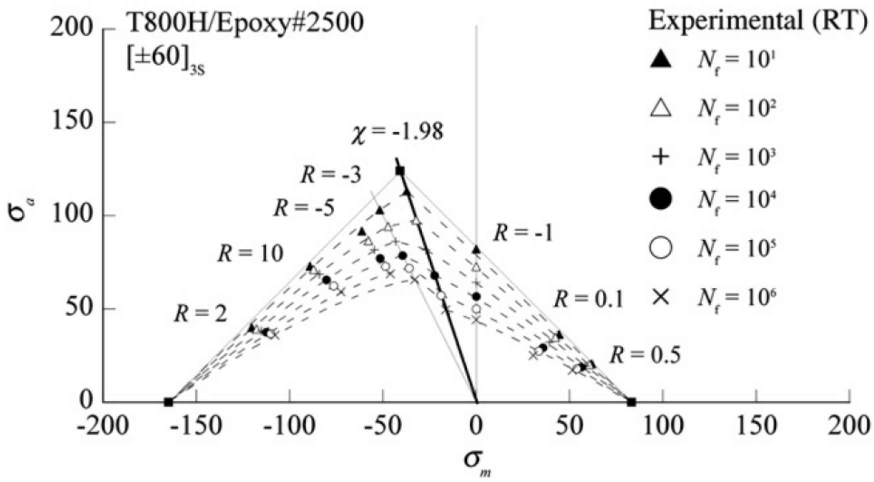

Figure 3.3: Three-segment anisomorphic CLD for a carbon-epoxy laminate with lay-up $[\pm 60]_{3S}$ showing constant life curves for different values of the fatigue life cycles, as well as radial lines corresponding to a constant R-ratio, reprinted from Kawai and Murata (2010).

For the three-segment anisomorphic model, three assumptions were made in addition to those for the two-segment model:

1. The fatigue behaviour of carbon-epoxy laminates under CA loading at any R-ratio can be predicted based on the behaviour under fatigue loading at both the critical R-ratio χ and the sub-critical R-ratio χ_S.

2. The CLLs in the centre segment can be defined using linear interpolation by connecting similar fatigue life datapoints on the critical and sub-critical radials.

3. The CLLs in the left and right segment can be described in a similar manner as for the two-segment model.

Next, the model steps of the three-segment anisomorphic model are provided.

Step 1-3
The method for establishing the three-segment CLD is similar to that for the two-segment anisomorphic model. However, additional fatigue life tests must be performed at $R = \chi_S$ to establish a second input S-N curve. The sub-critical R-ratio χ_S can be chosen arbitrarily but must fall within either of the two ranges defined by χ: $-\infty < \chi_S < \chi$ or $\chi \leq \chi_S < 0$. However, based on the evaluated laminates by Kawai and Murata (2010) and Kawai and Itoh (2014), the value of χ_S for laminates showing |UCS|>UTS can best be selected as $\chi_S < \chi$ in order to describe the most noteworthy distortions in the CLD. On the other hand, the value of χ_S for laminates characterised by UTS>|UCS|, to which also the two-segment anisomorphic model can be applied, should not influence the final predictions significantly.

Step 4
Similar to the two-segment model, fatigue life input data must be converted to a (ψ, N_f) form after which a curve can be fitted to the test data. Note that this procedure must be performed twice: once for $R = \chi$ and once for $R = \chi_S$. Furthermore, two fatigue strength ratios are identified: 1) a critical ratio ψ_χ and 2) a sub-critical ratio ψ_{χ_S}.

Step 5
For fitting of a curve to experimental data, Kawai and Murata (2010) suggest a different, more elaborated fitting curve compared to that used for the two-segment CLD (Equation 3.4), given as

$$2N_f = \frac{1}{K_\chi}\frac{1}{(\psi_\chi)^n}\frac{(1-\psi_\chi)^a}{\left(\psi_\chi - \psi_\chi^L\right)^b}, \tag{3.8}$$

where ψ_χ^L describes the (potential) fatigue limit for HCF. In addition to the laminate-specific fitting parameters K_χ, a, and n defined in Equation 3.4, a fourth fitting parameter b can be identified. Kawai and Murata (2010) recommend Equation 3.8 and do not consider the use of Equation 3.4 for the S-N curve description of the angle-ply laminates. However, the author of this work, as will be further argued in Chapter 4, recognises possibilities for the use of the two-segment S-N curve expression in the three-segment CLD approach. The selection of an S-N curve expression should not rely on the used CLD model but instead should be based on the appropriateness of an expression to the observed fatigue life trends. Nevertheless, this section will closely follow the method proposed by Kawai and Murata (2010) and only Equation 3.8 will be considered.

Step 6
The S-N curves fitted to input fatigue life data can be used to define CLL expressions. For each CLD segment, a corresponding CLL expression can be defined as (Kawai and Murata, 2010)

$$-\frac{\sigma_a - \sigma_a^{\chi}}{\sigma_a^{\chi}} = \left(\frac{\sigma_m - \sigma_m^{\chi}}{UTS - \sigma_m^{\chi}}\right)^{2-(\psi_\chi)^{k_T}} \quad \text{if} \quad \sigma_m^{\chi} \le \sigma_m \le UTS, \tag{3.9}$$

$$-\frac{\sigma_a - \sigma_a^{\chi}}{\sigma_a^{\chi} - \sigma_a^{\chi_s}} = \frac{\sigma_m - \sigma_m^{\chi}}{\sigma_m^{\chi_s} - \sigma_m^{\chi}} \quad \text{if} \quad \sigma_m^{\chi_s} \le \sigma_m < \sigma_m^{\chi}, \tag{3.10}$$

$$-\frac{\sigma_a - \sigma_a^{\chi_s}}{\sigma_a^{\chi_s}} = \left(\frac{\sigma_m - \sigma_m^{\chi_s}}{UCS - \sigma_m^{\chi_s}}\right)^{2-(\psi_\chi)^{k_C}} \quad \text{if} \quad UCS \le \sigma_m < \sigma_m^{\chi_s}. \tag{3.11}$$

Now, three expressions instead of two describe the CLLs and the transitional region is described using linear interpolation. In addition, two parameters (k_C and k_T) are added to the functions for the compressive and the tensile segment, respectively. These parameters are constants involved in describing the transition from a straight line to parabolas for a changing fatigue life. In the given approach, one should first assume k_T and k_C equal to 1.0 and then "adjust the values of these exponents manually taking into account the accuracy of prediction using the three-segment anisomorphic CFL diagram." However, it is the author's opinion that the procedure suggested by Kawai and Murata (2010) might not be appropriate. The advised method seems to employ datapoints used for validation purposes to determine the values of the exponents. In essence, it is no longer a predictive method but is instead a descriptive method of fatigue life data. Hence, it is not possible to guarantee the accuracy of predictions merely using data under $R = \chi$ and χ_S because the value of k_T and k_C must be assumed while the appropriate description of the CLL shape is still unknown. In this work, an improved method, not relying on validation data, is proposed in Chapter 5.

Step 7
CLL expressions for each segment can be combined to form a CLL over the entire mean stress range. Plotting several CLLs for different fatigue lives in one diagram leads to establishment of the CLD.

Step 8
Once CLL expressions have been established and a CLD has been constructed, S-N curves for different R-ratios can be predicted. This is done in a similar way as in the two-segment model by finding the intersection of the radial for the R-ratio of interest with CLLs for different values of N_f. The proper CLL expression from Equation 3.9 to 3.11 is selected based on the value of the mean stress. The radial is given by Equation 3.5.

Applicability
The three-segment anisomorphic model was evaluated using carbon-epoxy (T800H/2500) laminates with angle-ply lay-ups, namely $[\pm 30]_{3s}$, $[\pm 45]_{3s}$, and $[\pm 60]_{3s}$. As discussed in the previous section, the two-segment CLD is applicable to the former two laminates but not to the latter laminate. Kawai and Murata (2010) demonstrated that the three-segment CLD is applicable to all three laminates. Based on the obtained CLD and predicted S-N curves, it was concluded by Kawai and Murata (2010) that the predictive accuracy increases when using a CLD with three segments. Yet, some comments can be made. Firstly, the CLD for the $[\pm 60]_{3s}$-laminate shows an underprediction of the fatigue life for compression-dominated loading ($R < \chi$, i.e. $\sigma_m < \sigma_m^{\chi}$) and an overprediction for tension-dominated loading at $R = 0.1$. In addition, similar to the two-segment CLD, fatigue life predictions for C-C loading show larger disagreements with test data. Moreover, the employed datasets for validation are again small in size. Therefore, additional tests and evaluations must be performed for a valid conclusion on the predictive accuracy of the three-segment anisomorphic model for carbon-epoxy angle-ply lay-ups.

Kawai and Itoh (2014) evaluated the predictive performance of the three-segment CLD using UD carbon-epoxy (T800H/2500) laminates at different off-axis angles. A comparison with the two- and three-segment CLD was made and it was concluded that the use of the three-segment CLD “greatly” (Kawai and Itoh, 2014) improves the predictions. The predictions show an acceptable agreement with validation test datapoints but sometimes slightly under-predict the fatigue life of different R-ratios. To improve the predictive accuracy, Kawai and Itoh (2014) introduced a four-segment anisomorphic model that will be discussed in the next section.

3.4 Four-Segment Anisomorphic CLD

The four-segment anisomorphic CLD, proposed by Kawai and Itoh (2014), is an extended version of the two- and three-segment CLD to describe and predict fatigue lives of laminates showing large differences in mean stress sensitivity for different R-ratios. An example of a four-segment anisomorphic CLD is shown in Figure 3.4 for a carbon-epoxy laminate with lay-up $[30]_{16}$. The difference in mean stress sensitivity is clearly seen when comparing this CLD with that for the $[45/90/\text{-}45/0]_{2S}$-laminate shown in Figure 3.2. Large variations are seen on both the left and right side of the radial for $R = \chi$. The four-segment anisomorphic model is capable of describing these changes and was designed using on- and off-axis carbon-epoxy (T800H/2500) laminates with lay-ups $[0]_{16}$, $[10]_{16}$, $[15]_{16}$, $[30]_{16}$, $[45]_{16}$, and $[90]_{16}$.

Several additional assumptions are made for the four-segment anisomorphic model:

1. The fatigue behaviour of carbon-epoxy laminates under CA loading at any R-ratio can be predicted based on the behaviour under fatigue loading at the critical R-ratio χ, left auxiliary R-ratio χ_L, and the right auxiliary R-ratio χ_R.

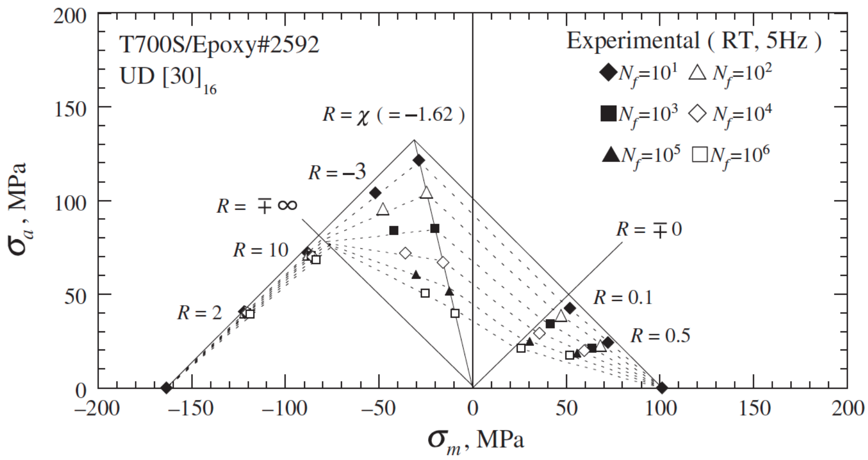

Figure 3.4: Four-segment anisomorphic CLD for a carbon-epoxy laminate with lay-up $[30]_{16}$ showing constant life curves for different values of the fatigue life cycles, as well as radial lines corresponding to a constant R-ratio, reprinted from Kawai and Itoh (2014).

2. The CLLs in the centre segments can be defined using linear interpolation by connecting similar fatigue life datapoints on the critical radial with those on the left and right auxiliary radials.

3. The predicted CLLs in the most left and right segments can be determined in a similar manner as for the three-segment model.

The four-segment CLD consists of four segments that are bounded by three radials. Consequently, additional fatigue life tests must be performed under two additional R-ratios besides the critical R-ratio, namely at 1) the left auxiliary R-ratio χ_L and 2) the right auxiliary R-ratio χ_R. Constructing the CLD and predicting S-N curves occurs in a similar manner as for the two- and three-segment CLD. Nonetheless, the specific procedure and the validation of the method are discussed next.

Step 1-3

The CLD is constructed using three input S-N curves at $R = \chi$, χ_L, and χ_R, where the following must hold:

$$-\infty < \chi_L \leq \chi \leq \chi_R < 0.$$

Both a left and a right auxiliary R-ratio were selected because, in contrast to the validation laminate ($[\pm 60]_{3S}$) for the three-segment CLD, the UD off-axis laminates show CLL distortions on both the left and right side of the $R = \chi$ radial. Including additional input data in both regions allows for an improved description of the CLLs. Kawai and Itoh (2014) suggest a value for the left and right auxiliary R-ratio as $\chi_L = -\infty$ and $\chi_R = 0$, respectively, or R-ratios that are in close vicinity of the suggested values (e.g., $R = 10$ and $R = 0.1$, respectively).

Step 4
Input fatigue life data under all three R-ratios (χ, χ_L, χ_R) must be converted in terms of the fatigue strength ratio (ψ, N_f). Note that three different strength ratios exist: one for each R-ratio, namely ψ_χ, $\psi_{\chi L}$ and $\psi_{\chi R}$.

Step 5
To the transformed data, an S-N curve function can be fitted. Kawai and Itoh (2014) suggest a normalised S-N curve expression similar to that used in the three-segment anisomorphic model, i.e. Equation 3.8. Here, a similar remark can be made as in the previous section concerning the application of this S-N curve function or a different function. This view will not be further debated in this section and the reader is referred to Chapter 4 for a more elaborate discussion.

Step 6
Input fatigue life data and fitted S-N curves can be used to define CLL expressions and subsequently the CLD. Four CLL expressions are defined, one for each CLD segment, where the CLLs in the centre two segments are defined using linear interpolation. The four CLL expressions are given as (Kawai and Itoh, 2014)

$$-\frac{\sigma_a - \sigma_a^{\chi_R}}{\sigma_a^{\chi_R}} = \left(\frac{\sigma_m - \sigma_m^{\chi_R}}{UTS - \sigma_m^{\chi_R}}\right)^{2-\left(\psi_{\chi_R}\right)^{k_T}} \quad \text{if} \quad \sigma_m^{\chi_R} \leq \sigma_m \leq UTS, \tag{3.12}$$

$$-\frac{\sigma_a - \sigma_a^{\chi_R}}{\sigma_a^{\chi_R} - \sigma_a^{\chi}} = \frac{\sigma_m - \sigma_m^{\chi_R}}{\sigma_m^{\chi} - \sigma_m^{\chi_R}} \quad \text{if} \quad \sigma_m^{\chi} \leq \sigma_m < \sigma_m^{\chi_R}, \tag{3.13}$$

$$-\frac{\sigma_a - \sigma_a^{\chi}}{\sigma_a^{\chi} - \sigma_a^{\chi_L}} = \frac{\sigma_m - \sigma_m^{\chi}}{\sigma_m^{\chi_L} - \sigma_m^{\chi}} \quad \text{if} \quad \sigma_m^{\chi_L} \leq \sigma_m < \sigma_m^{\chi}, \tag{3.14}$$

$$-\frac{\sigma_a - \sigma_a^{\chi_L}}{\sigma_a^{\chi_L}} = \left(\frac{\sigma_m - \sigma_m^{\chi_L}}{UCS - \sigma_m^{\chi_L}}\right)^{2-\left(\psi_{\chi_L}\right)^{k_C}} \quad \text{if} \quad UCS \leq \sigma_m < \sigma_m^{\chi_L}. \tag{3.15}$$

These CLL functions can be combined to create a CLL over the entire mean stress range in the CLD. Note that the parameters k_T and k_C are similar to those used in the three-segment anisomorphic model. The method of obtaining the values for these exponents is not described in detail by Kawai and Itoh (2014). Instead, it is suggested to assume a value of 1.0 for the parameters in case of a standard four-segment anisomorphic CLD. Comparable remarks can be made concerning the method of obtaining k_T and k_C as for the three-segment CLD, especially because no estimation method has been suggested for the four-segment CLD. However, this evaluation will not be restated in this section and the reader is referred to Section 3.3 for a more detailed assessment.

Step 7
To establish the CLD, CLLs for different fatigue lives must be plotted in the same diagram. This requires merging of the CLL expressions of each segment for constant values of the fatigue life.

Step 8

Similar to the previously described anisomorphic model versions, an S-N curve prediction can be made by finding the intersections of the radial for a specific R-ratio (Equation 3.5) with the appropriate CLLs for the considered mean stress (Equations 3.12 to 3.15).

Applicability

The four-segment CLD was validated by Kawai and Itoh (2014) using six UD carbon-epoxy (T800H/2500) laminates with different off-axis angles (0°, 10°, 15°, 30°, 45°, and 90°). Only the standard four-segment anisomorphic model was applied in which $k_T = k_C = 1.0$. The predicted CLD and S-N curves were compared with validation test data and it was found that the four-segment anisomorphic CLD is capable of making acceptable predictions for the fatigue life, thereby closely following the experimentally obtained datapoints. However, most predictions are slightly conservative, independent of the considered laminate, stress level or R-ratio. Note that, similar to the datasets used for validation of the two- and three-segment CLD, the datasets employed for the validation of the four-segment anisomorphic model are limited in their size (on average four specimens per S-N curve). Due to the small size of the datasets, which makes the S-N curve prone to errors, conclusions on the applicability of the model are only preliminary. Moreover, Kawai and Itoh (2014) have only provided a qualitative rather than a quantitative evaluation. For the latter, additional fatigue life tests must be performed.

3.5 Discussion

Three anisomorphic models have been identified in this chapter, namely the two-, three-, and four-segment CLD model. The two-segment CLD is the most simple model to implement and requires the least amount of test data as input (one S-N curve at $R = \chi$). The three- and four-segment CLD request a more extensive procedure, depending on two and three S-N curves as input, respectively ($R = \chi_S$, and $R = \chi_L$ and χ_R, respectively, in addition to $R = \chi$). Thereby, the latter two models directly counteract the initial advantage offered by the two-segment anisomorphic model: the small amount of fatigue life data needed as input because it results in the need to perform additional experimental fatigue life tests to obtain two and three S-N curves, respectively. This increases the expenses related to fatigue life predictions in terms of both time and costs. In Chapter 5, a CLD model is presented that resolves this aspect of the three- and four-segment CLDs by requiring only one S-N curve as input to provide fatigue life predictions.

All three anisomorphic models are based on the fatigue behaviour under the critical R-ratio χ. However, χ is not an R-ratio conventionally used for fatigue life tests and, consequently, experimental data is often not available at $R = \chi$. More conventional R-ratios applied during testing are $R =$ -1, 0.1 or 10. Therefore, when implementing the anisomorphic model, experimental data at a different R-ratio than the critical R-ratio is often used as input (often at R = -1 because it is closest to the real value of χ), which directly affects the predictive accuracy of the model. Thus, it can be seen as a disadvantage that the anisomorphic models are based on experimental data at $R = \chi$ because it makes them less widely and less easily applicable. For accurate predictions, it almost always implies that fatigue life tests must be performed, even when experimental fatigue life data at a different R-ratio is readily available. Chapter 4 and 5 each present a fatigue life prediction model that mitigates this aspect by allowing for input of fatigue life data obtained at either $R = 0.1$ or R = -1.

A third point of consideration, as previously discussed in the corresponding sections for each CLD model, is that the two-segment anisomorphic CLD is solely a fatigue life prediction model while this aspect is questionable for the three- and four-segment CLDs. The three- and four-segment CLD models include two additional exponents in the CLL functions, namely k_T and k_C, without providing a computational method to determine their values. If one assumes a value for these parameters solely based on the input fatigue life data, the model is a predictive fatigue life model but its predictive accuracy is unclear. The manner of determining the exponent values, as proposed by Kawai and Murata (2010), indicates a more descriptive method of the fatigue life behaviour because the values are selected by "taking into account the accuracy of prediction using the three-segment anisomorphic CFL diagram." This implies the use of other fatigue life test results in addition to the two S-N curves at $R = \chi$ and χ_S. Thereby, a necessity arises to conduct additional fatigue life tests on top of the two and three S-N curves already needed. Consequently, both time and cost expenses are further increased when employing the three- and four-segment CLD models. The CLD model presented in Chapter 5 diminishes the need for additional fatigue life tests by adapting the CLL expressions and removing exponents k_T and k_C from the function. Instead, another parameter is introduced whose value is directly dependent on the input static strength data rather than validation datasets.

Lastly, the anisomorphic models might not be fully applicable to C-C loading cases. Each model showed difficulty in fatigue life predictions of the C-C loading cases, specifically for $R = 2$ or 10. This can be caused by a variety of sources, for example, an inaccurate CLL definition or the large scatter seen in C-C fatigue life data. An improvement of the C-C predictive accuracy is of interest but will not be included in this work. Combined with concerns raised in Chapter 2 on C-C loading, it is decided to exclude these types of loadings in the adaptation of the anisomorphic model and instead focus on the fatigue life prediction of T-T and T-C loading cases using a single S-N curve.

In order to address the previously mentioned issues, except the prediction of C-C loading cases, two new CLD models are presented in this work. Chapter 4 suggests a fatigue life prediction model for laminates characterised by UTS>|UCS|, which is an adapted version of the two-segment model. For laminates characterised by the opposite, i.e. |UCS|>UTS, a CLD model is presented in Chapter 5, which allows for a reduction of the required input data compared to the three- and four-segment anisomorphic model. Both models only employ fatigue life data of one S-N curve related to a conventional

R-ratio of $R = 0.1$ or $R = -1.0$. In addition, no validation data is required for the model in Chapter 5 to obtain an estimation of the model parameters, which are solely based on static strength and fatigue life input data. Note that in this work, no CLD model is presented for carbon-epoxy laminates with UTS=|UCS| because no datasets are available to the author to verify which of the two models is applicable.

Chapter 4

Fatigue Life Prediction Model for UTS>|UCS|

The two-segment anisomorphic model, presented by Kawai and Koizumi (2007) for carbon fibre-reinforced epoxy laminates characterised by UTS > |UCS|, has been adapted such that experimental data obtained at a conventional R-ratio of either $R = 0.1$ or -1 can be employed rather than data obtained at the uncommon $R = \chi$. The proposed model does not distinguish between input data obtained at $R = 0.1$ or -1; the employed method is similar. This chapter commences with a section covering the methodology of the proposed model and discusses the adaptations made to the two-segment anisomorphic model. Each step of the model is discussed in detail and the differences with the two-segment anisomorphic model are stated for each model aspect. The second section of this chapter presents several datasets used to analyse the performance of the proposed model. Moreover, its predictive accuracy with respect to the two-segment anisomorphic model is evaluated. Section 4.3 provides a similar evaluation but instead by means of an experimental campaign.

4.1 Method

The general method of the proposed model will be presented in this section. First, an overview of the model and its assumptions are given and the method is illustrated by means of a flowchart. Next, every subsection provides details on different aspects of the method such as the required input or CLL expressions. Moreover, the differences with the two-segment anisomorphic by Kawai and Koizumi (2007) are discussed.

The proposed model is based on similar assumptions as the two-segment CLD, given in Section 3.2. Only the first assumption is altered, which is a direct consequence of a changing input R-ratio:

1. The fatigue behaviour of carbon-epoxy laminates under CA loading at any R-ratio (T-T and T-C) can be predicted based on the behaviour under fatigue loading at an R-ratio of either $R = 0.1$ or -1.

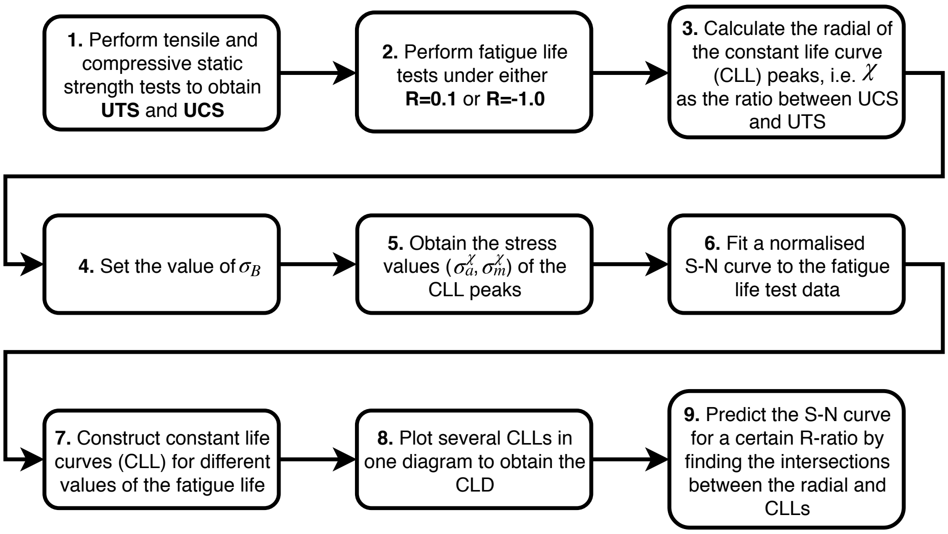

Figure 4.1: Flowchart depicting the proposed model for carbon-epoxy laminates characterised by UTS>|UCS|.

A flowchart of the steps taken to construct a CLD and predict S-N curves using the proposed model is shown in Figure 4.1. Next, a short explanation of each different step is provided. For a detailed description of each step, the reader is referred to the corresponding subsections. An example of the proposed CLD is shown in Figure 4.2

1. Static strength test data, in the form of UTS and UCS, is required as input to the model. (Subsection 4.1.1)

2. CA fatigue life tests are performed at either $R = 0.1$ or $R =$ -1.0. The R-ratio can be chosen by the user. (Subsection 4.1.1)

3. The value of the critical R-ratio χ can be calculated as the ratio between UCS and UTS (Equation 3.1).

4. The value of σ_B must be defined in order to determine ψ_χ in the next step. (Subsection 4.1.2)

5. The peak stress values on the $R = \chi$ radial are determined using the CLL expressions and fatigue life input data at $R = 0.1$ or -1. (Subsection 4.1.5)

6. A normalised S-N curve expression $\psi_\chi = f^{-1}(2N_f)$ is fitted to the calculated peak stress values for $R = \chi$ in order to describe the critical S-N curve. (Subsection 4.1.3)

7. CLLs for different values of the fatigue life N_f can be constructed using the fitted critical S-N curve. (Subsection 4.1.4)

8. The CLD is obtained by combining several CLLs in the same diagram. (Subsection 4.1.6)

9. An S-N curve at a different R-ratio than the input R-ratio can be predicted by determining intersections of the CLLs with the radial corresponding to the R-ratio of interest. (Subsection 4.1.7)

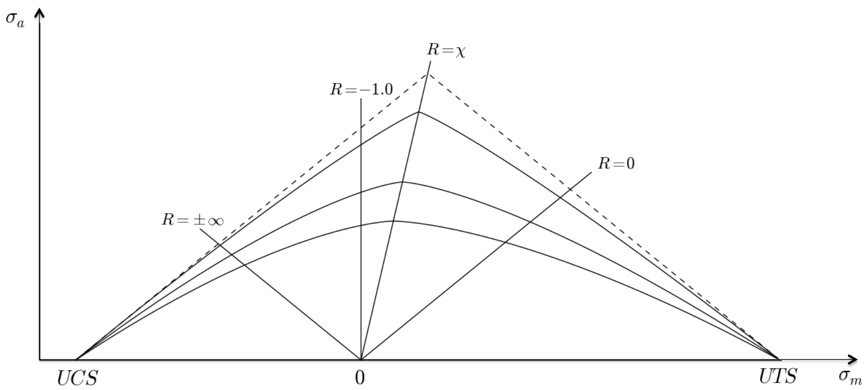

Figure 4.2: Proposed CLD model describing the fatigue behaviour of carbon-epoxy laminates characterised by UTS>|UCS|.

Note that there are large similarities between the proposed model and the two-segment model by Kawai and Koizumi (2007), presented in Chapter 3. Therefore, similar model aspects will not be explained in large detail, instead the reader is referred to Chapter 3 for additional clarification. The main differences between the models can be found in the used input data and the additional step to predict CLL peaks. Especially the second difference is large: where the two-segment anisomorphic model obtains the stress values for the CLL peaks directly by fitting a curve to fatigue life data at $R = \chi$, the proposed model requires solving of a set of equations, consisting of the CLL expression and the radial function for $R = \chi$ in order to find the CLL peaks. This additional model step is explained in detail in Subsection 4.1.5.

4.1.1 Input Data (Step 1 and 2)

The proposed model requires two experimental datasets as input. Firstly, similar to the two-segment CLD, it requires the values of UTS and UCS. Secondly, different from the two-segment CLD, experimental fatigue life data obtained at either $R = 0.1$ or -1 must be available. The required size of experimental datasets was discussed in Chapter 2.

4.1.2 Determination of χ and σ_B (Step 3 and 4)

Static strength and fatigue life input data can be used to determine the value for $R = \chi$ and σ_B in step 3 and 4, respectively. Similar to the two-segment anisomorphic model, the proposed method assumes that CLLs show an amplitude stress peak at the radial corresponding to the critical R-ratio χ and that the CLD can be defined using two segments bounded by the $R = \chi$ radial. Therefore, as will be seen in Subsection 4.1.5 for step 5, it is required to determine the exact location of these peaks. Consequently, it is required to determine the value of χ.

In addition to the critical R-ratio χ, the value of σ_B must be defined. This is also required for step 5 (Subsection 4.1.5), where the critical fatigue strength ratio ψ_χ is used in the CLL expressions. ψ is defined as in Equation 3.2. The value for σ_B is set as σ_B =UTS, independent of the input R-ratio and solely dependent on static strength data. Note that this is different from the two-segment anisomorphic model where σ_B is obtained using extrapolation of the S-N curve.

4.1.3 S-N Curve Expression (Step 6)

Several S-N curve functions are available of which several examples are provided in Appendix A. An S-N curve expression should provide an accurate description of the dataset. For example, if the experimental data shows a strong non-linearity, the use of a linear curve is not suitable. A detailed trade-off between different S-N curve expressions will not be conducted. Instead, in order to remain close to the anisomorphic model and allow for a straightforward comparison with the model proposed in this chapter, Equation 3.4 will be employed in the remainder of this work. This expression was preferred over Equation 3.8 because the latter employs five model parameters which implies the need of at least five experimental datapoints for fitting. An underdetermined system is obtained if less datapoints than fitting parameters are available (i.e., more equations than unknowns). Because a limited amount of experimental data is available for evaluation purposes (Section 4.2 and 4.3), Equation 3.4 was selected to avoid fitting difficulties. Nonetheless, note that for some laminates an improved description of the fatigue life test data might be obtained using a different S-N curve expression. These can be easily implemented by the reader since this will not alter any other steps of the model.

Note that in order to fit the curve to a dataset, it is required to transform fatigue life datapoints to the ratio ψ (Equation 3.2). After converting fatigue life data to the (ψ, N_f) format, Equation 3.4 can be fitted using a Least Squares Percentage Regression (LSPR) technique, discussed in detail in Appendix A. Once the values for the fitting parameters K_χ, a, and n are obtained, an S-N curve describing the fatigue life is obtained.

Note that, in the proposed model, it is not required to fit the curve to the input fatigue life data under $R = 0.1$ or $R = -1.0$. Yet, it is possible if one wants to describe test data. Instead, the curve must be fitted to the CLL amplitude stress peaks corresponding to $R = \chi$, as explained in more detail in Subsection 4.1.5.

4.1.4 Constant Life Lines (Step 7)

The CLLs are defined similar to the two-segment anisomorphic model and given by Equation 3.6 and 3.7. The CLL peaks are again located on the radial for $R = \chi$. Note that σ_a^χ and σ_m^χ, describing the peak stresses, are unknown because there is no fatigue life test data available under $R = \chi$. In order to construct the CLL, it is required to determine their values, for which the procedure is presented in the next subsection.

4.1.5 Determination of CLL Peaks and Peak S-N Curve (Step 5)

The two CLD segments are bounded by the radial corresponding to $R = \chi$ at which the CLL peaks are located. This is also shown in Figure 4.2. A range of related mean and amplitude stress combinations (σ_m^χ, σ_a^χ) on the $R = \chi$ radial can be determined as

$$\frac{\sigma_a^\chi}{\sigma_m^\chi} = \frac{1-\chi}{1+\chi}. \tag{4.1}$$

However, the fatigue life N_f corresponding to each (σ_m^χ, σ_a^χ)-combination is unknown: each CLL for a constant value of N_f intersects the radial, but its exact location of intersection is unknown. The intersection point of the CLL with the radial for $R = \chi$, and thus the location of the CLL peak (N_f, σ_m^χ, σ_a^χ), can be determined by combining the formulas for the CLL and the radial. Then, the set of equations that must be solved to obtain the peak locations is given as

$$\sigma_a^I = \sigma_a^\chi \left(1 - \left(\frac{\sigma_m^I - \sigma_m^\chi}{UTS - \sigma_m^\chi}\right)^{2-\psi_\chi}\right) \quad \text{if} \quad \sigma_m^\chi \leq \sigma_m^I \leq UTS, \tag{4.2}$$

$$\sigma_a^I = \sigma_a^\chi \left(1 - \left(\frac{\sigma_m^I - \sigma_m^\chi}{UCS - \sigma_m^\chi}\right)^{2-\psi_\chi}\right) \quad \text{if} \quad UCS \leq \sigma_m^I < \sigma_m^\chi, \tag{4.3}$$

$$\sigma_a^\chi = \sigma_m^\chi \frac{1-\chi}{1+\chi}. \tag{4.4}$$

The set of equations can now be solved for σ_m^χ and σ_a^χ using the experimental data input. Both UTS and UCS are known from static strength tests and fatigue life data for either $R = 0.1$ or $R =$ -1 is available. The fatigue life test datapoints can be used to define a range of unique combinations of $(N_f, \sigma_m^I, \sigma_a^I)$. Note that all stress value combinations for different N_f are located on one radial related to either $R = 0.1$ or $R =$ -1. The critical fatigue strength ratio ψ_χ is related to the stress level at the CLL peak and defined as Equation 3.2. In this equation, σ_B equals UTS and $\sigma_{\max}^\chi$ is a function of σ_m^χ and σ_a^χ, given as

- $\sigma_{\max}^\chi = \sigma_m^\chi + \sigma_a^\chi$ if $\sigma_m^\chi > 0$, i.e. if -1 $< \chi < 1$,
- $\sigma_{\max}^\chi = \sigma_m^\chi - \sigma_a^\chi$ if $\sigma_m^\chi < 0$, i.e. if $\chi <$ -1,
- $\sigma_{\max}^\chi = \sigma_a^\chi$ if $\sigma_m^\chi = 0$, i.e. if $\chi =$ -1.

Summarising, in order to find the locations of the CLL peaks located on the radial related to $R = \chi$, the set of Equations 4.2 to 4.4 must be solved. The variables UTS, UCS, and (σ_m^I, σ_a^I) stresses corresponding to the considered N_f are known from the input dataset. The ratio ψ_χ is a function of UTS, σ_m^χ, and σ_a^χ. Thereby, it becomes possible to solve the set of equations for σ_m^χ and σ_a^χ corresponding to N_f, resulting in a range of $(N_f, \sigma_m^\chi, \sigma_a^\chi)$-combinations. Note that the values of N_f are equal to those found during the fatigue life tests but that the corresponding stresses are different since they relate to a different R-ratio. Combining the stresses at $R = \chi$ for different fatigue lives, an S-N curve can be described for $R = \chi$ and the S-N curve expression defined in Subsection 4.1.3 can be fitted to the obtained peak stress combinations. Now, a continuous S-N curve for $R = \chi$ has been predicted. In the next subsection, an explanation is provided how to employ this newly obtained S-N curve to construct CLLs and a CLD.

4.1.6 Constant Life Diagram (Step 8)

Next, it is possible to construct CLLs and a CLD using the predicted CLL peaks. In the previous subsection, an S-N curve expression was fitted to the predicted CLL peaks, thereby obtaining a continuous function describing fatigue life-stress combinations on the $R = \chi$ radial. Now, for each value of N_f, it is possible to obtain the corresponding peak mean and amplitude stress combination $(N_f, \sigma_m^\chi, \sigma_a^\chi)$. Consequently, using Equations 3.6 and 3.7, it is possible to construct several CLLs for different fatigue lives. Combining these CLLs results in the CLD for the laminate. Note that, similar to the two-segment anisomorphic model, all CLLs converge to either σ_m =UTS or σ_m =UCS on the x-axis for $\sigma_a = 0$ (i.e., $R = 1$). The CLLs for $N_f = 1$, defining the CLD boundary, are reduced to linear curves, given as

$$
\begin{aligned}
\sigma_a &= UTS - \sigma_m \quad \text{if} \quad \sigma_m^\chi \leq \sigma_m \leq UTS, \\
\sigma_a &= UCS + \sigma_m \quad \text{if} \quad UCS \leq \sigma_m < \sigma_m^\chi.
\end{aligned}
\tag{4.5}
$$

4.1.7 S-N Curve Prediction (Step 9)

After the CLLs have been established, the mean S-N curves for different R-ratios can be predicted. This occurs in a similar manner as for the two-segment anisomorphic model by finding the intersection of the CLL with the radial corresponding to the R-ratio of interest. Details on the exact procedure of deriving an S-N curve from a CLD can be found in Section 3.2.

4.2 Validation using Datasets from Literature

To evaluate the performance of the model presented in this chapter, test data from several carbon-epoxy laminates found in literature is used. Each subsection discusses the results from the proposed model for one laminate separately. Moreover, each subsection includes a quantitive comparison between the predictive accuracies of the proposed model and the two-segment anisomorphic model by Kawai and Koizumi (2007).

Three carbon-epoxy laminates are employed to evaluate the predictive performance. In order to allow for a comparison with the two-segment anisomorphic model, evaluations can only occur using laminates for which fatigue life test results at $R = \chi$, 0.1, and -1 loading are available. Test results of an R-ratio close to $R = \chi$ (e.g., in some cases the value of χ approaches -1) can also be used to substitute for $R = \chi$. However, this might affect fatigue life predictions by the two-segment anisomorphic model. In order to perform a straightforward comparison of both models, this option will not be considered and only laminates for which test results at $R = \chi$ are available will be evaluated. However, these are not commonly available for laminates considered in literature and therefore the datasets of three laminates, presented by Kawai and Koizumi (2007), are employed. Their lay-ups are given as:

1. $[45/90/\text{-}45/0]_{2S}$
2. $[0/60/\text{-}60]_{2S}$
3. $[0/90]_{3S}$

Kawai and Koizumi (2007) did not only present the experimental datasets but also the fatigue life predictions by the two-segment anisomorphic model. In the next subsections, these will be employed in the comparison of the predictive accuracies. First, in Subsection 4.2.1, the employed error metrics will be considered.

4.2.1 Error Metrics

In order to compare the models, it is required to evaluate the fatigue life predictions made using each model with test results and subsequently compare their predictive accuracy. This subsection will commence with an explanation of the manner of comparison, after which each error metric is defined.

The most straightforward comparison is between the predicted S-N curve and individual test results. However, single datapoints, especially outliers, can largely influence the obtained quantitative errors, which can result in a misleading impression of the predictive accuracy. An improved evaluation can be obtained by fitting an S-N curve to the validation dataset. Subsequently, a comparison between the best-fit and the predicted S-N curve can be performed at each stress level corresponding to a test datapoint. This will minimise the influence of outliers on the obtained quantitative errors. Note that the difference in fatigue life must be compared for a given applied stress level rather than the stress level for a given fatigue life because the stress level is the independent variable while the corresponding fatigue life is the dependent variable (Chapter 2).

The difference between the predicted and true (following the best-fit S-N curve) fatigue life can be quantified by means of the relative difference. It is of importance to look at the relative rather than the absolute error because the latter will lead to an incorrect judgement of the predictive accuracy. For instance, a difference of 10 cycles at a true value of $N_f = 100$ will have a larger impact than a misprediction of 10 cycles on a true fatigue life of $N_f = 10^6$. Therefore, relative errors will be used, which will provide a comprehensible result of the true implications on all fatigue life scales (i.e., for $2N_f = 10^3$ to $2N_f = 10^6$).

Four error metrics will be employed, namely:

1. Mean Average Percentage Error (MAPE),
2. Mean Normalised Bias (MNB),
3. Root Mean Squared Percentage Error (RMSPE),
4. Sum of Squared Errors of Prediction (SSE).

MAPE provides an indication on the magnitude of the average percentage relative difference between the predicted and true mean fatigue life. It is defined as

$$\text{MAPE} = \frac{100\%}{n} \sum_{i=1}^{n} \left| \frac{T_i - M_i}{T_i} \right|, \tag{4.6}$$

where M_i and T_i are the predicted and true fatigue life, respectively, and n is the size of the test dataset.

MNB indicates whether the model over- or under-predicts the true fatigue life. Its value can be calculated using

$$\mathrm{MNB} = \frac{100\%}{n} \sum_{i=1}^{n} \frac{T_i - M_i}{T_i}. \tag{4.7}$$

The third error metric, RMSPE, is defined as

$$\mathrm{RMSPE} = \sqrt{\frac{1}{n} \sum_{i=1}^{n} \left(\frac{T_i - M_i}{T_i} \cdot 100\% \right)^2}. \tag{4.8}$$

Lastly, the SSE will be employed to provide an indication on the performance of the model. The previously introduced relative percentage errors have a disadvantage that the errors are biased (Shcerbakov et al., 2013). Under-predictions always lead to better results than over-predictions because for under-predictions the percentage error cannot exceed 100% (Tofallis, 2015). Since a comparison will be made of both models, also the logarithmic error measure SSE is introduced. This error measure provides an opposite effect: it penalises an under-prediction more than an over-prediction of the fatigue life. If a difference is seen between the models based on the SSE and the percentage errors, the models should be analysed more closely to judge which one results in more accurate predictions. The SSE is defined as

$$\mathrm{SSE} = \sum_{i=1}^{n} \left(\log\left(T_i\right) - \log\left(M_i\right) \right)^2. \tag{4.9}$$

A few additional remarks must be made before evaluating the models. Firstly, only fatigue life predictions are compared for the stress levels corresponding to experimental datapoints. This also implies that no comparison of the static strength prediction occurs. Secondly, in order to provide a forthright comparison of both models, the model by Kawai and Koizumi (2007) was slightly adapted by applying a LSPR method to fit Equation 3.4 rather than 'visual fitting' as originally employed by Kawai and Koizumi (2007) (Appendix A). This ensures that only the effect of a changing input dataset is compared. Moreover, the determination of σ_B for the two-segment CLD model was kept similar to the manner described by Kawai and Koizumi (2007). The last made remark relates to the employed errors; it is of importance to recognise that their values do not provide a decision on whether or not predictions made by each model are accurate. They merely provide an indication on the performance of the models with respect to one another. Moreover, note that it is only an indication; all error measures are biased and should only be evaluated in correspondence with the presented S-N curve figures.

4.2.2 $[45/90/-45/0]_{2S}$

The first laminate used for validation is a carbon-epoxy (T800H/3631) laminate with lay-up $[45/90/\text{-}45/0]_{2S}$ for which the experimental data was presented by Kawai and Koizumi (2007). The reader is referred to the corresponding paper for details on manufacturing and testing. The experimental data has also been included in Appendix D. Note that the dataset used for input and validation are limited in size; the smallest datasets corresponds to $R = \chi$ and consists of five fatigue life datapoints. The other three datasets ($R = 0.1$, 0.5, and -1) each contain six datapoints. A discussion on the risks related to small-sized datasets was provided in Chapter 2 and should be taken into account when assessing the provided evaluation. The focus in this subsection lies on the S-N curve and CLD predictions made using the proposed model, as well as its predictive accuracy compared to that of the two-segment CLD.

The critical stress ratio χ was found to equal -0.68. For the model proposed in this work, the critical S-N curve for $R = \chi$ was predicted using either input fatigue life data at $R = 0.1$ or -1 and Equation 3.4 was fitted to the obtained critical datapoints. For the two-segment anisomorphic CLD, Equation 3.4 was fitted directly to the experimental fatigue life datapoints. The values for the fitting parameters for both models are presented in Table 4.1.

Table 4.1: Model fitting parameters for the S-N curve describing the fatigue life under the critical R-ratio χ, determined using different input datasets (i.e., $R = 0.1$ and $R = -1$).

Input R-ratio	K_χ	a	n
$R = 0.1$	1.39	0.018	13.58
$R =$ -1	0.024	0.22	9.02
$R = \chi$	0.0084	0.27	9.14

The predicted CLDs by the proposed model are shown in Figure 4.3a and 4.3b when using the fatigue life datasets for $R = 0.1$ and -1 as input, respectively. Small differences are seen in the predicted CLDs. For example, when $R =$ -1 is used as input, fatigue lives are over-predicted for most load cases, while both over- and under-predictions are seen when $R = 0.1$ is used as input. Especially a large variation is seen in the predicted CLLs corresponding to $2N_f = 10^3$ and $2N_f = 10^4$: the predicted CLLs by means of $R = 0.1$ input data show lower stresses and are less accurate than those obtained using the $R =$ -1 dataset.

Next, the predicted S-N curves for different R-ratios will be discussed in more detail. The S-N curves, predicted using both models, are presented in Figure 4.4 for a) $R = 0.5$, b) $R = 0.1$, c) $R =$ -1, and d) $R = \chi =$ -0.68. In addition, the best-fit S-N curve (Equation 3.4) to the test dataset is shown by means of a dashed line. The error measures were determined for each predicted S-N curve and are included in Table 4.2.

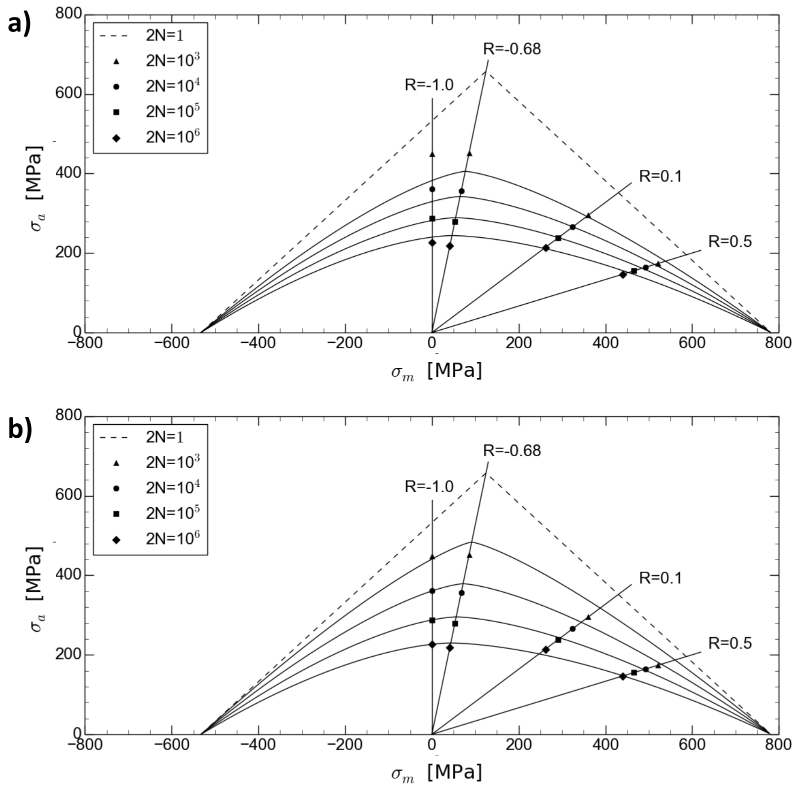

Figure 4.3: Constant fatigue life diagram for $[45/90/-45/0]_{2S}$ carbon-epoxy laminate, obtained using the proposed model with a) $R = 0.1$ and b) $R = -1.0$ fatigue life data as input.

Evaluating the results, it can be concluded that fatigue life predictions for $R = 0.5$ and 0.1 by means of the proposed model are slightly less accurate than the original two-segment CLD model. Yet, all predicted curves are in vicinity of the experimental data. The S-N curve predictions for $R = 0.5$ are similar by all models, showing a slight tendency to over-prediction. The predicted curves by $R = 0.1$ and χ are indicating a similar trend for $2N_f < 10^4$ but deviate for higher fatigue cycles; $R = 0.1$ predicts a less fatigue sensitive behaviour than $R = \chi$ but remains closer to the best-fit curve. $R =$ -1 shows larger over-predictions for lower values of N_f, which is also penalised by the error measures, as seen in Table 4.2. However, for higher fatigue lives, the curve intersects the best-fit curve and predicts lower fatigue lives. Evaluating Figure 4.4c for $R =$ -1, the S-N curve predictions by $R = \chi$ and 0.1 intersect one another at approximately $2N_f = 3 \cdot 10^4$. For lower fatigue cycle values, $R = \chi$ provides closer predictions, while $R = 0.1$ provides better predictions for higher fatigue cycles. From Table 4.2, it is clear that the bias for $R = 0.1$ is more than six times smaller than $R = \chi$. This effect can also be seen in Figure 4.4c in the predicted S-N curves: while the curve by $R = \chi$ underpredicts the fatigue life for all scales, the curve by $R = 0.1$ shows both under- and over-predictions, intersects the best-fit curve, and is in closer vicinity to the experimental data.

Table 4.2: Error metrics for the fatigue life prediction of $[45/90/-45/0]_{2S}$ by means of the proposed (input of $R = 0.1$ and $R = -1.0$) and two-segment anisomorphic CLD.

Input R-ratio	MAPE [%]	MNB [%]	RMSPE [%]	SSE [-]
	R=0.5			
$R = 0.1$	330.85	330.85	344.7	12.6
$R =$ -1	423.1	423.1	534.27	15.16
$R = \chi$	113.3	100.7	150.5	3.93
	R=0.1			
$R =$ -1	113.3	108.9	141.4	3.76
$R = \chi$	26.5	-9.86	31.4	1.02
	R=-1.0			
$R = 0.1$	66.8	7.33	78.2	5.06
$R = \chi$	45.4	-45.4	45.9	2.35
	R=χ			
$R =$ -1	99.86	99.86	100.0	2.40
$R = 0.1$	91.2	48.50	142.7	3.09

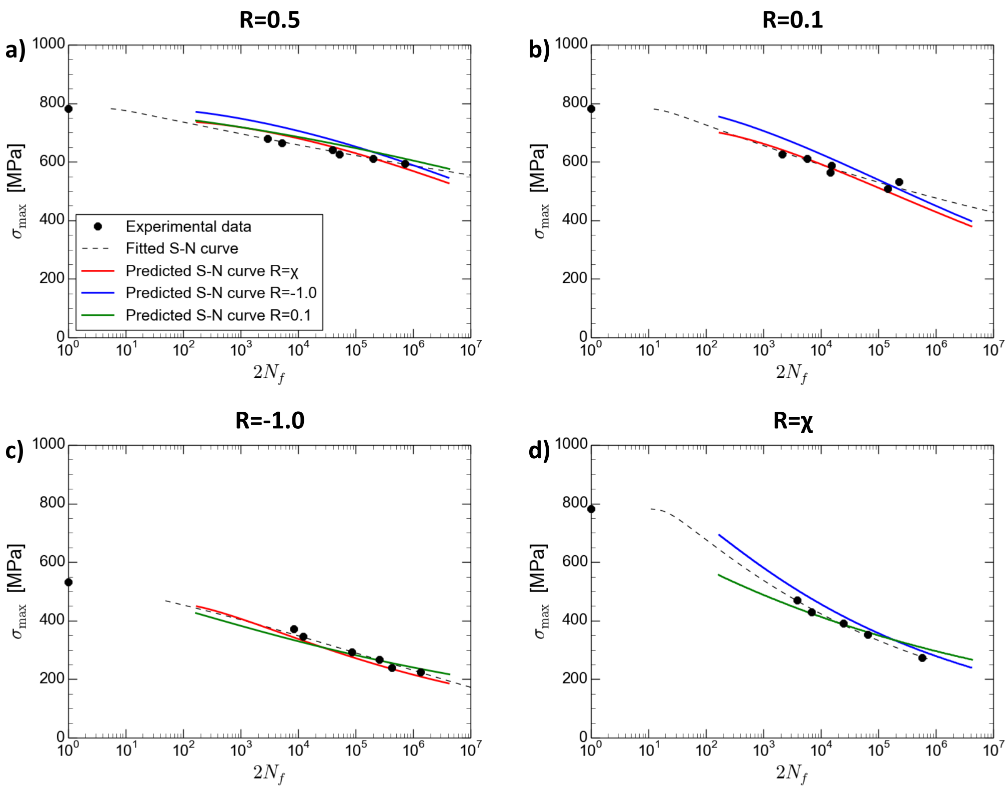

Figure 4.4: Fatigue life predictions for $[45/90/-45/0]_{2S}$ by the proposed model (input $R = 0.1$ or $R = -1.0$) and the two-segment CLD (input $R = \chi$). In addition, experimentally obtained fatigue lives are depicted. Fitted and predicted S-N curves are shown for a) $R = 0.5$, b) $R = 0.1$, c) $R = -1.0$, and d) $R = \chi$. The legend is the same for all figures.

4.2.3 $[0/60/-60]_{2S}$

The carbon-epoxy (T800H/3631) laminate with lay-up $[0/60/\text{-}60]_{2S}$ can be used to validate the proposed model. Experimental test results for this laminate were presented by Kawai and Koizumi (2007) and the reader is referred to the corresponding paper for details on manufacturing and testing. The employed test datapoints have been included in Appendix D. Note that the employed fatigue life datasets are limited with the dataset corresponding to R = -1 consisting of five test results (including 1 run-out) and the datasets for the other R-ratios consisting of six datapoints. This can influence the conclusions made on the predictive accuracy of the models in this subsection.

The critical R-ratio χ is -0.53 with UTS= 880.5 MPa and UCS= -465.1 MPa. The model fitting parameters for Equation 3.4, fitted to the predicted $R = \chi$ fatigue life datapoints using the model proposed in this chapter, are presented in Table 4.3. The fitting parameters are shown for both cases: when R = 0.1 and when R = -1 fatigue life data is used as input. In addition, the values of the fitting parameters are included when fitting Equation 3.4 directly to experimental datapoints obtained at $R = \chi$.

Table 4.3: Model fitting parameters for the S-N curve describing the fatigue life under the critical R-ratio χ, determined using different input datasets (i.e., $R = 0.1$ and $R = -1$).

Input R-ratio	$\mathbf{K}_\chi$	**a**	**n**
$R = 0.1$	0.0042	0.30	13.27
R = -1	$5.34 \cdot 10^{-5}$	0.51	3.67
$R = \chi$	0.0019	0.34	9.88

The predicted CLDs by the proposed model are presented in Figure 4.5a and 4.5b when $R = 0.1$ and -1 data is used as input, respectively. Datapoints representing fatigue lives for different R-ratios, derived by fitting an S-N curve expression through the experimental dataset, have also been included in the CLD. Small differences are seen between the two CLDs: where the CLD in Figure 4.5a shows equally spaced CLLs, the CLD in Figure 4.5b indicates a large LCF plateau, followed by a rapid decrease in stress for higher N_f values. Next, the CLDs can be used to predict S-N curves for different R-ratios, as discussed next. The S-N curves are also predicted using the two-segment anisomorphic model, of which the CLD is presented by Kawai and Koizumi (2007), and a comparison between both models is provided.

The S-N curve fitting to the $R = 0.1$ fatigue life dataset initially posed challenges caused by an outlier. This outlier, i.e. ($\sigma_{\max}$, $2N_f$)=(748.5 MPa, 1818), greatly influenced the fitted curve as shown in Figure 4.6. Consequently, this also impacted CLD and fatigue life predictions by the proposed model. An improved fitting is presented in Figure 4.7b, of which the fitting parameters have been included in Table 4.3. Note that the improved fitting was employed for the previous presented CLD prediction in Figure 4.5a.

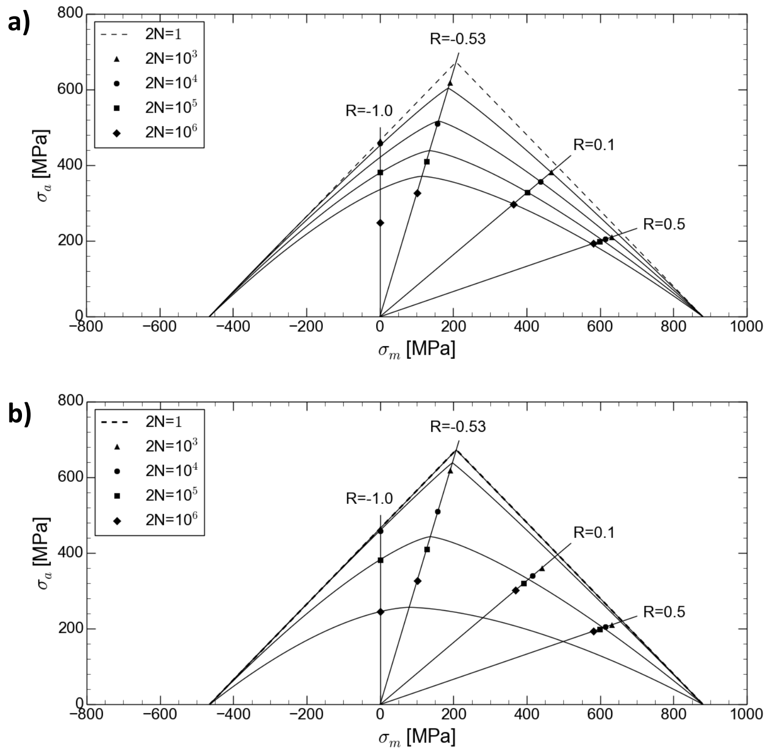

Figure 4.5: Constant fatigue life diagram for $[0/60/-60]_{2S}$ carbon-epoxy laminate, obtained using the proposed model with a) $R = 0.1$ and b) $R = -1.0$ fatigue life data as input.

Figure 4.7 presents the predicted S-N curve for a) $R = 0.5$, b) $R = 0.1$, c) $R =$ -1, and d) $R = \chi =$ -0.53 by the model proposed in this work and the two-segment anisomorphic CLD. The corresponding error measures are determined for each predicted S-N curve and included in Table 4.4. Instantly, the shape of the predicted S-N curves by $R =$ -1 stands out. It is different from the other S-N curves, both predicted and fitted, and the predictions are less accurate than those obtained using $R = 0.1$ and $R = \chi$. This effect is caused by the $R =$ -1 dataset from which these predictions where derived. As seen in Figure 4.7c, four datapoints are concentrated in one fatigue life region and one run-out is present. This leads to a best-fit S-N curve with a large LCF plateau followed by a large fatigue life sensitivity. Employing the $R =$ -1 dataset leads to an extrapolation of the predictions to lower and higher fatigue lives of which the accuracy is not guaranteed by the proposed model. It is expected that when additional fatigue life tests are performed at $R =$ -1 for different stress levels, thereby obtaining an input dataset describing a larger fatigue life range, improved prediction results will be acquired.

Noticeable in Table 4.4 are the error measures for the $R = 0.1$ fatigue life predictions which indicate a slightly better prediction when $R =$ -1 is used as input rather than $R = \chi$. When evaluating Figure 4.7b, one would expect a better performance by $R = \chi$.

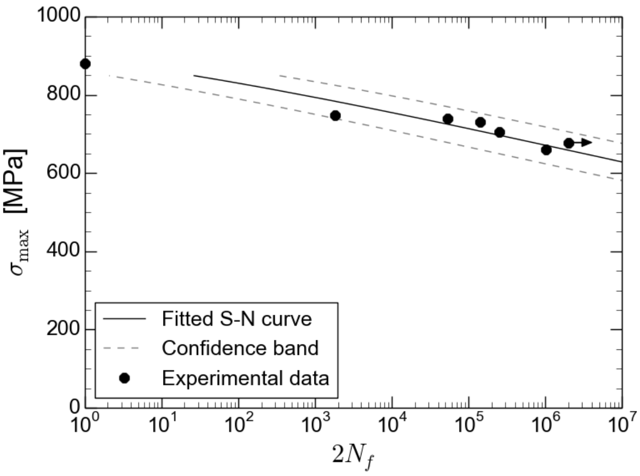

Figure 4.6: Fitted S-N curve to $R = 0.1$ experimental validation data containing outlier ($\sigma_{\max}$, $2N_f$)=(748.5 MPa, 1818), including experimental validation data and a 90% confidence band.

The conclusion based merely on the error measure is caused by the validation dataset of $R = 0.1$. The $R = 0.1$ dataset consists of applied stress levels that are in close range of one another, only the corresponding fatigue lives describe a slightly wider range but lack in values for $2N_f < 5 \cdot 10^4$. Remember that the error measures are calculated by evaluating the difference in fatigue life on each stress level of the dataset. In the applied stress range, both predicted S-N curves are in vicinity of one another and the best-fit curve. This results in low values of the error measures and a conclusion that $R = 0.1$ results in better predictions. Evaluating Figure 4.7b, a different conclusion should be drawn. This again demonstrates the importance of a good and wide-ranged experimental dataset, not only those used as input but also for those used for validation purposes.

Table 4.4: Error metrics for the fatigue life prediction of $[0/60/-60]_{2S}$ by means of the proposed model (input of $R = 0.1$ and $R = -1.0$) and two-segment anisomorphic CLD.

Input R-ratio	MAPE	MNB	RMSPE	SSE
	R=0.5			
$R = 0.1$	448.3	433.7	611.7	13.04
$R =$ -1	1813	1774	2884	32.95
$R = \chi$	340.1	292.6	487.8	12.32
	R=0.1			
$R =$ -1	37.98	-22.24	46.65	2.82
$R = \chi$	57.57	-57.57	58.53	3.50
	R=-1.0			
$R = 0.1$	96.70	-8.23	108.6	9.07
$R = \chi$	60.70	-60.70	68.67	8.85
	R=χ			
$R =$ -1	307.6	289.3	448.6	11.29
$R = 0.1$	156.5	153.6	219.0	5.60

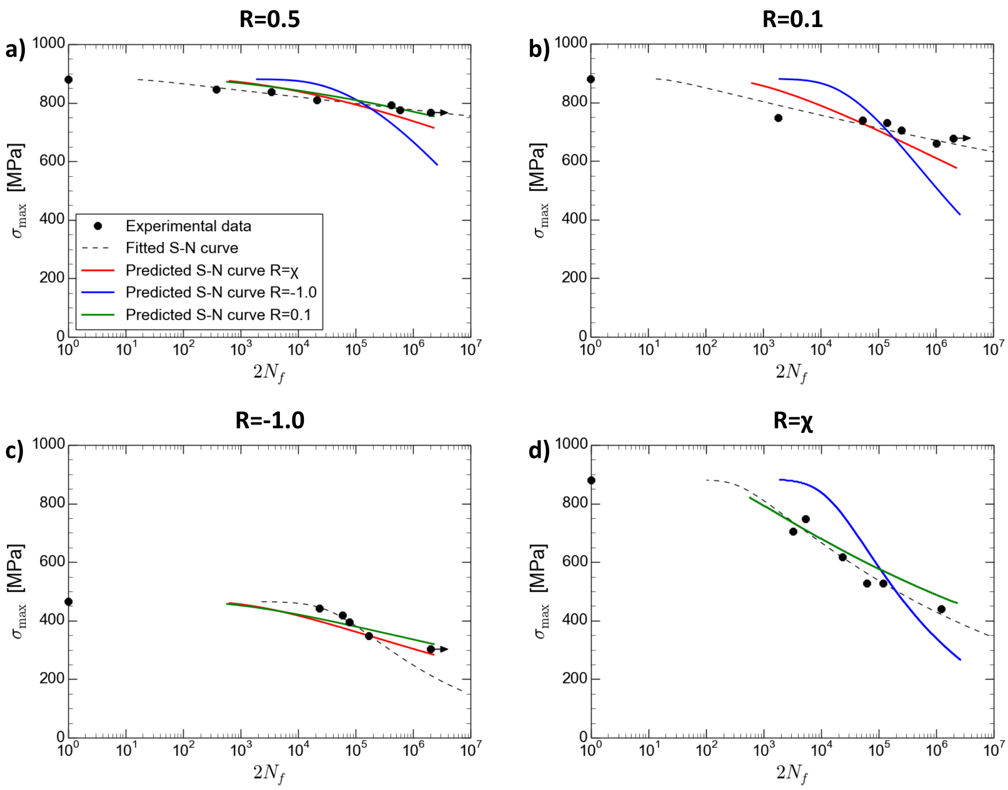

Figure 4.7: Fatigue life predictions for $[0/60/-60]_{2S}$ by the proposed model (input $R = 0.1$ or $R = -1.0$) and the two-segment CLD (input $R = \chi$). In addition, experimentally obtained fatigue lives are depicted. Fitted and predicted S-N curves are shown for a) $R = 0.5$, b) $R = 0.1$, c) $R = -1.0$, and d) $R = \chi$. The legend is the same for all figures.

4.2.4 $[0/90]_{3S}$

The third laminate used for validation of the proposed model is a carbon-epoxy (T800H/2500) laminate with a cross-ply lay-up $[0/90]_{3S}$ of which the experimental test results for this laminate were presented by Kawai and Koizumi (2007). The datasets are included in Appendix D. The datasets for each R-ratio are limited in size. The smallest dataset corresponds $R = 0.1$ and consists of only two datapoints while the largest available dataset corresponds to $R = \chi$ and contains six datapoints. Except for $R = \chi$, datasets do not contain a sufficient number of test results considering the recommendations by ASTM (1980 (2015)) (Chapter 2). Conclusions based on the validation provided in this subsection are only preliminary and it is recommended to include additional test data. Yet, the evaluation is performed using this laminate to allow for a comparison with the two-segment anisomorphic model.

The critical stress ratio χ equals -0.44 with UTS = 1414.1 MPa and UCS = -618.0 MPa. Note that UTS and UCS were determined by Kawai and Koizumi (2007) using only one specimen for each test. For more reliable results, it is recommended to perform additional static strength tests. Equation 3.4 is fitted to the experimental data and the predicted fatigue lives for $R = \chi$, for which the fitting parameters are presented in Table 4.5.

Table 4.5: Model fitting parameters for the S-N curve describing the fatigue life under the critical R-ratio χ, determined using different input datasets (i.e., $R = 0.1$ and $R = -1$).

Input R-ratio	K_χ	a	n
$R = 0.1$	0.12	0.13	10.91
$R =$ -1	2.29	$1.0 \cdot 10^{-6}$	14.49
$R = \chi$	1.27	0.022	12.97

The CLLs, predicted using fatigue life data at $R = 0.1$ or $R =$ -1 as input to the model presented in this chapter, are shown in Figure 4.8a and 4.8b, respectively. In addition, fatigue lives derived from S-N curves fitted through the experimental datasets have been included. For both CLDs, it is seen that the model predicts fatigue lives similar to the experimental data and between the two CLDs only minimal differences can be found. The CLD predicted using the two-segment anisomorphic model has been presented by Kawai and Koizumi (2007). Next, the S-N curve predictions for different R-ratios derived from the CLDs are compared with experimental test results.

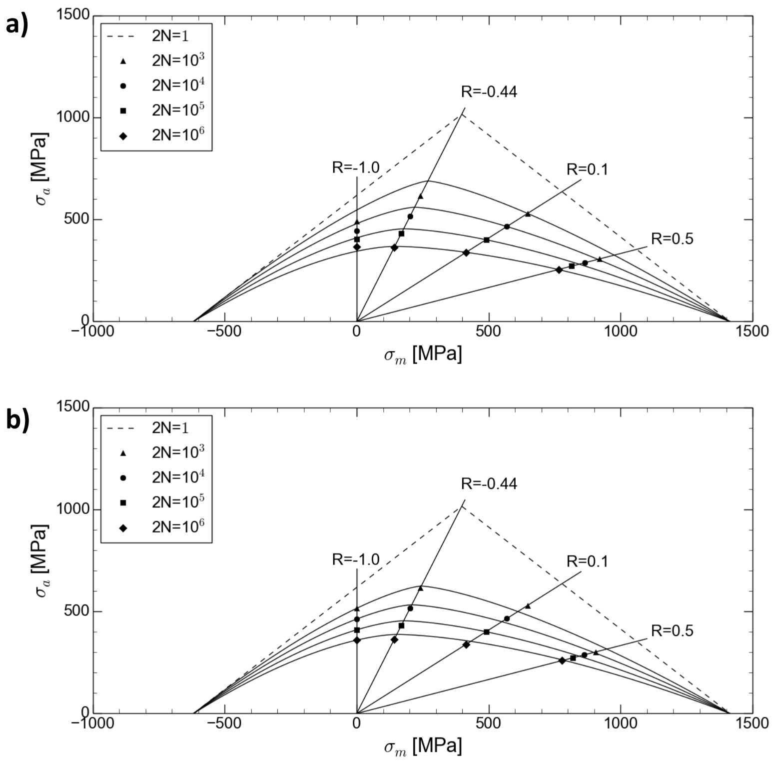

Figure 4.8: Constant fatigue life diagram for $[0/90]_{3S}$ carbon-epoxy laminate, obtained using the proposed model with a) $R = 0.1$ and b) $R = -1.0$ fatigue life data as input.

Fatigue life predictions for the $[0/90]_{3S}$-laminate are shown in Figure 4.9. The S-N curves are predicted for four R-ratios, namely a) R = 0.5, b) R = 0.1, c) R = -1, and d) $R = \chi$ = -0.44, using three different R-ratios as input, i.e. $R = \chi$, R = 0.1, and R = -1. In Table 4.6, the corresponding error measures are presented. In Figure 4.9a) it is seen that the S-N curves for R = 0.5 all provide predictions in close correspondence with the two experimental datapoints corresponding to fatigue life cycles in the range of $10^5 < 2N_f < 10^6$ while for lower fatigue lives an over-prediction occurs. For $R = 0.1$, the S-N curve predictions by R = -1 are in closer proximity to the best-fit curve than $R = \chi$, as also confirmed by the error measures in Table 4.6. The predicted S-N curves for R = -1 (Figure 4.9c) show small differences and are in proximity of the best-fit curve to the validation dataset. Table 4.6 indicates a slightly better predictive performance by R = 0.1, most likely caused by the more accurate prediction of the three datapoints in the range: $3 \cdot 10^5 < 2N_f < 8 \cdot 10^5$.

Table 4.6: Error metrics for the fatigue life prediction of $[0/90]_{3S}$ by means of the proposed model (input of $R = 0.1$ and $R = -1.0$) and two-segment anisomorphic CLD.

Input R-ratio	MAPE	MNB	RMSPE	SSE
	R=0.5			
$R = 0.1$	749.6	749.6	1057	15.34
$R =$ -1	347.5	347.5	429.8	8.50
$R = \chi$	223.1	207.0	302.4	5.56
	R=0.1			
$R =$ -1	37.16	-21.57	42.96	0.80
$R = \chi$	56.14	-56.14	57.45	1.66
	R=-1.0			
$R = 0.1$	63.95	5.28	78.28	1.76
$R = \chi$	48.28	-42.88	53.34	2.85
	R=χ			
$R = 0.1$	150.5	150.5	184.1	5.13
$R =$ -1	88.81	88.81	105.1	2.69

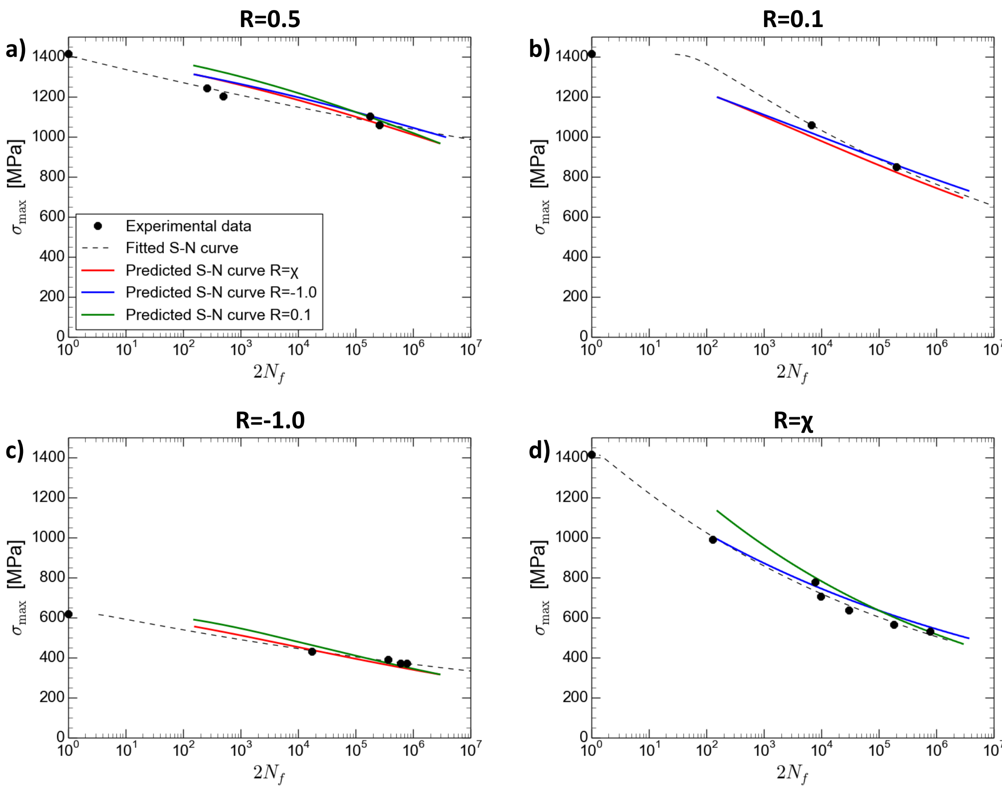

Figure 4.9: Fatigue life predictions for $[0/90]_{3S}$ by the proposed model (input $R = 0.1$ or $R = -1.0$) and the two-segment CLD (input $R = \chi$). In addition, experimentally obtained fatigue lives are depicted. Fitted and predicted S-N curves are shown for a) $R = 0.5$, b) $R = 0.1$, c) $R = -1.0$, and d) $R = \chi$. The legend is the same for all figures.

4.2.5 Conclusion

Fatigue life predictions made using the model proposed in this chapter for three carbon-epoxy laminates found in literature, characterised by UTS>|UCS|, have been compared with predictions made using the two-segment anisomorphic CLD by Kawai and Koizumi (2007). Based on the presented evaluations, it can be concluded that the fatigue life prediction model proposed in this chapter is capable of providing a similar accuracy as the two-segment anisomorphic CLD model by Kawai and Koizumi (2007) for the considered carbon-epoxy laminates. Moreover, the predictions for the evaluated laminates lie in the same order of magnitude as the experimental fatigue life data.

Evaluating the results in detail, a general trend can be discovered for the prediction of $R = 0.5$ loading. This loading ratio is always slightly over-predicted, independent of which model is employed. For the other three considered R-ratios, no clear trend can be identified among the models and S-N curve predictions are always centrally located through the experimental data. Note that these conclusions are based on experimental datasets of which some consisted of less datapoints than the prescribed minimum of six by (Chapter 2), which might have influenced the results significantly, as seen for the $[0/60/\text{-}60]_{2S}$-laminate. Therefore, the analysis provided in this subsection can only be seen as preliminary and it is strongly recommended to perform additional evaluations of the predictive accuracy by reviewing additional laminates as well as larger datasets. Only in such a way, a reliable conclusion on the predictive accuracy of the proposed model with respect to the two-segment anisomorphic model can be obtained.

4.3 Validation using an Experimental Campaign

In order to further validate the proposed model, an experimental campaign was designed and executed. Several carbon-epoxy specimens of the same lay-up were manufactured and tested to assess the predictive accuracy of the model. The first subsection concisely outlines the main steps taken in the experimental campaign. This is followed by a subsection providing an evaluation of the results using both the two-segment anisomorphic and the adapted CLD model.

4.3.1 Experimental Campaign: Process

This subsection outlines the steps taken during the experimental campaign; starting at laminate manufacturing up to the testing procedures that were followed.

Material

The material used for manufacturing of the specimens is a Hexcel *AS4/8552* UD prepreg ply. The *AS4* fibres are continuous carbon fibres while the *8552* resin is an amine cured epoxy resin. Even though the material had passed its expiration date at the time of manufacturing, its tackiness was judged as sufficient for usage.

Laminate and specimen manufacturing

A laminate with an average thickness of 2.285 mm and a $[90/0/90]_{2S}$ lay-up was manufactured from the $AS4/8552$ prepreg. A hand lay-up was conducted and a debulking procedure was performed after every three plies. After lay-up, the laminate was cured in an autoclave following a cycle recommended by the manufacturer. The curing cycle has been included in Appendix B.

After curing, the laminate was roughly cut using a Carat liquid-cooled diamond saw, followed by more precise cutting using a Proth Industrial liquid-cooled saw to obtain the rectangular specimens. Specimens of two different nominal sizes were cut. On the one hand, for the static strength and T-T tests, specimens with a length of 250 mm and a width of 25 mm were cut according to ASTM standard D3039/D3039M and D3479/3479M (ASTM, 1971 (2017)) (ASTM, 1976 (2012)). On the other hand, for the compressive strength and T-C tests, specimens with a length of 140 mm and a width of 12 mm were cut following ASTM standard D6641/D6641M (ASTM, 2001).[1] The specimens for compressive strength and T-C tests are smaller in order to reduce the chance of buckling during compressive loads because it was decided to not include an ABD during testing since this will likely alter the test results (Chapter 3). To avoid buckling during compressive loading, ASTM standard D6641/D6641M (ASTM, 2001) recommends a gauge length of 12 mm. However, due to limitations of the fatigue testing machine, the minimum gauge length during testing equals 17 mm. Any specimen showing buckling failure was omitted from the final results. An overview of the specimen geometry and number of specimens for each type of test is shown in Table 4.7. Note that the number of specimens depends on the considered R-ratios. The selection of R-ratios for testing is discussed in more detail in the paragraphs on the testing procedure.

After cutting of the specimens, their sizes were measured and inspected for any damage visible to the naked-eye. In addition, paper tabs with a thickness of approximately 0.15 mm were glued on both ends of each specimen for an increased clamping grip during testing. The adhesive used for this purpose is cyanoacrylate (also known as super glue).

Table 4.7: Performed tests with corresponding geometry and number of tests.

Test type	Number of tests	Specimen geometry
Tensile strength test	4	250x25 mm
Compressive strength test	6	140x12 mm
Fatigue life test (T-T): $R = 0.1$	8	250x25 mm
Fatigue life test (T-C): $R = -1.0$	22	140x12 mm
Fatigue life test (T-C): $R = \chi$	14	140x12 mm

[1] A more recent version of this standard (ASTM, 2001 (2016)) suggests a nominal width and gauge length of 13 mm. However, a cutting plate for the Proth Industrial tool was available that was based on the previous version of the standard. Due to the small difference in width, it was chosen to follow the earlier version of the standard rather than the most recent version.

Testing Procedure

Two types of tests were performed during the experimental campaign: 1) static strength and 2) fatigue life tests. All tests were performed using an in-house developed 60kN fatigue machine with hydraulic grip. No attempt was made to control temperature or humidity during testing. All tests were performed at room temperature (~ 23°C).

Tensile and compressive static strength tests were displacement controlled at a nominal rate of 2.0 and 1.3 mm/min following ASTM standard D3039/D3039M (ASTM, 1971 (2017)) and D6641/D6641M (ASTM, 2001 (2016)), respectively. The tensile and compressive tests were repeated for four and six samples, respectively.

Contrary to the static strength tests, fatigue life tests were load controlled. Testing occurred at three R-ratios: 0.1, -1.0, and χ and at a testing frequency of 10 Hz. Data for the first two R-ratios is needed as input to the model. The latter R-ratio can be used for validation purposes of the CLD and S-N curve predictions, as well as a comparison with the two-segment anisomorphic model. Tests were performed at several stress levels for each R-ratio. Testing at each stress level was repeated with up to four specimens to guarantee an appropriate sample and representative description of the fatigue behaviour for the considered laminate. In such manner, the effect of a possible outlier or run-out on the final S-N curve can be reduced. Note that small variations in in the applied stress might exist between specimens at the same level due to the fact that the testing machine is load controlled and minimal variations in geometry exist between specimens.

Fatigue life tests were terminated at $N_f = 10^6$ cycles. After reaching one million cycles, tests are stopped and the specimen is considered as a run-out. Fatigue life testing is only performed under T-T and T-C loading conditions and not under C-C loading. C-C loading was omitted from testing based on issues related to these type of tests, as discussed in more detail in Chapter 2.

The total number of tests performed at each R-ratio is summarised in Table 4.7. Note that for $R = 0.1$, a smaller number of fatigue life tests was performed in comparison with the other two R-ratios. This is a result from issues originating during testing. For example, several specimens failed in the clamp region or failed prematurely. This led to an unexpected large number of censored test results and, consequently, a lower number of accepted test results for S-N curve establishment. Due to time constraints and machine availability, it was not possible to perform additional fatigue life tests for a more representative sample of the fatigue behaviour at $R = 0.1$. However, the minimum number of tests for one S-N curve, as prescribed by ASTM (1980 (2015)), was reached. On the other hand, for $R = -1$, a large number of fatigue life tests were performed due to testing at several frequencies other than 10 Hz. Note that these test results have been included in Appendix C but are not considered in the evaluation of the fatigue life prediction models.

4.3.2 Experimental Campaign: Results

The results of the experimental campaign are discussed in this subsection. First, the static strength test results are presented for both the tensile and compressive tests. This is followed by fatigue life test results which are presented by means of S-N curves.

Static Strength Tests

Four static tensile tests have been performed to determine UTS, whose value is, on average, 684.6 MPa. Furthermore, six compressive static tests have been performed to determine UCS. On average, UCS equals 411.5 MPa. Table 4.8 provides an overview of the static strength test results, as well as the mean failure stress value, standard deviation, and coefficient of variation, where the latter two provide an indication of the uniformity of both specimens and testing process.

Table 4.8: Tensile and compressive static strength test results.

Tensile Static Strength		Compressive Static Strength	
Specimen	Failure Stress [MPa]	Specimen	Failure Stress [MPa]
S03	662.4	S36	405.1
S04	672.5	S39	402.5
S11	688.0	S43	411.5
S13	715.5	S44	414.9
		S45	422.8
		S46	412.4
Mean Failure Stress	684.6 MPa	Mean Failure Stress	411.5 MPa
Sample Standard Deviation	23.14 MPa	Sample standard Deviation	7.24 MPa
Coefficient of Variation	3.38%	Coefficient of Variation	1.76%

Fatigue Life Tests

Fatigue life tests have been performed at three R-ratios, namely at one T-T type loading (i.e., $R = 0.1$), and two T-C type loadings (i.e., $R = \chi =$ -0.60, and $R =$ -1). The fatigue life test results are presented by means of S-N curves and a CLD. The test data has been included in Appendix C.

The S-N curves for $R = 0.1$, $R = \chi$, and $R =$ -1 are presented in Figure 4.10. Equation 3.4 was fitted to the experimental data to describe the S-N curve. Note that for the $R = 0.1$ data, also two datapoints obtained under $f = 5$ Hz were included to expand the size of the dataset.

The considered laminate shows a large fatigue insensitivity, resulting in large scatter in the obtained fatigue life results, especially for $R = 0.1$. This is as expected based on the results by Nijssen (2010), who showed that larger scatter in fatigue life data is seen for FRPs insensitive to fatigue, as discussed in detail in Chapter 2. The laminate is most

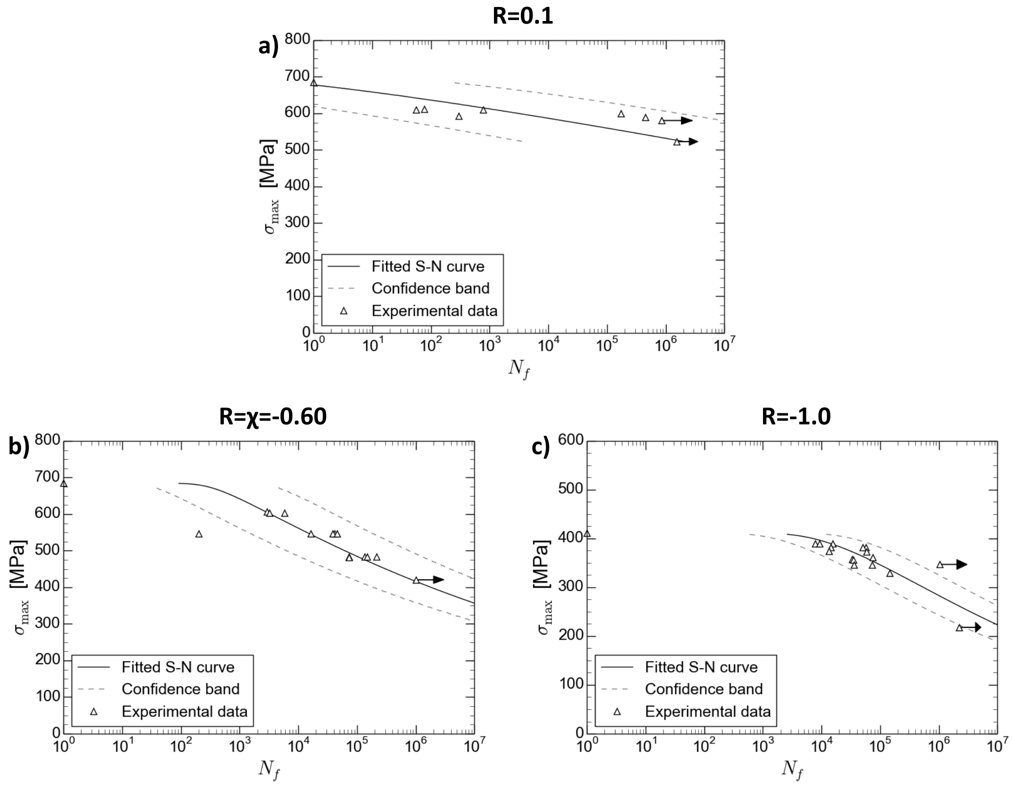

Figure 4.10: Experimental fatigue life data for $R = 0.1$, $\chi = -0.60$, and -1. Thick lines represent the fitted mean S-N curves and the dashed lines represent a 90% confidence band.

sensitive to fatigue loading at an R-ratio of $R = \chi$ while the lowest sensitivity is seen for $R = 0.1$: the S-N curve for $R = 0.1$ describes a rather horizontal linear line while the curve is more steep for $R = \chi$ and $R =$ -1. However, the data for the T-C load types is mostly located in the mid-cycle range while data in the fatigue life scale of $N_f > 10^5$ or LCF is limited. This results in fitted curves showing a large LCF plateau, followed by a more steeply decreasing curve. Preferably, additional tests are performed at higher and lower stress levels to obtain test results in all fatigue life scales. However, due to time constraints and test machine availability, this was not possible in the scope of this work.

All samples under $R =$ -1 loading failed in a compressive failure mode while all samples under $R = 0.1$ failed in a tensile failure mode. For $R = \chi$, the final failure modes were mixed; some specimens showed tensile failure while others showed compressive failure. This can be an indication that a hypothesis made by Kawai and Koizumi (2007) that a failure mode transition occurs at or near $R = \chi$ is true. Moreover, if the latter is true, it is a confirmation of the reliability of the static tensile and compressive tests, which resulted in a good approximation of the critical R-ratio χ. The focus of this thesis is not on the different damage mechanisms seen in fatigue loading and therefore this aspect will not be further discussed in this work

4.3.3 Fatigue life Predictions

Fatigue life data for the carbon-epoxy laminate with lay-up $[90/0/90]_{2S}$ under $R = \chi$ loading, presented in the previous subsection and in Appendix C, was used as input to the two-segment anisomorphic model by Kawai and Koizumi (2007) to predict the fatigue behaviour at $R = 0.1$ and $R =$ -1. Moreover, fatigue life data for $R = 0.1$ and $R =$ -1 was used as input to the model proposed in this chapter to predict $R = \chi$ and $R =$ -1, and $R = 0.1$ and $R =$ -1, respectively. The results are used for a comparison of the predictive accuracy of the two models.

The critical stress ratio for the considered laminate equals $\chi =$ -0.60. For the two-segment anisomorphic model, Equation 3.4 was fitted to the experimental dataset for $R = \chi$ and its model fitting parameters are presented in Table 4.9. The table also shows the model fitting parameters for the predicted critical S-N curve by means of the proposed model with $R = 0.1$ or $R =$ -1 as input.

Table 4.9: Model fitting parameters for the S-N curve describing the fatigue life under the critical R-ratio χ.

Input R-ratio	K_χ	a	n
$R = \chi = -0.60$	0.0020	0.34	14.50
$R = 0.1$	4.92	$1.00 \cdot 10^{6}$	25.70
$R = -1$	$1.59 \cdot 10^{-4}$	0.46	8.05

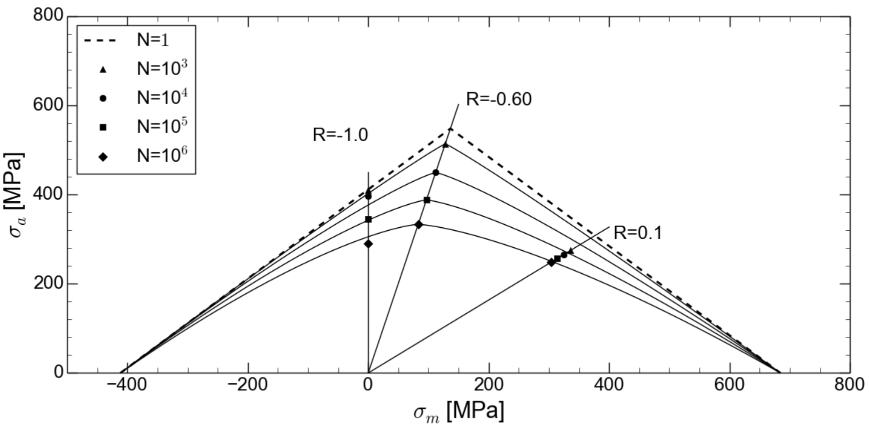

Figure 4.11: Constant fatigue life diagram for $[90/0/90]_{2S}$ carbon-epoxy laminate, obtained using the two-segment anisomorphic model with $R = \chi = -0.60$ fatigue life data as input.

The CLD predicted using the two-segment anisomorphic model is shown in Figure 4.11. It can be seen that the $R = 0.1$ datapoints are located closely together, as expected from the experimental dataset. Moreover, they are located in the predicted CLL range corresponding to $10^5 < N_f < 10^6$, which means that for lower fatigue lives, higher stresses are predicted by the model. For R = -1, an over-prediction is seen for the fatigue lives corresponding to the higher fatigue life scales ($N_f = 10^6$) while an under-prediction is expected for the lower fatigue lives ($N_f = 10^3 \sim 10^4$). For $N_f = 10^5$, the predicted CLL intersects with the fitted datapoint at $R = 0.1$. Based on the obtained CLD, it can be seen that a relative long and flat LCF plateau can be expected for R = -1, as well as a gradual S-N curve slope because the CLLs are located close to the static strength line.

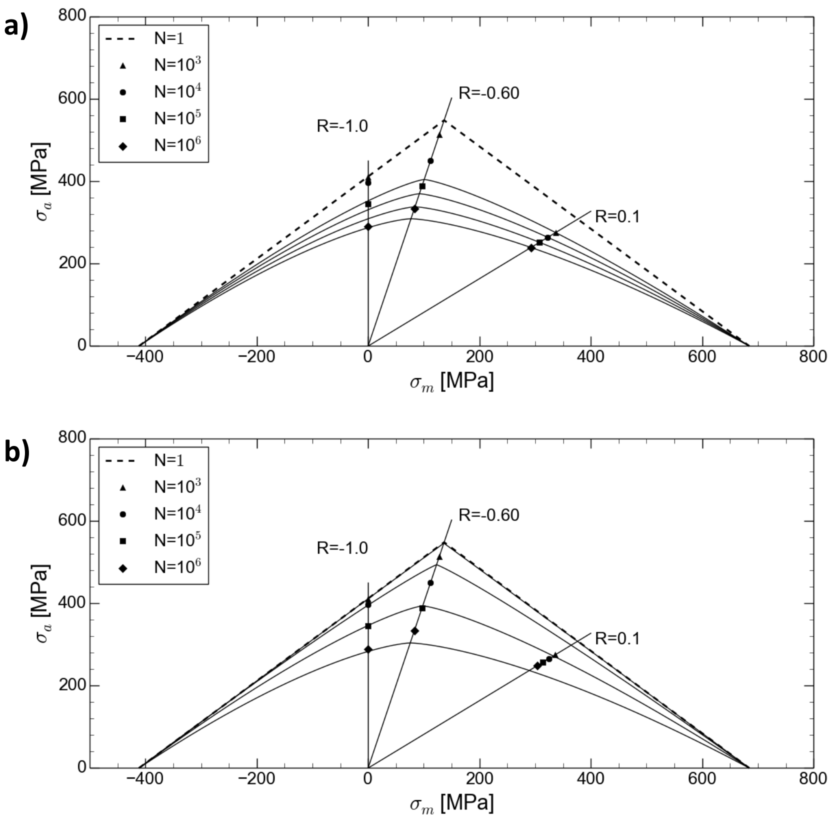

Figure 4.12: Constant fatigue life diagram for $[90/0/90]_{2S}$ carbon-epoxy laminate, obtained using the proposed model with a) $R = 0.1$ and b) $R = -1.0$ fatigue life data as input.

The CLDs, including the predicted CLLs, are shown in Figure 4.12a and 4.12b when using fatigue life data corresponding to $R = 0.1$ and -1 as input to the proposed model, respectively. For the first case, where $R = 0.1$ data is used as input, an under-prediction is seen for $R = \chi$ and R = -1. Only for $N_f = 10^6$, the CLL curve intersects the datapoint at R = -1. The CLD predicted by means of fatigue life data for R = -1, results in a large LCF plateau, visible by means of the CLLs for $N_f = 10^3$ and $N_f = 10^4$ which are close to the static strength line. This results in an over-prediction of the fatigue lives at

$R = \chi$ for the lower fatigue life scales. In addition, an under-prediction is seen for the higher fatigue life values at $R = \chi$. For $R = 0.1$, both under- and over-predictions are seen when $R =$ -1 is used as input to the proposed model, as seen in Figure 4.12b. The datapoints are located closely together while the predicted CLLs show a wider range. The concentration of the validation data for $R = 0.1$ is caused by the input dataset for $R = 0.1$, which showed large scatter for similar stress levels, resulting in an almost linear horizontal curve with low fatigue sensitivity. This affects the estimated fatigue lives for $R = 0.1$ and therefore also the validation dataset used to evaluate the predictive accuracy of the proposed model, as seen in Figure 4.12.

The presented CLDs can be used to derive S-N curve predictions for $R = 0.1$, $R = \chi$, and $R =$ -1. These are shown in Figure 4.13a, 4.13b, and 4.13c, respectively, and the values of the error metrics are included in Table 4.10. Due to the limited size of the experimental campaign, only two curves can be compared for each R-ratio. Moreover, the datasets showed large scatter, which influences the conclusions made in this subsection.

When evaluating Table 4.10 and Figure 4.13, it is instantly clear that all three models seem to have difficulties predicting the fatigue behaviour under different R-ratios. The predicted curve by the two-segment anisomorphic model for $R =$ -1 seems closest to the experimental data, followed by the prediction for $R = \chi$ by the proposed model using $R =$ -1 as input. For the latter case, the error measures in Table 4.10 indicate poor predictions compared to when $R = 0.1$ is used as input. However, one has to keep in mind that the MAPE, MNB, and RMSPE penalise over-predictions more than under-predictions. When $R = 0.1$ is employed as input, the predicted fatigue life is under-predicted, resulting in lower error measures. This is confirmed by the value of the SSE, which indicates improved results when $R =$ -1 is employed. Moreover, note that the error measures are calculated based on all available experimental datapoints, even though this requires an extrapolation of the predictions when $R =$ -1 data is used as input. Improved results will thus be obtained when only interpolation is considered.

The fatigue life for $R =$ -1 is under-predicted when $R = 0.1$ is used as input to the proposed model and the two-segment anisomorphic model will lead to better results. The under-predictions by $R = 0.1$ for $R =$ -1 are likely caused by the nature of the $R = 0.1$ dataset. The predicted S-N curves for $R = 0.1$ are not describing the fatigue behaviour, independent of the used model, as is also confirmed by the error measures. The shape of the S-N curve with respect to the fitted curve seems most similar using the two-segment anisomorphic model but it results in large over-predictions of the higher stress levels. Moreover, the predictions by the proposed model, using $R =$ -1 data as input, are affected by the limited fatigue life scale in the $R =$ -1 dataset.

Overall, based on the results for the carbon-epoxy (AS4/8552) laminate obtained by means of an experimental campaign, no general conclusion can be made on which model results in more accurate predictions with respect to the experimental data. This is mostly caused by the fatigue life datasets used as input and validation, which show large scatter or do not contain datapoints on all fatigue life scales, thereby affecting the made predictions and the obtained predictive accuracy.

Table 4.10: Error metrics for the fatigue life prediction of $[90/0/90]_{2S}$ by means of the proposed model (input of $R = 0.1$ and $R = -1.0$) and two-segment anisomorphic CLD.

Input R-ratio	MAPE	MNB	RMSPE	SSE
	R=0.1			
$R =$ -1	$5.41 \cdot 10^3$	$5.41 \cdot 10^3$	$6.30 \cdot 10^3$	88.98
$R = \chi$	$4.07 \cdot 10^3$	$4.07 \cdot 10^3$	$4.50 \cdot 10^3$	79.52
	R=-1.0			
$R = 0.1$	98.89	-98.89	98.90	432.6
$R = \chi$	50.30	-47.88	55.02	13.00
	R=χ			
$R = 0.1$	98.06	-98.06	98.07	256.8
$R =$ -1	134.7	134.7	167.5	10.09

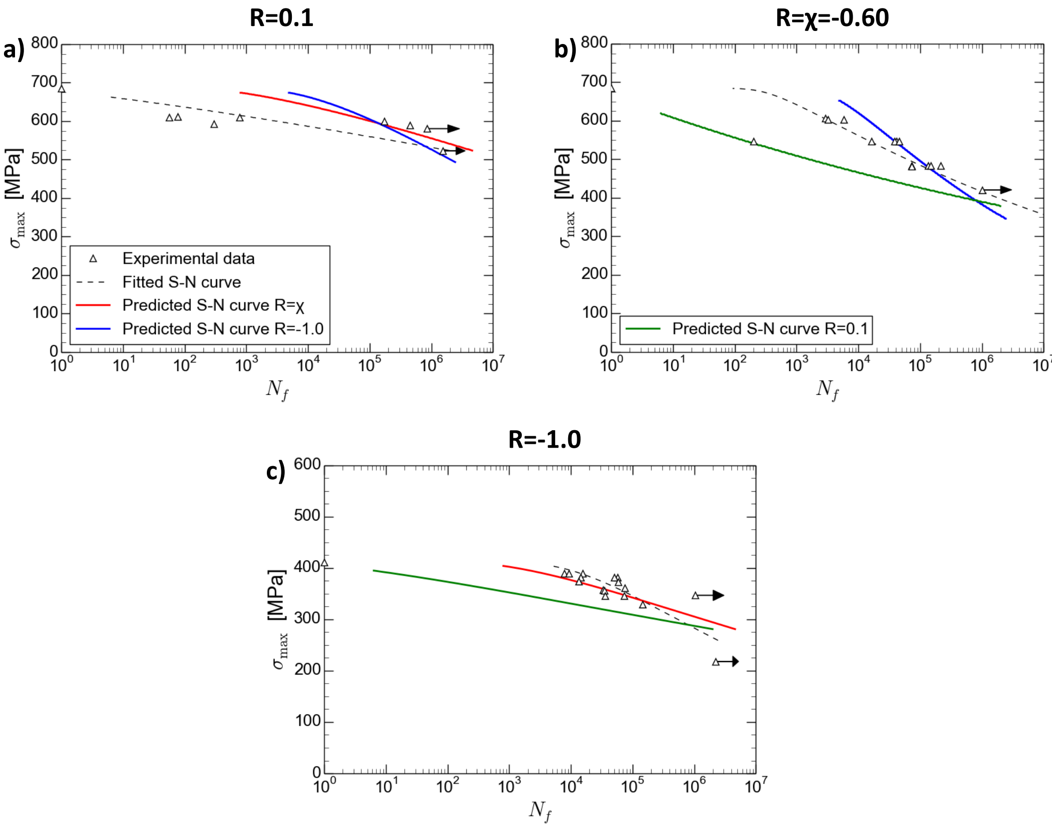

Figure 4.13: Fatigue life predictions for $[90/0/90]_{2S}$ by the proposed model (input $R = 0.1$ or $R = -1.0$) and the two-segment CLD (input $R = \chi$). In addition, experimentally obtained fatigue lives are depicted. Fitted and predicted S-N curves are shown for a) $R = 0.1$, b) $R = -1.0$ and c) $R = \chi$. The legend is the same for all figures.

Chapter 5

Fatigue Life Prediction Model for |UCS|>UTS

The model presented in this chapter is applicable to carbon fibre-reinforced epoxy laminates characterised by |UCS| > UTS. It only requires static strength data in the form of UTS and UCS and fatigue life data at one R-ratio corresponding to either $R = 0.1$ or -1. Similar to the model proposed in Chapter 4, the method does not distinguishes whether fatigue life test data for $R = 0.1$ or -1 is used as input. The same procedure for fatigue life predictions, as outlined in this chapter, can be employed.

The set-up of this chapter is similar to that of Chapter 4, thereby allowing for a straightforward comparison of both models. The first section outlines the proposed model, the steps to be taken for fatigue life prediction and the made assumptions. Each step of the model is discussed, as well as any differences with the three- and four-segment anisomorphic model by Kawai and Murata (2010) and Kawai and Itoh (2014) discussed in Section 3.3 and 3.4, respectively. Section 5.2 provides an evaluation of the predictive accuracy of the presented model compared to that of the anisomorphic models by means of fatigue life datasets for carbon-epoxy laminates found in literature.

5.1 Method

This section presents a fatigue life prediction model for carbon fibre-reinforced epoxy laminates characterised by |UCS|>UTS. First, an overview of the method is given by means of a flowchart and each step is shortly described. Each subsection provides a detailed explanation of one model procedure, as well as the differences with the three- and four-segment anisomorphic model.

The proposed model is based on four main assumptions, which are different from the three- and four-segment anisomorphic models:

1. The fatigue behaviour of carbon-epoxy laminates under CA loading at any R-ratio can be predicted based on the behaviour under fatigue loading at an R-ratio of either $R = 0.1$ or -1.
2. The shape of the CLLs in the right segment is dependent on the ratio between UCS and UTS.
3. The CLLs in the middle segment can be determined using linear interpolation between datapoints on the radials of $R = \chi$ and $R = \pm\infty$ for similar fatigue lives.
4. All CLLs intersect the left radial boundary ($R = \pm\infty$) in the top tenth percentile.

The first assumption is a consequence of a change in the input R-ratio with respect to the three- and four-segment anisomorphic CLD. The source and validity of the second to fourth assumption relates to the definition of the CLLs, which is further discussed in Section 5.1.4.

A flowchart illustrating the methodology of the presented model is shown in Figure 5.1 and each step is concisely described next. For a detailed description of each model step, the reader is referred to the corresponding subsections. An example of the proposed CLD shape is provided in Figure 5.2

1. Static strength test data, in the form of UTS and UCS, is required as input to the model. (Subsection 5.1.1)
2. CA fatigue life tests are performed at either $R = 0.1$ or $R = -1.0$. The R-ratio can be chosen by the user. (Subsection 5.1.1)
3. The critical R-ratio χ can be calculated as the ratio between UCS and UTS.
4. The value of σ_B must be defined in order to determine ψ_χ in the next step. (Subsection 5.1.2)
5. A function describing stress values on the radial segment boundaries (i.e., $R = \chi$ and $R = \pm\infty$) must be defined based on the static strength and fatigue life input data. (Subsection 5.1.5)

   5.1. The critical S-N curve ($R = \chi$) must be determined in order to describe the intersections of the CLLs with the radial.

   5.1.a The stress values (σ_m^χ, σ_a^χ) on the radial $R = \chi$ are calculated using the CLL expressions and fatigue life input data.

   5.1.b A normalised S-N curve $\psi_\chi = f^{-1}(2N_f)$ is fitted to the stress values (σ_m^χ, σ_a^χ) for $R = \chi$ in order to describe the critical S-N curve. (Subsection 5.1.3)

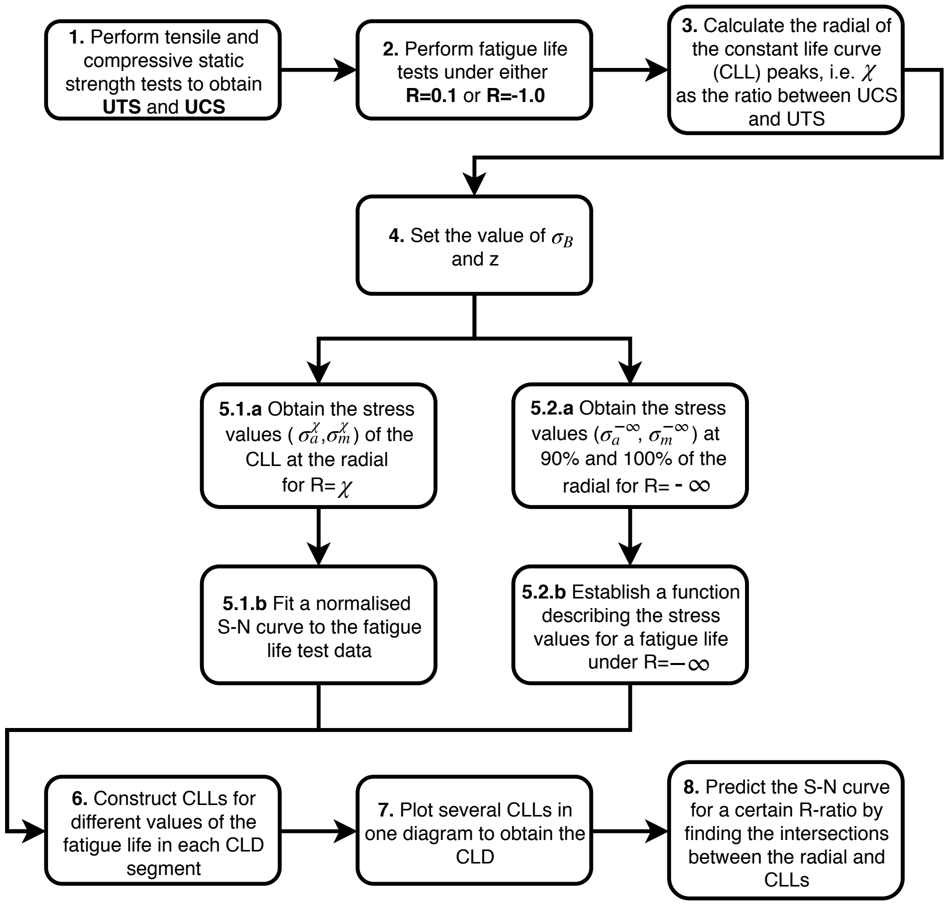

Figure 5.1: Flowchart depicting the proposed model for carbon-epoxy laminates characterised by |UCS|>UTS.

5.2. The S-N curve for $R = \pm\infty$ must be determined in order to describe the intersections of the CLLs with the radial. (Subsection 5.1.5)

5.2.a Stress values ($\sigma_m^{\pm\infty}$, $\sigma_a^{\pm\infty}$) on the radial $R = \pm\infty$ are calculated in order to describe the stress interval in which all CLLs are located. This interval is defined as the upper tenth percentile of the radial.

5.2.b The stress values ($\sigma_m^{\pm\infty}$, $\sigma_a^{\pm\infty}$) are used to obtain a function describing the location of intersection of each CLL with the $R = \pm\infty$ radial.

6. CLLs for different values of the fatigue life N_f can be constructed for each CLD segment using the functions defining the stress values at which the CLLs intersect the two boundary radials (i.e., $R = \chi$ and $R = \pm\infty$). (Subsection 5.1.4)

7. The CLD is obtained by depicting several CLLs for each segment in the same diagram. (Subsection 5.1.6)

8. An S-N curve for a different R-ratio than the input R-ratio can be predicted by determining intersections of the CLLs with the radial corresponding to the R-ratio of interest. (Subsection 5.1.7)

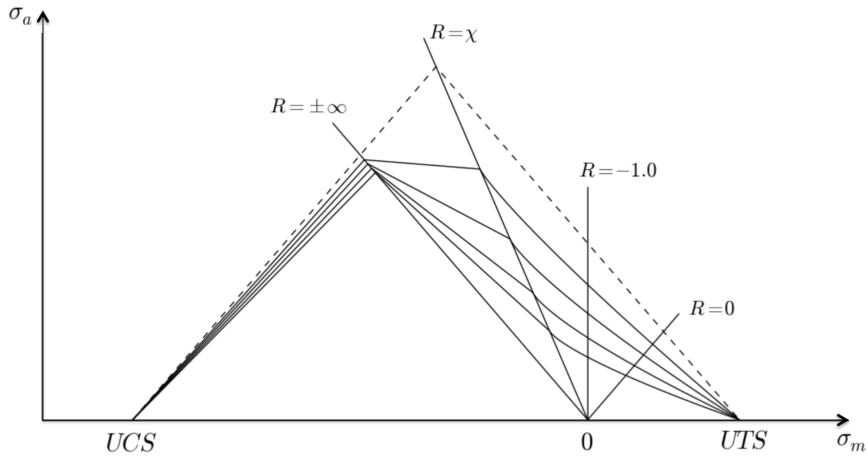

Figure 5.2: Proposed CLD model describing the fatigue behaviour of carbon-epoxy laminates characterised by |UCS|>UTS.

5.1.1 Input Data (Step 1 and 2)

Similar to the model presented in Chapter 4, applicable to laminates showing UTS>|UCS|, the model proposed in this chapter employs static strength data and CA fatigue life data. Test data on both tensile and compressive ultimate static strength is required. In addition, a sufficient number of fatigue life datapoints at either $R = 0.1$ or -1 are needed in the form of the applied CA stresses and numbers of cycles to failure. Note the difference with the three- or four-segment anisomorphic model that require fatigue life datasets for $R = \chi$ and $R = \chi_S$ or $R = \chi$, $R = \chi_L$, and $R = \chi_R$, respectively. Thus, less fatigue life datasets are required, namely one versus two and three, respectively.

5.1.2 Determination of χ and σ_B (Step 3 and 4)

As discussed in Sections 3.3 and 3.4, the CLLs for laminates characterised by |UCS|>UTS no longer show an amplitude stress peak in the vicinity of the $R = \chi$ radial. The method in this chapter adheres to this, as can be seen in Figure 5.2. However, one of the two CLD segment boundaries (between the middle and right segment) has been defined at the $R = \chi$ radial. Therefore, it is required to establish the value of χ, which is defined similar as for previously discussed models (Equation 3.1). Note that no experimental data is required to establish the stress values at this radial; these will be determined in step 5.1 (Subsection 5.1.5).

The value of σ_B must also be defined to establish the fatigue strength ratio ψ, as defined in Equation 3.2. For the laminates considered in this model, where |UCS|>UTS, σ_B is set equal to σ_B =|UCS|. Note that this definition of σ_B is different from that in the anisomorphic models where σ_B is obtained using S-N curve extrapolation to $N_f = 1$.

5.1.3 S-N Curve Expression (Step 5.1.b)

Similar to the method proposed in Chapter 4, an LSPR technique is employed to fit Equation 3.4 to the datapoints. Again, it is not required to fit the function to the input data but only has to be fitted to the critical datapoints for $R = \chi$ (Step 5.1.b) as shown in the flowchart (Figure 5.1). Note that the employed S-N curve expression is different than that of the three- and four-segment anisomorphic approach. For these models, an elaborated function was suggested by Kawai and Murata (2010) and Kawai and Itoh (2014), namely Equation 3.8. As discussed in Chapter 4, Equation 3.4 is preferred over Equation 3.8, mainly due to the size of the validation datasets used in this work that do not allow for the combined use of Equation 3.8 and LSPR. However, the model allows for implementation of a different S-N curve function which does not require the adaptation of any other model steps.

5.1.4 Constant Life Lines (Step 6)

The CLD is divided into three segments as seen in Figure 5.3:

1. $\sigma_m^\chi \leq \sigma_m \leq$ UTS (T-T and T-C fatigue loads),
2. $\sigma_m^{-\infty} \leq \sigma_m \leq \sigma_m^\chi$ (T-C fatigue loads),
3. UCS $\leq \sigma_m \leq \sigma_m^\infty$ (C-C fatigue loads),

where σ_m is the varying mean stress and σ_m^χ and $\sigma_m^{\pm\infty}$ are the mean stresses corresponding to $R = \chi$ and $R = \pm\infty$, respectively. For the first two segments, expressions for the CLLs can be constructed. Note that the proposed fatigue life prediction model is not applicable to the 3$^{\text{rd}}$ segment consisting of C-C fatigue loads due to concerns raised in Chapter 2 and 3. Therefore, no CLL suggestions for this segment are made in this work.

The definition of the CLD segments is different from the three- or four-segment anisomorphic CLD. The three-segment anisomorphic CLD also consists of three segments, however, the segment boundaries are only equal when χ_S is assumed as $\chi_S = \pm\infty$. Then, CLL definitions can be compared directly, as will be shown in the discussion of each CLL expression. The four-segment anisomorphic CLD consists of one additional CLD segment and thus one additional segment boundary. As discussed in Section 3.4, the segment boundaries are defined by the radials corresponding to $R = \chi$, χ_L, and χ_R. However, when χ_L is assumed as $\chi_L = \pm\infty$, as in the standard four-segment anisomorphic model, similarities in segment definitions can be found. The first, most right, segment of the

CLD in this study is similar to the combination of the two right segments of the four-segment anisomorphic model (defined by $R = \chi$, and χ_R). Moreover, the definition of the centre segments is equal, as well as that of the most left segment. This allows for a simplification in the CLL comparison. Next, an overview of the CLL expressions is provided, followed by a detailed description of the CLL derivations and a comparison with the CLL definitions employed in the three- and four-segment anisomorphic models.

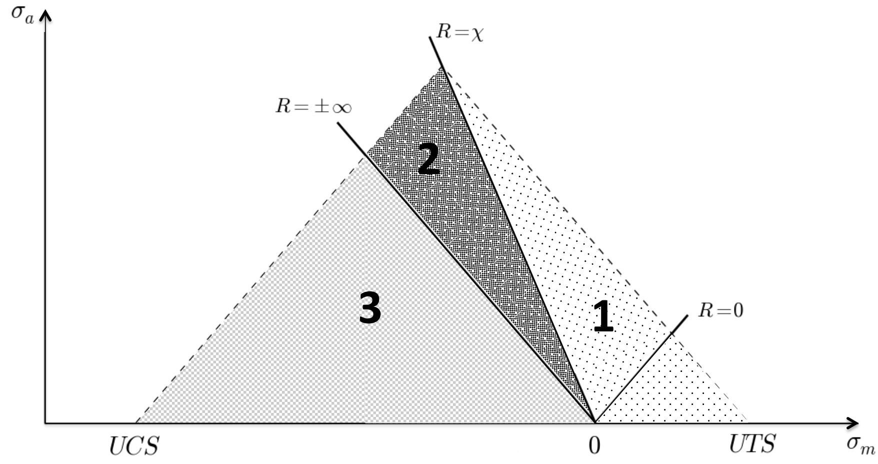

Figure 5.3: Proposed CLD model for carbon-epoxy laminates characterised by |UCS|>UTS, divided into three segments.

Overview of CLLs

For the first two CLD segments, CLL expressions have been established. Only two CLLs are given since the CLD segment for C-C loading is not considered in this work. Summarising, based on the value of σ_m, the CLLs are given as

$$-\frac{\sigma_a - \sigma_a^\chi}{\sigma_a^\chi} = \left(\frac{\sigma_m - \sigma_m^\chi}{UTS - \sigma_m^\chi}\right)^{(2-\psi_\chi)^z} \quad \text{if} \quad \sigma_m^\chi \leq \sigma_m \leq UTS, \tag{5.1}$$

$$\frac{\sigma_a - \sigma_a^\chi}{\sigma_a^\chi - \sigma_a^{\pm\infty}} = \frac{\sigma_m - \sigma_m^\chi}{\sigma_m^\chi - \sigma_m^{\pm\infty}} \quad \text{if} \quad \sigma_m^{-\infty} \leq \sigma_m \leq \sigma_m^\chi. \tag{5.2}$$

By combining the two expressions, a CLD can be established for the laminate of interest. This procedure is explained in more detail in the next subsection. First, a detailed description of the derivation of each CLL is provided, as well as a definition of the function variables.

CLL formulation for $\sigma_{\mathbf{m}}^{\chi} \leq \sigma_{\mathbf{m}} \leq$ UTS (Segment 1)

The right segment is bounded by the radial corresponding to $R = \chi$, the static strength CLL ($N_f = 1$), and the x-axis. The CLL in this segment is expressed as Equation 5.1, where the exponent z is defined as

$$\begin{aligned} z &= 1.0 && \text{if } \text{-}1.0 < \chi < 0.0, \\ z &= \frac{1}{4}(\chi + 1) && \text{if } \text{-}\infty \leq \chi < 1.0. \end{aligned} \tag{5.3}$$

The definition of the CLL in the right segment of the CLD is comparable to that of the model presented in Chapter 4. The CLLs converge to $\sigma_m = UTS$ on the x-axis and intersect the radial of $R = \chi$ in (σ_m^{χ}, σ_a^{χ}). However, a slight adaptation has been made by including exponent z. This exponent provides a shape transformation of the CLLs based on the value of χ. From the CLDs published by Kawai and Murata (2010) and Kawai and Itoh (2014), it can be concluded that for a decreasing value of χ, the shape of the CLLs changes accordingly. For |UCS| $\approx$ UTS (χ = -1.0), the CLLs can be closely described using a linear curve, i.e. $z = 0.0$. If the value of χ further decreases (i.e., |UCS|$\ll$UTS), the CLLs start to follow a convex shape. The proposed expression for z describes this shape transition of the CLLs based on the value of $R = \chi$. For laminates showing UTS>|UCS| (i.e., -1.0 $< R <$ 0.0) the value of z equals 1.0. This suggests a discontinuity in the value of z at χ = -1.0. However, due to large differences seen in the CLDs for laminates showing |UCS|>UTS with respect to laminates showing UTS>|UCS|, this discontinuity was deemed acceptable.

The proposed CLL definition (Equation 5.1) can be compared with that of the three-segment anisomorphic model (Equation 3.9) since the definition of the right CLD segment is equal for both models. The expressions for the CLL are similar and the only variation is seen in the exponent; where Kawai and Murata (2010) apply an exponent k_T to ψ_{χ}, this study applies an exponent z to $(2-\psi_{\chi})$ to control the shape of the CLL. In addition, Kawai and Murata (2010) select the value of k_T based on the predicted CLD while the value of z in this study is based on experimentally found values for UTS and UCS.

Comparison of the CLL expression with that of the four-segment anisomorphic model is less straightforward. When employing the standard four-segment anisomorphic CLD as proposed by Kawai and Itoh (2014), the two most right CLD segments, confined by $R = \chi$ and $R = \chi_R$, are similar to the first segment in this study. Thus, the CLL proposed in this study for the first segment (Equation 5.1) can be compared with two CLL expressions (Equation 3.12 and 3.13). Equation 3.12 is comparable to Equation 5.1, however, small differences arise. The main distinction is the inclusion of the exponent k_T by Kawai and Itoh (2014), similar to the three-segment CLD, while this study applies z, dependent on UTS and UCS. Moreover, Equation 3.12 is only valid until the radial for $R = \chi_R$ while Equation 5.1 is applicable until $R = \chi$. To define the CLL in the range $\chi < R < \chi_R$ in the four-segment anisomorphic model, Equation 3.13 is employed, which is a linear curve.

CLL formulation for $\sigma_{\mathbf{m}}^{-\infty} \leq \sigma_{\mathbf{m}} \leq \sigma_{\mathbf{m}}^{\chi}$ (Segment 2)
The middle segment of the CLD is bounded by two radials corresponding to $R = \chi$ and $R = \pm\infty$ and the static strength CLL ($N_f = 1$). The CLL intersects the $R = \chi$ radial at (σ_m^{χ}, σ_a^{χ}), which is the same location as the CLL defined for the first segment. The intersection of the CLL and the $R = \pm\infty$ radial on the left side of the CLD segment is less obvious. From fatigue life data published by Kawai and Murata (2010) and Kawai and Itoh (2014) on laminates characterised by |UCS|>UTS, it was judged that all CLLs intersect the radial corresponding to $R = \pm\infty$ in the top region of the radial. Closer evaluation allows for concluding that this narrow region can be described as approximately the upper 10% of the $R = \pm\infty$ radial.

In order to define an expression for the CLL in the middle segment, it is required to first define an expression for the upper 10% of the radial. The radial corresponding to $R = \pm\infty$ and the static strength CLL (i.e., $\psi = 1.0$, $N_f = 1$) intersect at ($\sigma_m^{100\%}$, $\sigma_a^{100\%}$). The static strength CLL is known to intersect the x-axis in $\sigma_m = UCS$ and peak at the $R = \chi$ radial in (σ_m^{χ}, σ_a^{χ}). Note that the latter also describes the peak of the complete CLD. The static strength CLL can be described by

$$\sigma_a^{\psi=1.0} = \frac{\sigma_a^{\chi}}{\sigma_m^{\chi} - UCS} \left(\sigma_m^{\psi=1.0} - UCS\right), \tag{5.4}$$

where ($\sigma_m^{\psi=1.0}$, $\sigma_a^{\psi=1.0}$) is a variable mean and amplitude stress combination located on the CLL. The values for σ_m^{χ} and σ_a^{χ} can be determined using UTS and UCS, by defining σ_m^{χ} in Equation 4.1 as

$$\sigma_m^{\chi} = \frac{UCS + UTS}{2}. \tag{5.5}$$

Using the static strength CLL, the intersection with the radial corresponding to $R = \pm\infty$ can be found, where the radial for $R = \pm\infty$ is defined as

$$\sigma_a = \sigma_m \frac{1 - (\pm\infty)}{1 + (\pm\infty)}. \tag{5.6}$$

When $\sigma_a^{\psi=1.0}$ in Equation 5.4 equals σ_a in Equation 5.6, the intersection of the two curves is found and consequently ($\sigma_m^{100\%}$, $\sigma_a^{100\%}$) is obtained by solving

$$\sigma_a^{\psi=1.0} = \sigma_a^{100\%}, \tag{5.7}$$

$$\sigma_m \frac{1 - (\pm\infty)}{1 + (\pm\infty)} = \frac{\sigma_a^{\chi}}{\sigma_m^{\chi} - UCS} \left(\sigma_m^{100\%} - UCS\right). \tag{5.8}$$

The top of the radial corresponding to $R = \pm\infty$, i.e. ($\sigma_m^{100\%}$, $\sigma_a^{100\%}$), defines the upper bound of the 10% top of the $R = \pm\infty$ radial. The lower bound can be described as 90%

of the mean and amplitude stress of the upper bound, i.e. ($\sigma_m^{90\%}$, $\sigma_a^{90\%}$), given as

$$\sigma_m^{90\%} = 0.9 \cdot \sigma_m^{100\%}, \tag{5.9}$$
$$\sigma_a^{90\%} = 0.9 \cdot \sigma_a^{100\%}. \tag{5.10}$$

The top tenth percentile of the $R = \pm\infty$ radial is now defined by the lower bound ($\sigma_m^{90\%}$, $\sigma_a^{90\%}$), upper bound ($\sigma_m^{100\%}$, $\sigma_a^{100\%}$), and Equation 5.6. A set of equations, describing the intersection stresses of a CLL and the radial, is given as Equation 5.6 and

$$\sigma_a^{\pm\infty} = \frac{0.1 \cdot \sigma_a^{100\%}}{\log_{10}(10^6)} \log_{10}(N_f). \tag{5.11}$$

In Equation 5.11, N_f is the fatigue life of the considered CLL, $\sigma_a^{90\%}$ and $\sigma_a^{100\%}$ describe the top tenth percentile of the $R = \pm\infty$ radial, and ($\sigma_m^{\pm\infty}$, $\sigma_a^{\pm\infty}$) is the mean and amplitude stress combination for which a CLL corresponding to a certain value of N_f intersects the $R = \pm\infty$ radial.

This assumed expression takes several aspects into account. Firstly, it is given that the static strength CLL intersects the radial of $R = \pm\infty$ in ($\sigma_m^{100\%}$, $\sigma_a^{100\%}$). Secondly, it is assumed that the CLL for $N_f = 10^6$ intersects the $R = \pm\infty$ radial in ($\sigma_m^{90\%}$, $\sigma_a^{90\%}$). Note that this assumption directly relates to the applicability boundary of the model of not considering HCF predictions (i.e., $N_f > 10^6$). Lastly, it is assumed that CLLs for different values of N_f do not intersect one another. Consequently, $\sigma_m^{\pm\infty}$ and $\sigma_a^{\pm\infty}$ must always be decreasing for an increasing N_f. A condition that is met by the proposed fatigue life prediction model.

Both the left and right bound of the CLLs in the middle segment of the CLD have been defined. The right bound of a CLL is defined as the intersection of the CLL with the radial corresponding to $R = \chi$, i.e. (σ_m^{χ}, σ_a^{χ}) while the left bound is defined as ($\sigma_m^{\pm\infty}$, $\sigma_a^{\pm\infty}$) on the $R = \pm\infty$ radial. Next, the shape of the CLLs between these two points can be defined. The CLL is described using linear interpolation between the lower and upper bound, of which its validity will be demonstrated in Section 5.2. Equation 5.2 is used to describe the CLLs in the middle segment, where σ_m and σ_a are the mean and amplitude stress on the CLL for a certain value of N_f, $\sigma_m^{\pm\infty}$ and $\sigma_a^{\pm\infty}$ are the mean and amplitude stress, respectively, at which the CLL intersects the $R = \pm\infty$ radial, and σ_m^{χ} and σ_a^{χ} are the mean and amplitude stress, respectively, at which the CLL intersects the $R = \chi$ radial.

The differences between the middle segments of the model proposed in this chapter and of the three-segment anisomorphic CLD by Kawai and Murata (2010) are minimal; the expressions for the CLL are similar since both models assume a linear relation (Equation 3.10 versus Equation 5.2). The main difference between the models lies in the determination of the left bound of the CLL. The model proposed in this chapter assumes that the left segment boundary is always defined by the $R = \pm\infty$ radial while the three-segment anisomorphic model by Kawai and Murata (2010) defines it by the sub-critical R-ratio χ_S which can be chosen arbitrarily. When χ_S is assumed to equal $\chi_S = \pm\infty$, the segments and CLL definitions become equal.

The third segment in the four-segment anisomorphic model by Kawai and Itoh (2014) is similarly defined as the second segment of the CLD in this study. The former is bounded by the radials for $R = \chi_L$ and $R = \chi$ while the latter is bounded by radials for $R = \pm\infty$ and $R = \chi$. If χ_L is set equal to $\pm\infty$, as is assumed in the standard four-segment anisomorphic model, the segments become equal and the CLLs can be compared. Both models assume a linear shaped CLL (Equation 3.14 versus Equation 5.2). The main difference is seen in the determination of the stress coordinates on the boundary radials: where the four-segment anisomorphic model determines the intersections of the CLLs with the radials by means of experimental data, the proposed model calculates these by means of a set of equations.

5.1.5 Determination of CLL Intersections with the Segment Boundary Radials (Step 5)

The static strength and fatigue life input data can be combined with the CLL definitions to construct the CLD, as will be discussed in the next subsection. However, before the CLD can be established, it is required to determine the location of intersection of the CLLs with the $R = \chi$ and $R = \pm\infty$ radials in order to define the CLL expressions. The steps required to find the stress values of the intersections are described in this subsection. The method is different from the three- and four-segment anisomorphic models where the stresses on the segment boundaries are obtained by means of an experimental campaign.

The first intersection of the CLL is with the $R = \chi$ radial: $(\sigma_m^\chi,\ \sigma_a^\chi)$. The $R = \chi$ radial defines the boundary between the middle and right segment. The exact location of intersection can be determined based on the input fatigue life datapoints for either $R = 0.1$ or -1. It is known that all input fatigue life datapoints lie on one radial described by Equation 3.5, where R equals 0.1 or -1.0, dependent on the input data. Each datapoint describes an applied CA fatigue load, characterised by its mean σ_m and amplitude σ_a stress and corresponding fatigue life: $(N_f, \sigma_m, \sigma_a)$. The input fatigue life datapoints always lie in the right CLD segment ($\sigma_m^\chi \leq \sigma_m \leq UTS$), irrespective of whether it corresponds to $R = 0.1$ or $R = -1.0$. The intersection of a CLL with these datapoints must be found in order to allow for derivation of the values for $(\sigma_m^\chi,\ \sigma_a^\chi)$. The CLL in the right segment can be used for this purpose and is defined as Equation 5.1.

The CLL expression (Equation 5.1) is based on the values of the mean and amplitude stress where the curve intersects the radial for $R = \chi$ (i.e., $(\sigma_m^\chi,\ \sigma_a^\chi)$). Moreover, the equation contains the ratio ψ_χ, whose value was previously defined in Equation 3.2 and is directly dependent on the values for $(\sigma_m^\chi,\ \sigma_a^\chi)$. In addition, the value of the exponent z (Equation 5.3) is dependent on the value of χ and thus on both UTS and UCS values. Lastly, the CLL expression contains variable mean and amplitude stress coordinates located on the CLL (σ_m, σ_a). By combining the CLL expression (Equation 5.1) with the equation for the radial (Equation 4.1), a set of equations is obtained that is defined as

$$\begin{aligned} \sigma_a^I &= \sigma_a^\chi \left(1 - \left(\frac{\sigma_m^I - \sigma_m^\chi}{UTS - \sigma_m^\chi}\right)^{(2-\psi_\chi)^z}\right) \quad \text{if} \quad \sigma_m^\chi \leq \sigma_m^I \leq UTS, \\ \sigma_a^\chi &= \sigma_m^\chi \frac{1-\chi}{1+\chi}. \end{aligned} \tag{5.12}$$

In this set of equations, z and UTS are known quantities while σ_m^I and σ_a^I are the test datapoints used as input to the model (i.e., (N_f, σ_m, σ_a)). Next, it is possible to solve for (σ_m^χ, σ_a^χ) when ψ_χ is written as a function of the stresses under $R = \chi$. Then, the fatigue life-stress combinations located on the $R = \chi$ radial are obtained as (N_f, σ_m^χ, σ_a^χ) and each found combination corresponds to a datapoint from the input dataset (N_f, σ_m, σ_a). This procedure is repeated for each input datapoint. Once all datapoints (N_f, σ_m^χ, σ_a^χ) for $R = \chi$ are obtained, it is possible to fit Equation 3.4 through the datapoints following a LSPR method (of which the derivation is outlined in Appendix A). Using the fitted ψ-$2N_f$ curve, a continuous function of (N_f, σ_m^χ, σ_a^χ)-combinations is obtained describing the intersection of the CLL with the $R = \chi$ radial.

Note that it is also possible to fit Equation 3.4 to the datapoints of the input dataset, and to solve the set of Equations 5.12 for each value of N_f using the corresponding stress values of the fitted curve. Consequently, this method will lead to a more computationally expensive model than the first proposed method because the set of Equations 5.12 has to be solved more often. Moreover, it does not provide a higher predictive accuracy and the predicted S-N curves are similar for both methods. Therefore, the former method is suggested, resulting in a less computationally expensive model.

Next, it is possible to establish the CLL boundary between the middle and left CLD segment, defined as the radial corresponding to $R = \pm\infty$. Firstly, it is required to determine the boundaries of the top 10% segment of the $R = \pm\infty$ radial by means of the procedure outlined in Subsection 5.1.4. This results in two mean and amplitude stress combinations, namely 1) ($\sigma_m^{100\%}$, $\sigma_a^{100\%}$) and 2) ($\sigma_m^{90\%}$, $\sigma_a^{90\%}$). Then, a continuous function describing the location of intersection ($\sigma_m^{\pm\infty}$, $\sigma_a^{\pm\infty}$) of CLLs for different N_f values with the $R = \pm\infty$ radial is obtained using Equation 5.6 and 5.11.

The functions describing the CLL intersections with the segment boundary radials can be used to finalise the CLL definitions (Equation 5.1 and 5.2). Subsequently, these can be used to establish a CLD for the laminate. The next subsection covers the CLL and CLD construction in more detail.

5.1.6 Constant Life Diagram (Step 7)

The establishment of functions defining the intersections of the CLLs with the segment boundary radials ($R = \chi$ and $R = \pm\infty$) in terms of the mean and amplitude stresses ((σ_m^χ, σ_a^χ) and ($\sigma_m^{\pm\infty}$, $\sigma_a^{\pm\infty}$)), as discussed in the previous subsection, allows for construction of CLLs and consequently a CLD. For each N_f, the intersections are determined by means of Equation 5.6, and 5.11, which are used to define the CLL expressions for each segment (Equation 5.1 and 5.2). Combining the CLLs of each segment allows for establishment of the complete CLD. All CLLs converge to σ_m =UCS or σ_m =UTS on the x-axis for $\sigma_a = 0$ (i.e., $R = 1$). Moreover, the CLD is bounded by means of the x-axis and two linearly shaped CLLs corresponding to $N_f = 1$, given as Equation 4.5. Note that the main aspects of the CLD are similar to that in the three- and four-segment anisomorphic CLDs; differences are seen in the segment and CLL definitions, as well as the input datasets employed for the latter.

5.1.7 S-N Curve Prediction (Step 8)

Combining the CLD segments and the corresponding CLL definitions allows for construction of the complete CLD as shown in the previous subsection. Consequently, S-N curves can be predicted for different R-ratios. This occurs in a similar manner as in the three- and four-segment anisomorphic model. All datapoints of the R-ratio of interest are known to lie on one radial corresponding to this R-ratio, where the radial is defined as Equation 3.5. If the intersection of a CLL for a specified value of N_f with this radial is found and this is repeated for a wide range of N_f values, it is possible to derive the S-N curve of interest. The set of equations that must be solved is given as Equations 5.1, 5.2, and 3.5 where the appropriate CLL expression must be chosen based on the considered value for σ_m and thereby on the R-ratio of interest. Note that only (σ_m, σ_a) is unknown in this set of equations. The points of intersection (σ_m^χ, σ_a^χ) and ($\sigma_m^{\pm\infty}$, $\sigma_a^{\pm\infty}$) with segment boundary radials have been determined previously while ψ_χ is a function of (σ_m^χ, σ_a^χ). Lastly, UTS and UCS are required as input and the exponent z is a function of these two variables (Equation 5.3).

5.2 Validation using Datasets from Literature

The previously proposed model is validated in this section by evaluating its predictive performance using two carbon-epoxy laminates. The employed datasets for these laminates originate from literature, more specifically: they were presented by Kawai and Murata (2010) and Kawai and Itoh (2014). Due to time constraints of this work, no experimental campaign was conducted as in Chapter 4. The lay-ups of the considered laminates are $[\pm 60]_{3S}$ and $[45]_{16}$. A quantitative comparison of its performance with respect to the four-segment CLD by Kawai and Itoh (2014) is included as well. Only a comparison with the four-segment CLD model is provided and not with the three-segment CLD model due to its similarity with the four-segment CLD. Predictions using the four-segment CLD model are made using several S-N curves and thereby using more fatigue life data than the proposed model. The use of additional input data can enhance the predictive accuracy, however, should be minimal for the acceptance of the proposed model. The R-ratios used for comparison are different from the input R-ratios, i.e. either $R = 0.5$, -3, -5, or -10. Each subsection will present a comparison for a different laminate lay-up, namely $[\pm 60]_{3S}$ and $[45]_{16}$ in Subsection 5.2.1 and 5.2.2, respectively. The employed error measures are similar to those discussed in Section 4.2.1.

5.2.1 $[\pm 60]_{3S}$

A carbon-epoxy laminate (T800H/2500) with lay-up $[\pm 60]_{3S}$ is used for validation of the model proposed in this chapter. Its experimental data was presented by Kawai and Murata (2010) and is also included in Appendix D. For details on manufacturing and testing, the reader is referred to the corresponding paper. The datasets are limited in size with on average five datapoints per R-ratio. Fatigue life tests were performed at two T-T R-ratios ($R = 0.1$ and $R = 0.5$) and four T-C R-ratios ($R =$ -1, $R = \chi =$ -1.98, $R =$ -3, and $R =$ -5). The absolute value of UCS is almost twice the size of UTS (-164.8 MPa versus 83.3 MPa), resulting in a value for χ of -1.98. The values of the fitting parameters for the critical S-N curve, predicted using $R = 0.1$ and -1 as input to the proposed model, are presented in Table 5.1. Moreover, in the four-segment anisomorphic model, input data at $R = 0.1$, $R =$ -1, and $R = \chi$ is employed to which Equation 3.4 is fitted. The corresponding fitting parameters are presented in Table 5.2. Note that the four-segment anisomorphic model was not yet applied by Kawai and Murata (2010) or Kawai and Itoh (2014) to this laminate. However, improved results with the standard four-segment anisomorphic model were obtained compared to the standard[1] three-segment anisomorphic model.[2] For that reason, the four-segment anisomorphic model, rather than the three-segment CLD, will be employed for comparison with the proposed model.

Table 5.1: Model fitting parameters for the S-N curve describing the fatigue life under the critical R-ratio χ, determined using different input datasets (i.e., $R = 0.1$ and $R = -1$).

Input R-ratio	$\mathbf{K}_\chi$	**a**	**n**
$R = 0.1$	0.011	0.27	9.04
$R =$ -1	$9.40 \cdot 10^{-3}$	0.28	9.47

[1] The standard three-segment anisomorphic model has been assumed as $R = \chi =$ -1.98 and $R = \chi_S = 10$, with $k_T = k_C = 1$.

[2] The results of the comparison have not been included in this report because it is not the focus of this work to compare the two-, three-, and four-segment anisomorphic models.

Table 5.2: Model fitting parameters for the S-N curves fitted to the fatigue life data under the R-ratio $R = \chi$, $R = 0.1$, and $R = 10$.

R-ratio	K_χ	a	n
$R = \chi$	0.41	0.083	15.37
$R = 0.1$	$4.59 \cdot 10^{-3}$	0.33	18.24
$R = 10$	2.02	$1.00 \cdot 10^{-6}$	87.69

The CLDs predicted by the proposed model are shown in Figure 5.4a and 5.4b using fatigue life data at $R = 0.1$ and -1 as input, respectively. Both CLDs show similarities, with fatigue life predictions for $R > \chi$ close to experimental data while those for $R < \chi$ show larger inconsistencies. In the next two paragraphs, the S-N curves predicted using the CLDs are presented and discussed in more detail with respect to the experimentally obtained data. Moreover, a comparison is made with the predictions by the four-segment anisomorphic CLD.

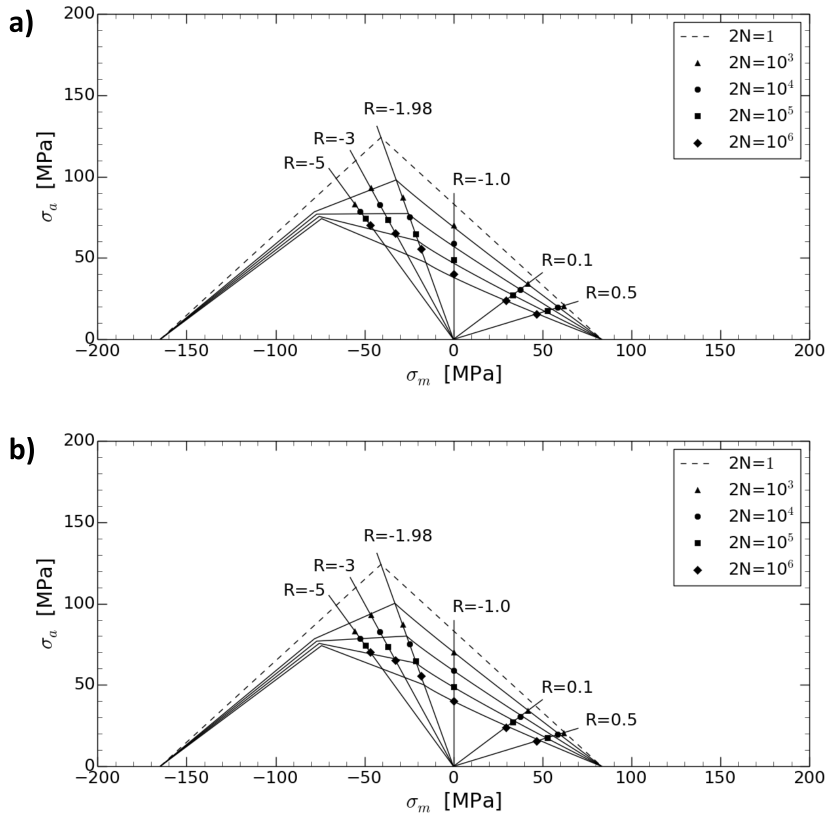

Figure 5.4: Constant fatigue life diagram for $[\pm 60]_{3S}$ carbon-epoxy laminate, obtained using the proposed model with a) $R = 0.1$ and b) $R = -1.0$ fatigue life data as input.

The predicted S-N curves are shown in Figure 5.5 for a) R = 0.5, b) R = -3, and c) R = -5. Only these three R-ratios can be used for comparison because the four-segment CLD model requires input of fatigue life data of the other three R-ratios. Moreover, the proposed model requires the input of either R = 0.1 or R = -1 fatigue life data. Besides the predicted S-N curves, each diagram includes a best-fit S-N curve (Equation 3.4) to the test data, obtained using a LSPR method (Appendix A) and shown by means of a dashed line. The error measures for all models are presented in Table 5.3.

From Figure 5.5 and Table 5.3, it can be seen that the predictions by the model proposed in this chapter are stable and show only small differences for a changing input R-ratio. The differences with the four-segment anisomorphic model are larger. For R = 0.5, fatigue life predictions by the three models are adjacent and describe the best-fit curve closely. For both R = -3 and -5, all predicted S-N curves show larger deviations from the best-fit S-N curve and do not seem to represent the fatigue behaviour under this T-C type loading. However, the proposed model (both input of R = 0.1 and -1) outperforms the four-segment anisomorphic model predictions for both R-ratios. Note that the values of MAPE, MNB, and RMSPE are similar for all three models (Table 5.3). However, this is caused by the under-prediction of the fatigue life by the four-segment anisomorphic model. Evaluating the SSE values, larger differences are seen since SSE penalises under-predictions more than over-predictions.

Table 5.3: Error metrics for the fatigue life prediction of $[\pm 60]_{3S}$ by means of the proposed model (input of $R = 0.1$ and $R = -1.0$) and four-segment anisomorphic CLD (input of $R = 0.1$, $R = \chi$, and $R = 10$).

Input R-ratio	MAPE [%]	MNB [%]	RMSPE [%]	SSE [-]
	R=0.5			
R = 0.1	71.66	-71.66	74.83	13.37
R = -1	64.64	-50.60	67.13	8.25
Four-segment	83.28	-12.27	97.13	6.12
	R=-3.0			
R = 0.1	73.60	-73.60	74.35	6.53
R = -1	62.74	-62.74	64.14	3.75
Four-segment	90.42	-90.42	90.42	16.53
	R=-5.0			
R = 0.1	73.60	-73.60	74.35	6.53
R = -1	114.1	77.71	149.6	3.93
Four-segment	79.01	-79.01	80.12	16.13

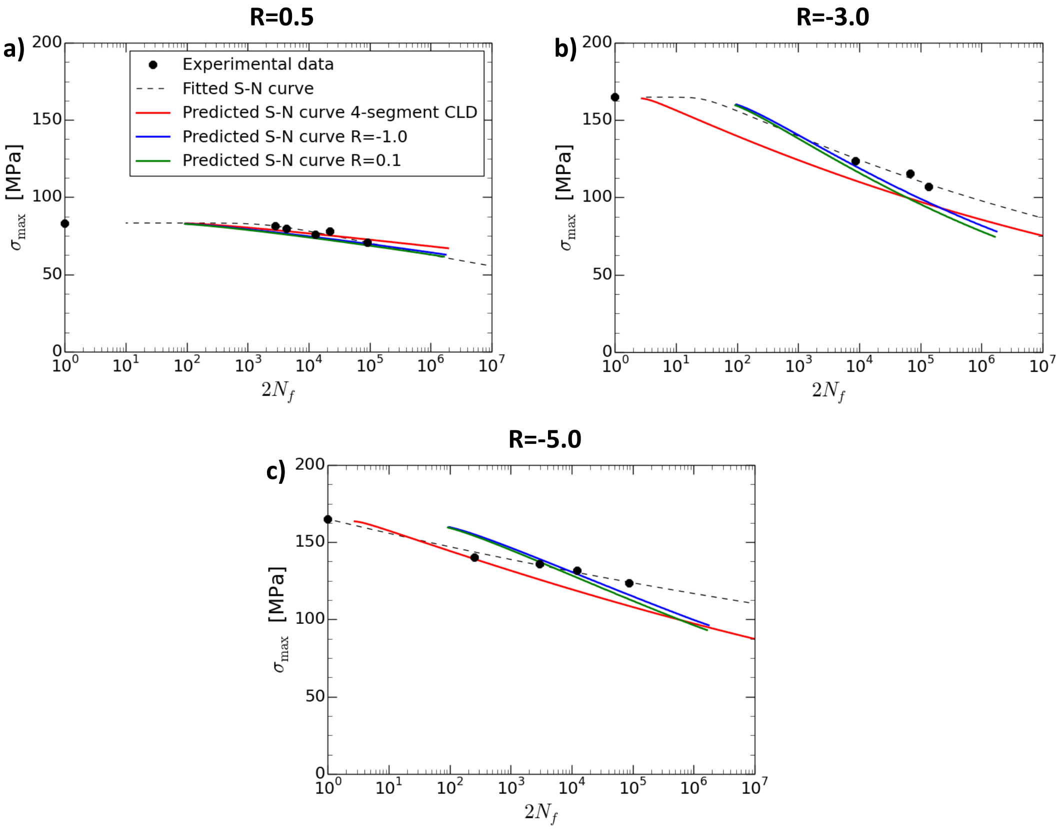

Figure 5.5: Fatigue life predictions for $[\pm 60]_{3S}$ by the proposed model (input $R = 0.1$ or $R = -1.0$) and the four-segment CLD (input $R = 0.1$, χ, and 10). In addition, experimentally obtained fatigue lives are depicted. Fitted and predicted S-N curves are shown for a) $R = 0.5$, b) $R = -3.0$, and c) $R = -5.0$. The legend is the same for all figures.

5.2.2 $[45]_{16}$

The second laminate used for validation of the proposed model is an off-axis UD carbon-epoxy laminate (T700S/2592) with lay-up $[\pm 45]_{16}$. Experimental fatigue life data for different R-ratios was presented by Kawai and Itoh (2014). Note that fatigue life data was presented by means of diagrams and the presumed values have been included in Appendix D. Datasets are again limited in size with some datasets only consisting of three tests. Datasets for five R-ratios are available, namely $R = 0.1$, 0.5, -1, χ, and -10. Note that for $R =$ -10, the datapoints show a large variability in fatigue life, which does not allow for a close fitting of an S-N curve through the data. It is expected that some of these datapoints are outliers and that an improved image of the fatigue behaviour at R = -10 can be achieved when additional fatigue life tests are performed. Note that the nature of the R = -10 dataset influences the evaluations made in this subsection. The critical R-ratio for the $[45]_{16}$-laminate equals $R = \chi$ = -2.46 with UTS= 61.6 MPa and UCS= -151.6 MPa. Both R = 0.1 and R = -1 were used as input to evaluate the predictive accuracy of the model presented in this chapter and the fitting parameters for the critical S-N curve are included in Table 5.4. For the four-segment anisomorphic CLD, Equation 3.4 is fitted to experimental data at $R = \chi$, 0.1, and 10. Its fitting parameter values are included in Table 5.5.

Table 5.4: Model fitting parameters for the S-N curve describing the fatigue life under the critical R-ratio χ, determined using different input datasets (i.e., $R = 0.1$ and $R = -1$).

Input R-ratio	K_χ	a	n
$R = 0.1$	0.23	0.11	9.48
R = -1	$2.95 \cdot 10^{-3}$	0.35	5.04

Table 5.5: Model fitting parameters for the S-N curves fitted to the fatigue life data under the R-ratio $R = \chi$, $R = 0.1$, and $R = 10$.

R-ratio	K_χ	a	n
$R = \chi$	0.029	0.22	7.82
$R = 0.1$	0.056	0.20	18.16
$R = 10$	$1.22 \cdot 10^{-3}$	0.19	24.18

The CLDs predicted using $R = 0.1$ and -1 as input to the model considered in Section 5.1 are presented in Figure 5.4a and 5.4b, respectively. The CLD predicted by the four-segment anisomorphic CLD has been presented by Kawai and Itoh (2014). CLLs for fatigue lives corresponding to $2N_f = 10^4 \sim 10^6$ are alike, independent of input R-ratio, and resemble the trend of the fatigue life test data. Even though both diagrams shown in Figure 5.4 are similar, a prominent contrast is seen in the CLL for $2N_f = 10^3$, which is largely different for both T-T and T-C loading. For higher stress values, slight under-predictions of fatigue life are seen for R = -1 and $R = \chi$ when R = 0.1 is used as input, while an over-prediction is seen for $R = 0.1$ and $R = 0.5$ when R = -1 is used as input. This difference becomes more clear in the discussion on the S-N curve predictions provided next, where also a comparison with the predictions made by the four-segment anisomorphic model is included.

The error metrics for both models are shown in Table 5.6. The predicted S-N curves, as well as the best-fit curve (Equation 3.4), for a) R = 0.5 and b) R = -10 are shown in Figure 5.7. Predictions at only two R-ratios can be compared for all models because of the difference in input R-ratio. In addition, to enrich the evaluation, a comparison is made between two models for R = -1, shown in Figure 5.7c, and for $R = \chi$, shown in Figure 5.7d, between the different inputs for the proposed model. Note that predictions made using the proposed model with R = -1 as input might be influenced by the limited size of the R = -1 dataset, which only consists of three test datapoints.

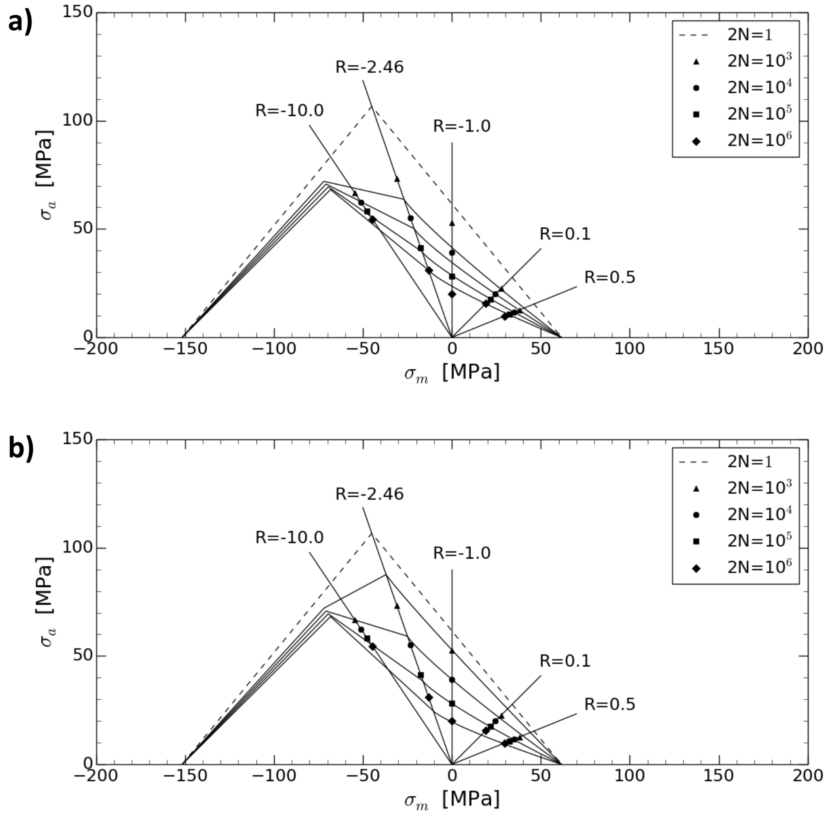

Figure 5.6: Constant fatigue life diagram for $[45]_{16}$ carbon-epoxy laminate, obtained using the proposed model with a) $R = 0.1$ and b) $R = -1.0$ fatigue life data as input.

Firstly, the predictions by each model for loading at $R = 0.5$, shown in Figure 5.7a, can be compared. All three models over-predict fatigue lives on all scales. On the one hand, the S-N curves by the four-segment CLD and the proposed model using $R = 0.1$ data as input are almost parallel to the best-fit curve to the experimental data. On the other hand, the predicted S-N curve using R = -1 fatigue life data as input to the proposed model shows a more sensitive fatigue behaviour. However, the fatigue life prediction made by the four-segment anisomorphic model shows the largest inaccuracies, as seen in Table 5.6 while the predictions based on $R = 0.1$ fatigue life data result in the most accurate predictions. This is also seen in Figure 5.7, where the curve is located closest and parallel to the best-fit curve.

A second comparison can be made by evaluating predictions for R = -10. The prediction made by the proposed model using $R = 0.1$ fatigue life data results in an S-N curve located in vicinity of the best-fit curve. The other two S-N curves, predicted using the four-segment CLD model and the proposed model using R = -1 as input, result in S-N curve shapes that are not in correspondence with the experimental validation data. Note that this conclusion cannot be made when merely looking at the values given in Table 5.6, which indicate that the four-segment CLD results in the best predictions. The size of the error measures is caused by two aspects, namely 1) the validation dataset and 2) the nature of the error metrics. Firstly, the validation dataset shows large variability in fatigue life for similar applied maximum stresses. Secondly, the error metrics are biased by penalising over- and under-predictions differently. This demonstrates the importance of evaluating both the error measures and the obtained curves simultaneously.

The third and fourth comparison for R = -1 and χ, respectively, are only made between two predictions. The predicted curves are shown for R = -1 in Figure 5.7c, and show small variations. The four-segment model is capable of providing more accurate predictions than the proposed model (using $R = 0.1$ fatigue life data as input) for the stress levels of the validation datapoints, which is confirmed by the error metrics in Table 5.6. Note that for lower stress levels, the proposed model seems to provide more accurate predictions, however, the best-fit curve in this fatigue life scale has been extrapolated. The predictions for $R = \chi$ by the proposed model using a different input R-ratio, i.e. $R = 0.1$ and -1, are shown in Figure 5.7d. Both curves are in vicinity of the best-fit curve and the experimental datapoints but show a different fatigue sensitivity. This results in reversed over- and under-predictions of fatigue life by the two curves. The latter is also quantified by the SSE error measure which is almost equivalent for both models.

Table 5.6: Error metrics for the fatigue life prediction of $[45]_{16}$ by means of the proposed model (input of $R = 0.1$ and $R = -1.0$) and four-segment anisomorphic CLD (input of $R = 0.1$, $R = \chi$, and $R = 10$).

Input R-ratio	MAPE [%]	MNB [%]	RMSPE [%]	SSE [-]
	R=0.5			
$R = 0.1$	604.0	604.0	618.8	15.10
R = -1	$1.65{\cdot}10^3$	$1.65{\cdot}10^3$	$2.19{\cdot}10^3$	27.09
Four-segment	$1.55{\cdot}10^4$	$1.55{\cdot}10^4$	$2.66{\cdot}10^4$	90.05
	R=-10.0			
$R = 0.1$	947.6	974.6	979.0	28.14
R = -1	377.0	354.7	594.9	10.84
Four-segment	74.19	-25.61	81.27	9.89
	R=-1.0			
$R = 0.1$	80.79	-80.79	81.38	10.81
Four-segment	35.65	-35.65	43.86	1.42
	R=χ			
$R = 0.1$	42.31	-37.91	46.38	4.01
R = -1	59.34	7.73	74.72	4.11

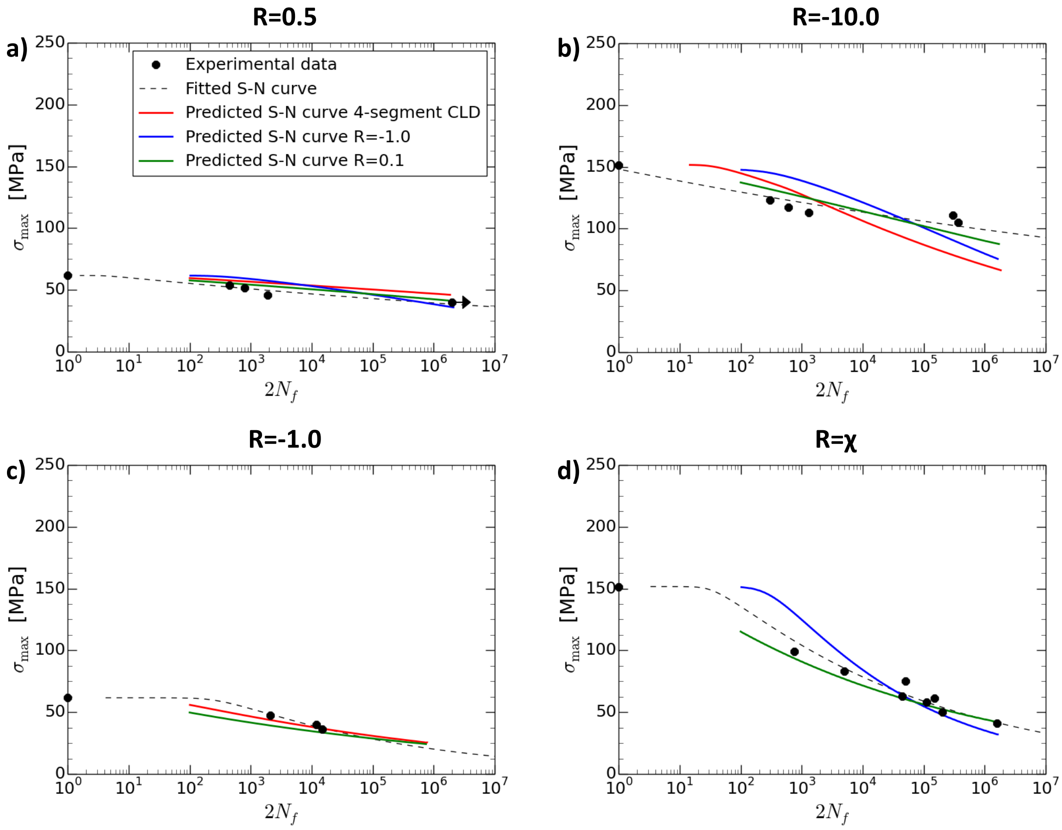

Figure 5.7: Fatigue life predictions for $[45]_{16}$ by the proposed model (input $R = 0.1$ or $R = -1.0$) and four-segment CLD (input $R = 0.1$, χ, and 10). In addition, experimentally obtained fatigue lives are depicted. Fitted and predicted S-N curves are shown for a) $R = 0.5$, b) $R = -10.0$, and c) $R = -1.0$. The legend is the same for all figures.

5.2.3 Conclusion

The predictive accuracy of the proposed model has been evaluated in this section. Moreover, a comparison with the standard four-segment anisomorphic model was made. Two cases were used for comparison, namely 1) a carbon-epoxy (T800H/2500) laminate with angle-ply lay-up of $[\pm 60]_{3S}$ and 2) a carbon-epoxy (T700S/2592) laminate with an off-axis UD lay-up of $[45]_{16}$. All made fatigue life predictions using the proposed and four-segment anisomorphic model were in vicinity of experimental data. Predictions are either similar between the models or show improvements when employing the proposed model.

One general trend in fatigue life predictions can be observed. Namely, for R-ratios related to T-C loading at $R < \chi$, both models show difficulties in predicting the fatigue life behaviour. An under-prediction is seen for lower stress values while an over-prediction is seen for higher stress values and the four-segment anisomorphic model has a stronger tendency to under-predict fatigue life. For the model proposed in this work, these results can be an indication that one of the made assumptions might not be completely valid. Firstly, an assumption was made on the intersection of the CLLs with the $R = \pm\infty$ radial. Based on the S-N curve predictions, the CLL intersection with the $\pm\infty$ radial should occur at lower stress values for lower fatigue lives while those for higher values of N_f should intersect the $\pm\infty$ radial at higher stresses. However, when also taking into account the predictions by the four-segment anisomorphic model, another conclusion can be drawn. The four-segment anisomorphic model shows a slightly lower predictive accuracy in the T-C fatigue life predictions for $R < \chi$ than the proposed model while the four-segment anisomorphic CLD employs fatigue life data in the vicinity of $R = \pm\infty$ (namely $R = 10$). Since also inaccurate fatigue life predictions have been obtained using experimental data, this might be an indication that the assumed linear CLL shape, employed in both models for T-C loading at $R < \chi$, is inaccurate. Instead, based on the obtained results, CLLs for lower values of N_f should have a more convex shape, resulting in lower stress values for a similar N_f, while CLLs for higher fatigue lives should have a concave shape. Whether the assumption of a linear-shaped CLL is valid can only be confirmed by performing more tests to obtain additional S-N curves for $R < \chi$.

The predictive accuracy of the proposed model with respect to the four-segment anisomorphic CLD is either similar or improved. This is unexpected because it was anticipated that the four-segment anisomorphic CLD would perform better in all cases. The four-segment anisomorphic CLD employs more experimental data which is related to all fatigue life scales: while the proposed model makes additional assumptions on the CLL curve shape, the four-segment anisomorphic CLD employs three S-N curves in each fatigue loading type region (T-T, T-C, and C-C). The difference in predictive accuracy might be caused by the use of an LSPR method (Appendix A), which is different from the visual method employed by Kawai and Itoh (2014). Moreover, a less elaborate curve fitting function (Equation 3.4) was employed in this section than that proposed by Kawai and Itoh (2014) (Equation 3.8) because the datasets, due to their size, do not always allow for the use of the latter equation in combination with the LSPR method. However, the fitting of the S-N curve function to the input data was deemed acceptable and therefore its influence is expected to be minimal. Lastly, the use of the standard four-segment anisomorphic CLD, where $k_T = k_C = 1$, might not be applicable for the considered laminates and the values of these exponents might require adaptation. However, for arguments described in Chapter 3, this results in a descriptive model rather than a predictive model and is deemed not appropriate.

Each of the previously described aspects can be a source for the lower than expected predictive accuracy of the four-segment anisomorphic CLD. However, for an unambiguous comparison with the proposed model, these alterations had to be made to the four-segment anisomorphic CLD. Moreover, the perception is that the effect of these aspects on the final outcome, except in case of the exponents, should be minimal. Therefore, even though this result was unforeseen, one can conclude that, for the two considered carbon fibre-reinforced epoxy laminates, the predictive accuracy of the proposed model is similar or improved with respect to that of the standard four-segment anisomorphic model.

Chapter 6

Conclusions

In this work, two fatigue life prediction models were presented for carbon fibre-reinforced epoxy laminates characterised by either UTS>|UCS| or |UCS|>UTS. Predictions are made for T-T and T-C loading cases based on a single S-N curve. These models have been proposed based on the research questions formulated in Chapter 1. The first research question is restated and addressed next.

> How to adapt the anisomorphic fatigue life prediction model such that a different input dataset can be used to minimise the number of required S-N curves and allow for a more conventional stress ratio?

The adaptation of the two-segment anisomorphic model resulted in the proposed model applicable to carbon-epoxy laminates characterised by UTS>|UCS|. An additional model step was included, which allowed for the derivation of the critical S-N curve from input fatigue life data obtained at either R = 0.1 or R = -1. This resulted in a model that predicts the fatigue life of carbon-epoxy laminates based on a single experimental S-N curve related to R = 0.1 or R = -1. The amount of experimental input data was not reduced with respect to the two-segment anisomorphic model. However, a more conventional stress ratio than the critical R-ratio can now be employed.

The adaptation of the three- and four-segment anisomorphic model resulted in the proposed model applicable to carbon-epoxy laminates showing |UCS|>UTS. Experimental results, presented by Kawai and Murata (2010) and Kawai and Itoh (2014), were reviewed and the anisomorphic model was adapted to include an assumption concerning the shape of the CLLs near the segment boundary between T-C and C-C loading. Moreover, an additional CLL-shape dependency on the UTS and UCS value was included. This resulted in a model that predicts the fatigue life of carbon-epoxy laminates based on a single experimental S-N curve related to $R = 0.1$ or $R = -1$. The amount of experimental input data was reduced compared to the three- and four-segment anisomorphic model, which require two and three S-N curves, respectively, of which one related to the critical R-ratio. Thus, not only a more conventional R-ratio can be employed as input to the models but also less experimental tests are required.

A second research question was defined in Chapter 1 related to the predictive accuracy of the proposed models. This research question is restated and answered as follows.

> What is the relative predictive performance of the proposed model with respect to the anisomorphic fatigue life model when comparing similar laminates tested in constant amplitude loading at different stress ratios (T-T and T-C)?

The relative predictive performance of the proposed model with respect to the two-segment anisomorphic model was evaluated by means of experimental data of three laminates from literature characterised by UTS>|UCS|. Moreover, an experimental campaign was conducted on a fourth laminate. For these laminates, the proposed model was capable of providing a similar predictive accuracy as the two-segment anisomorphic model. Moreover, the CLD model allowed for fatigue life predictions in similar fatigue life scales as experimental results. However, S-N curves for $R = 0.5$ were slightly over-predicted for all considered laminates, independent of whether the adapted model or the original two-segment anisomorphic model was used. The previously presented conclusion is only preliminary; the datasets employed in this study were limited in size. Chapter 7 provides a recommendation concerning additional evaluations of the predictive accuracy of the presented model.

The relative predictive performance of the proposed model for laminates characterised by |UCS|>UTS was assessed with respect to the four-segment anisomorphic model. A comparison was made using experimental data of two laminates from literature. For the two considered laminates, the model presented in this work allows for a similar or improved accuracy in the fatigue life prediction of T-T and T-C loading with respect to the four-segment anisomorphic model. This was not foreseen since the proposed model employs only one S-N curve as input compared to three by the four-segment anisomorphic CLD. Most likely, this is caused by an improvement in the assumed CLL shape. Thus, employing more experimental data does not necessarily lead to improved fatigue life predictions. Noticeable was the reduction in predictive accuracy of both models for T-C loads at $R < \chi$. This is seemingly caused by a linear assumed CLL which might not be suitable. Similar to the first model, the datasets employed for evaluation were limited in size. The conduction of additional evaluations will result in a strengthened verdict of the predictive accuracy, as recommended in Chapter 7.

Chapter 7

Recommendations

Several recommendations can be made related to the presented models. The most important recommendation regards the establishment of the predictive accuracy of the proposed models. Datasets employed in this work were mainly found in literature and are limited in their size: the size of the datasets was often smaller than the minimum number of tests results recommended by the ASTM standard (ASTM, 1980 (2015)). This can have greatly affected the obtained results. By performing additional evaluations, both for the same laminates with an extended dataset, as well as for carbon-epoxy laminates with different lay-ups, a better indication of the applicability of the models can be obtained.

The current set-up of both models allows for the use of an S-N curve related to either R = 0.1 or R = -1 without adapting the employed methodology. In theory, if the assumed CLL functions are accurate, the set-up of the model allows for the input of fatigue life data related to any R-ratio for the first model (applicable to UTS>|UCS|) and of any R-ratio in the range $\chi \leq R < 1$ for the second model (applicable to |UCS|>UTS). In both models, the critical S-N curve is derived directly from the input fatigue life data before establishing the complete CLL functions, which allows for the input of a different R-ratio. It can be of interest to investigate the predictive accuracy when other R-ratios are used as input. Moreover, in a similar manner also the simultaneous input of experimental data of several S-N curves can be evaluated; since it is always required to first predict the critical S-N curve, input datapoints obtained under different R-ratios can be employed. Then, the predicted critical fatigue lives can be combined and a curve can be fitted through the datapoints to obtain a critical S-N curve based on experimental input data from different R-ratios. This can be of interest when more than one S-N curve is readily available.

The previous recommendation relies on the assumption that the assumed CLL functions are suitable. However, as discussed in Chapter 6, slight over-predictions, by both the proposed and two-segment anisomorphic model, are obtained in the fatigue life prediction of $R = 0.5$ for laminates showing UTS>|UCS|. A further evaluation of the fatigue life behaviour for $R > 0.1$, as well as a study into an appropriate CLL shape for this region, can be of interest in future work.

For the second model, it has been assumed that all CLLs intersect the $R = \pm\infty$ radial in the top tenth percentile for $2N_f < 10^6$. However, since not much fatigue life data is available in literature for carbon-epoxy laminates showing |UCS|>UTS, it is unclear whether this assumption is true for all cases. Additional laminates should be evaluated to assess whether this assumption is valid. Moreover, it needs to be addressed whether the assumed CLL shapes are applicable. As discussed in Chapter 6, S-N curve predictions for $R < \chi$ show less correspondence with experimental results. Based on the presented results, improved predictions might be obtained using a convex CLL shape for low fatigue lives and a concave CLL shape for higher fatigue lives rather than a linear CLL for all fatigue life scales (Section 5.2).

Large scatter is often seen in fatigue life data of FRPs. To assess the influence of this variability, the set-up of a confidence band around the estimated S-N curves can be considered, as well as the influence of scatter in the input data on the final fatigue life predictions. In future work, it is possible to expand this concept to Probabilistic S-N (P-S-N) curves and, consequently, P-CLD curves, thereby allowing for an assessment of the uncertainty seen in fatigue life predictions.

The proposed fatigue life prediction models only consider uni-axial CA T-T and T-C fatigue loading. Firstly, the models can be expanded to include the prediction of C-C loads, however, this will require additional considerations regarding C-C testing. Secondly, multi-axial VA loading is more common than uni-axial CA loading when a structure is in-service. The models proposed in this work for uni-axial CA loading can be used as a base for the development of more elaborated fatigue life predictions models, taking into account different loading types while employing the benefits of limited experimental efforts required for the input.

Related to different loading types, the effects of changing environmental conditions, such as temperature and humidity on the fatigue life, can also be considered, as well as the prediction thereof. Potentially, the methods can be expanded to include predictions on these aspects.

The current work has focussed on carbon fibre-reinforced epoxy laminates. However, in future work the applicability of the models for different CFRP or even other FRP, such as GFRP laminates, should be investigated. For both the first and second model, an initial assumption has been made regarding the influence of the critical R-ratio. So far, this critical R-ratio has only been considered for carbon-epoxy laminates and it is unclear whether its impact is similar for other materials. For example, the first model assumes that the CLLs peak at the critical R-ratio; it can be of interest to evaluate whether this is true for other FRP materials as well.

The last made recommendation relates to the number of fatigue life data in one S-N curve. Currently, large numbers of fatigue life tests are required for the establishment of one reliable S-N curve. Research should be focussed on minimising experimental efforts related to one S-N curve. If this can be minimised, even further reductions in the required number of tests can be obtained when combining it with the models proposed in this work. This will result in a CLD model that is capable of providing predictions of the fatigue life for carbon-epoxy laminates in T-T or T-C loading based on less experimental datapoints at one conventional S-N curve.

Bibliography

Andersons, J., and Y. Paramonov, 2011: Applicability of empirical models for evaluation of stress ratio effect on the durability of fiber-reinforced creep rupture-susceptible composites. *Journal of Materials Science*, **46**, 1705–1713.

ASTM, 1971 (2017): Standard Test Method for Tensile Properties of Polymer Matrix Composite Materials. Standard, ASTM International, West Conshohocken, PA, USA. doi:10.1520/D3039_D3039M-17, URL http://www.astm.org/.

ASTM, 1976 (2012): Standard Test Method for Tension-Tension Fatigue of Polymer Matrix Composite Materials. Standard, ASTM International, West Conshohocken, PA, USA. doi:10.1520/D3479_D3479M-12, URL http://www.astm.org/.

ASTM, 1980 (2015): Standard Practice for Statistical Analysis of Linear or Linearized Stress-Life (S-N) and Strain-Life (ε-N) Fatigue Data. Standard, ASTM International, West Conshohocken, PA, USA. doi:10.1520/E0739-10R15, URL http://www.astm.org/.

ASTM, 2001: Standard Test Method for Determining Compressive Properties of Polymer Matrix Composite Laminates Using a Combined Loading Compression (CLC) Test Fixture. Standard, ASTM International, West Conshohocken, PA, USA. URL http://www.astm.org/.

ASTM, 2001 (2016): Standard Test Method for Compressive Properties of Polymer Matrix Composite Materials Using a Combined Loading Compression (CLC) Test Fixture. Standard, ASTM International, West Conshohocken, PA, USA. doi:10.1520/D6641_D6641M-16E01, URL http://www.astm.org/.

Bach, P., 1992: Fatigue properties of glass- and glass/carbon-polyester composites for wind turbines. ECN-C-92-072, Netherlands Energy Research Centre (ECN), Petten, Netherlands.

Barron, V., M. Buggy, and N. McKenna, 2001: Frequency effects on the fatigue behaviour on carbon fibre reinforced polymer laminates. *Journal of Materials Science*, **36**, 1755–1761.

Beheshty, M., and B. Harris, 1998: A constant-life model of fatigue behaviour for carbon-fibre composites: the effect of impact damage. *Composites Science and Technology*, **58**, 9–18.

Beheshty, M., B. Harris, and T. Adam, 1999: Empirical fatigue-life model for high-performance fibre composites with and without impact damage. *Composites Part A: Applied Science and Manufacturing*, **30**, 971–987.

Boerstra, G., 2007: The multislope model: a new description for the fatigue strength of glass reinforced plastic. *International Journal of Fatigue*, **29**, 1571–1576.

Caprino, G., and A. D'Amore, 1998: Flexural fatigue behaviour of random continuous-fibre-reinforced thermoplastic composites. *Composites Science and Technology*, **58**, 957–965.

Epaarachchi, J., and P. Clausen, 2003: An empirical model for fatigue behavior prediction of glass fibre-reinforced plastic composites for various stress ratios and test frequencies. *Composites Part A: Applied Science and Manufacturing*, **34**, 313–326.

Gathercole, N., H. Reiter, T. Adam, and B. Harris, 1994: Life prediction for fatigue of T800/5245 carbon-fibre composites: I. Constant-amplitude loading. *International Journal of Fatigue*, **16**, 523–532.

Harris, B., 2003: A parametric constant-life model for prediction of the fatigue lives of fibre-reinforced plastics. *Fatigue in Composites: Science and Technology of the Fatigue Response of Fibre-Reinforced Plastics*, B. Harris, Ed., Woodhead Publishing Limited, 546–568.

Harris, B., N. Gathercole, J. Lee, H. Reiter, and T. Adam, 1997: Life-prediction for constant-stress fatigue in carbon-fibre composites. *Phil. Trans. R. Soc. (London)*, **355**, 1259–1294.

Hexcel, 2016: *HexPly 8552 Epoxy Matrix Product Datasheet*. Hexcel, URL http://www.hexcel.com/user_area/content_media/raw/HexPly_8552_eu_DataSheet.pdf.

Jarosch, E., and A. Stepan, 1970: Fatigue properties and test procedures of glass reinforced plastic rotor blades. *Journal of the American Helicopter Society*, **15**, 33–41.

Kassapoglou, C., 2007: Fatigue life prediction of composite structures under constant amplitude loading. *Journal of Composite Materials*, **41**, 2737–2754.

Kawai, M., 2010: Fatigue life prediction of composite materials under constant amplitude loading. *Fatigue Life Prediction of Composites and Composite Structures*, A. Vassilopoulos, Ed., Woodhead Publishing Limited, 177–219.

Kawai, M., and N. Itoh, 2014: A failure-mode based anisomorphic constant life diagram for a unidirectional carbon/epoxy laminate under off-axis fatigue loading at room temperature. *Journal of Composite Materials*, **48**, 571–592.

Kawai, M., and M. Koizumi, 2007: Nonlinear constant fatigue life diagrams for carbon/epoxy laminates at room temperature. *Composites Part A: Applied Science and Manufacturing*, **38**, 2342–2353.

Kawai, M., and Y. Matsuda, 2012: Anisomorphic constant fatigue life diagrams for a woven fabric carbon/epoxy laminate at different temperatures. *Composites Part A: Applied Science and Manufacturing*, **43**, 647–657.

Kawai, M., Y. Matsuda, and R. Yoshimura, 2012: A general method for predicting temperature-dependent anisomorphic constant fatigue life diagram for a woven fabric carbon/epoxy laminate. *Composites Part A: Applied Science and Manufacturing*, **43**, 915–925.

Kawai, M., and T. Murata, 2010: A three-segment anisomorphic constant life diagram for the fatigue of symmetric angle-ply carbon/epoxy laminates at room temperature. *Composites Part A: Applied Science and Manufacturing*, **41**, 1498–1510.

Kawai, M., Y. Yagihashi, H. Hoshi, and Y. Iwahori, 2013: Anisomorphic constant fatigue life diagrams for quasi-isotropic woven fabric carbon/epoxy laminates under different hygro-thermal environments. *Advanced Composite Materials*, **22**, 79–98.

Kawai, M., and K. Yano, 2016a: Anisomorphic constant fatigue life diagrams of constant probability of failure and prediction of P–S–N curves for unidirectional carbon/epoxy laminates. *Composites Part A: Applied Science and Manufacturing*, **83**, 323–334.

Kawai, M., and K. Yano, 2016b: Probabilistic anisomorphic constant fatigue life diagram approach for prediction of P–S–N curves for woven carbon/epoxy laminates at any stress ratio. *Composites Part A: Applied Science and Manufacturing*, **80**, 244–258.

Kensche, C., 1995: Influence of composite fatigue properties on lifetime predictions of sailplanes. *Presented at XXIV OSTIV Congress, Omarama, New Zealand*, **19**, 69–76.

Kohout, J., and S. Věchet, 2001: A new function for fatigue curves characterization and its multiple merits. *International Journal of Fatigue*, **23**, 175–183.

Little, R., and E. Jebe, 1975: *Manual on statistical planning and analysis for fatigue experiments*. ASTM Special Technical Publication 588, American Society for Testing and Materials.

Lopes, C., O. Seresta, Y. Coquet, Z. Gürdal, P. Camanho, and B. Thuis, 2009: Low-velocity impact damage on dispersed stacking sequence laminates. Part I: Experiments. *Composites Science and Technology*, **69**, 926–936.

Naito, K., 2014: Effect of strain rate on tensile properties of carbon fiber epoxy-impregnated bundle composite. *Journal of Materials Engineering and Performance*, **23**, 708–714.

Nijssen, R., 2005: Tensile and compressive tests on standard OB specimens. Technical report. OB_TG1_R014 rev. 003, OPTIMAT.

Nijssen, R., 2006: Fatigue life prediction and strength degradation of wind turbine rotor blade composites. Ph.D. thesis, TU Delft.

Nijssen, R., 2010: Phenomenological fatigue analysis and life modelling. *Fatigue Life Prediction of Composites and Composite Structures*, A. Vassilopoulos, Ed., Woodhead Publishing Limited, 47–78.

Nijssen, R., O. Krause, and T. Philippidis, 2004: Benchmark of lifetime prediction methodologies. Technical report. OB_TG1_R012 rev. 001, OPTIMAT.

Owen, M., 1970: Fatigue testing of fibre reinforced plastics. *Composites*, **1**, 346–355.

Philippidis, T., and A. Vassilopoulos, 2002: Complex stress state effect on fatigue life of GRP laminates. Part I, experimental. *International Journal of Fatigue*, **24**, 813–823.

Post, N., and J. Case, S.W. Lesko, 2008: Modeling the variable amplitude fatigue of composite materials: A review and evaluation of the state of the art for spectrum loading. *International Journal of Fatigue*, **30**, 2064–2086.

Reifsnider, K., W. Stinchcomb, and T. O'Brien, 1977: Frequency effects on a stiffness-based fatigue failure criterion in flawed composite specimens. *Fatigue of Filamentary Composite Materials*, K. Reifsnider, Ed., ASTM International, 171–184.

Ronold, K., and A. Echtermeyer, 1996: Estimation of fatigue curves for design of composite laminates. *Composites Part A: Applied Science and Manufacturing*, **27**, 485–491.

Rotem, A., and H. Nelson, 1989: Failure of a laminated composite under tension-compression fatigue loading. *Composites Science and Technology*, **36**, 45–62.

Schijve, J., 2009: *Fatigue of Structures and Materials*. Springer Science & Business Media, B.V.

Sendeckyj, G., 1981: Fitting models to composite materials fatigue data. *Test Methods and Design Allowables for Fibrous Composites*, C. Chamis, Ed., American Society for Testing and Materials, 245–260.

Sendeckyj, G., 2001: Constant life diagrams - a historical review. *International Journal of Fatigue*, **23**, 347–353.

Shcerbakov, M., A. Brebels, N. Shcherbakova, A. Tyukov, J. T.A., and V. Kamaev, 2013: A survey of forecast error measures. *World Applied Sciences Journal*, **24**, 171–176.

Taniguchi, N., T. Nishiwaki, and H. Kawada, 2007: Tensile strength of unidirectional CFRP laminate under high strain rate. *Advanced Composite Materials*, **16**, 167–180.

Tofallis, C., 2008: Least squares percentage regression. *Journal of Modern Applied Statistical Methods*, **7**, 526–534.

Tofallis, C., 2015: A better measure of relative prediction accuracy for model selection and model estimation. *Journal of the Operational Research Society*, **66**, 1352–1362.

Vassilopoulos, A., 2010: Introduction to the fatigue life prediction of composite materials and structures: Past, present and future prospects. *Fatigue Life Prediction of Composites and Composite Structures*, A. Vassilopoulos, Ed., Woodhead Publishing Limited, 1–44.

Vassilopoulos, A., and T. Keller, 2011: *Fatigue of Fiber-reinforced Composites*. Springer Science+Business Media, B.V.

Vassilopoulos, A., B. Manshadi, and T. Keller, 2010a: Influence of the constant life diagram formulation on the fatigue life prediction of composite materials. *International Journal of Fatigue*, **32**, 659–669.

Vassilopoulos, A., B. Manshadi, and T. Keller, 2010b: Piecewise non-linear constant life diagram formulation for FRP composite materials. *International Journal of Fatigue*, **32**, 1731–1738.

Xia, Y., Y. Wang, Y. Zhou, and S. Jeelani, 2007: Effect of strain rate on tensile behavior of carbon fiber reinforced aluminum laminates. *Materials Letters*, **61**, 213–215.

Appendix A

S-N Curves

S-N curves can be fitted to fatigue life experimental datapoints to describe the change in fatigue life for different applied CA stresses. Both the expression used to describe these curves and the manner of fitting are of importance and are discussed in this appendix. Section A.1 considers four different S-N curve functions. Thereafter, Section A.2 introduces a curve fitting technique. Kawai and his colleagues did not specify the method used for curve fitting the ψ-$2N$ relation to experimental data at the critical R-ratio χ. However, it is presumed by the author of this work that the values of the curve fitting parameters (K_χ, a, n) have been identified by means of visual fitting[1]. Visual fitting will inherently not lead to the most optimal values for the curve fitting parameters. Instead, a regression analysis can result in a better descriptive function. Therefore, a new procedure to estimate the values for K_χ, a, and n will be proposed in Section A.2.

A.1 S-N Curve Functions

Several expressions can be employed to describe the S-N curve. Two expressions most commonly used are the 1) power and 2) exponential S-N curve, of which the use has been recommended by ASTM (1980 (2015)). The power-law relation (also known as the Basquin relation) is a log-log function and defined as (Vassilopoulos and Keller, 2011)

$$\sigma = \sigma_0 N^{-\frac{1}{k}}, \tag{A.1}$$

$$N\sigma^m = C, \tag{A.2}$$

[1] Kawai and Yano (2016a) present a similar curve fitting procedure to that used in the two-segment anisomorphic model, where the values of the model parameters "were identified by visually fitting" the function to experimental fatigue life data.

where C, k, m, and σ_0 are model parameters that are estimated based on fatigue life data by performing a linear regression.

When use is made of a lin-log diagram rather than a log-log diagram, the exponential formulation is often employed, given as

$$\sigma_a = A - B\left(\log\left(\bar{N}\right)\right)^C, \tag{A.3}$$

$$\sigma_a = A - B\log\left(\bar{N}\right). \tag{A.4}$$

It employs three curve fitting parameters A, B, and C, while $\bar{N}$ is the average number of cycles to failure. A simplified version is obtained when $C = 1$ (i.e., Equation A.4).

For the two-, three-, and four-segment anisomorphic CLD model, different S-N curve expressions have been proposed. Kawai and Koizumi (2007) introduced an equation for the two-segment CLD, defined as

$$2N_f = \frac{2}{K_\chi}\frac{(1-\psi)^a}{\psi^n}, \tag{A.5}$$

which consists of three model fitting parameters K_χ, a, and n. For the three-, and four-segment anisomorphic CLD, an elaborated S-N curve expression was proposed by Kawai and Murata (2010) and Kawai and Itoh (2014), given as

$$2N_f = \frac{1}{K_\chi}\frac{1}{(\psi_\chi)^n}\frac{(1-\psi_\chi)^a}{\left(\psi_\chi - \psi_\chi^L\right)^b}, \tag{A.6}$$

which employs five model parameters rather than three, namely K_χ, a, b, n, and ψ_χ^L.

A.2 Curve Fitting Technique

In this section, a curve fitting technique to estimate the fitting parameters K_χ, a, and n is presented. In this work, Equation A.5 is employed for reasons discussed in detail in Chapter 4. Therefore, the curve fitting technique presented in this appendix is shown only for Equation A.5. However, the presented method can be adapted for other S-N curve functions. In Subsection A.2.1, a maximum likelihood function is established that can be used to find estimates for the fitting parameters. Next, the maximum likelihood approach is combined with a LS regression technique to obtain values for the estimates in Subsection A.2.2.

A.2.1 Derivation Maximum Likelihood Function

Equation A.5 is fitted to a dataset and is considered to describe the mean fatigue life for each stress level. The variation in fatigue life data around the curve can be described using a representative probability distribution. It is assumed that fatigue life data at a constant stress level follows a log-normal distribution around the best-fit curve. The errors are independent log-normal errors e that can be added to the S-N curve equation as

$$2N_f = \frac{2}{K_\chi}\frac{(1-\psi)^a}{\psi^n}\cdot e. \tag{A.7}$$

A log-normal distribution will provide a normal distribution on the log-scale. When the previous equation is rewritten by taking the logs, the errors become additive:

$$\ln(2N_f) = \ln(2) - \ln(K_\chi) - n\ln(\psi) + a\ln(1-\psi) + \ln(e). \tag{A.8}$$

For the derivation of this equation it has been assumed that all three fitting parameters (K_χ, a, and n) are real and positive. In addition, it is given that both ψ and N_f are real and positive numbers, and that the range is of ψ is given as

$$0 \leq \psi \leq 1.$$

Because it was assumed that the independent errors e follow a lognormal distribution, it can be concluded that the independent errors $\ln(e)$ follow a normal distribution $N\left(0,\sigma^2\right)$. Consequently, N_f also follows a normal distribution per stress level since $\ln(2N_f)$ is described by the best-fit curve and independent errors, and is given as

$$\ln(2N_f) = m(\psi, a, K_\chi, n) + \ln(e), \tag{A.9}$$

where $m(\psi, K_\chi, a, n)$ describes the best-fit curve model. As previously mentioned, it has been assumed that the best-fit curve describes the mean of the normal distribution. Thus, the errors $\ln(e)$ will describe the variance of the normal distribution. In other words, $\ln(2N_f)$ follows a normal distribution with a mean $\mu = m(\psi, K_\chi, a, n)$ and variance σ^2 ($N\left(\mu,\sigma^2\right)$).

Next, a maximum likelihood function L can be expressed that has to be minimised to obtain an estimate for the model fitting parameters and variance. As aforementioned, it has been assumed that the fatigue life for a constant stress level can be described using a normal distribution $N(\mu,\sigma^2)$ on the log-scale. Accordingly, the maximum likelihood function is defined as

$$L = \prod_{i=1}^{M} f_{\mu,\sigma}\left(\psi_i, a, K_\chi, n\right) = \prod_{i=1}^{M}\frac{1}{\sigma\sqrt{2\pi}}e^{-\frac{1}{2}\left(\frac{\ln(2N_{f_i})-m(\psi_i,a,K_\chi,n)}{\sigma}\right)^2}. \tag{A.10}$$

The likelihood function L can be rewritten by taking the logs of Equation A.10, resulting in the log-likelihood function l defined as

$$l = \ln L = -M\ln(\sigma) - M\ln(\sqrt{2\pi}) - \frac{1}{2\sigma^2}\sum_{i=1}^{M}\left(\ln(2N_{f_i}) - m\left(\psi_i, a, K_\chi, n\right)^2\right). \tag{A.11}$$

An estimate for each fitting parameter, as well as for the mean and variance of the normal distribution, is obtained by taking the partial derivatives of the log-likelihood function with respect to a, K_χ, n, μ, and σ. The manner of taking the partial derivatives is shown next.

Partial derivative w.r.t. mean μ

First, the partial derivative of the log-likelihood function l with respect to the mean μ is evaluated. The mean μ of the normal distribution was previously defined as the best-fit curve through the fatigue life dataset as:

$$\begin{aligned} \mu &= m\left(\psi_i, a, K_\chi, n\right), \\ &= \ln(2) - \ln(K_\chi) - n\ln(\psi) + a\ln(1-\psi). \end{aligned} \tag{A.12}$$

The partial derivative of l (Equation A.11) with respect to μ is then given as

$$\frac{\partial l}{\partial \mu} = \frac{M}{\sigma^2}\left(\overline{\ln(2N_f)} - \mu\right) = 0, \tag{A.13}$$

where M is the total number of datapoints. For this equation to equal zero, the expression in the brackets must approach zero. Therefore the following must hold, which is also the definition of the mean:

$$\frac{\partial l}{\partial \mu} = 0 \text{ if } \mu = \overline{\ln(2N_f)}. \tag{A.14}$$

Partial derivative w.r.t. variance σ

The partial derivative with respect to the variance σ is presented as

$$\frac{\partial l}{\partial \sigma} = -\frac{M}{\sigma^3}\left(\sigma^2 - \frac{1}{M}\sum_{i=1}^{M}\left(\ln(2N_f) - \mu\right)^2\right) = 0. \tag{A.15}$$

For the partial derivative to equal zero, the expression in the brackets must approach zero. This provides an estimator for the variance σ^2 of the normal distribution, given as

$$\frac{\partial l}{\partial \sigma} = 0 \text{ if } \sigma^2 = \frac{1}{M}\sum_{i=1}^{M}\left(\ln(2N_f) - \mu\right)^2. \tag{A.16}$$

However, the obtained expression for σ^2 is biased, which must be corrected for. A bias-corrected estimator for σ^2 is given by

$$s^2 = \frac{1}{M-p}\sum_{i=1}^{M}\left(\ln(2N_f) - \mu\right)^2, \tag{A.17}$$

where $(M-p)$ is the Degrees Of Freedom (DOF) of the model and μ is described by the best-fit curve through the datapoints.

Partial derivative w.r.t. fitting parameters K_χ, a, n
The partial derivatives of the log-likelihood function with respect to each fitting parameter (K_χ, a, and n) are given by

$$\frac{\partial l}{\partial K_\chi} = 0 \text{ if } \sum_{i=1}^{M} \left(\ln(2N_f) - m\left(\psi_i, a, K_\chi, n\right)\right) \frac{\partial m\left(\psi_i, a, K_\chi, n\right)}{\partial K_\chi}, \tag{A.18}$$

$$\frac{\partial l}{\partial a} = 0 \text{ if } \sum_{i=1}^{M} \left(\ln(2N_f) - m\left(\psi_i, a, K_\chi, n\right)\right) \frac{\partial m\left(\psi_i, a, K_\chi, n\right)}{\partial a}, \tag{A.19}$$

$$\frac{\partial l}{\partial n} = 0 \text{ if } \sum_{i=1}^{M} \left(\ln(2N_f) - m\left(\psi_i, a, K_\chi, n\right)\right) \frac{\partial m\left(\psi_i, a, K_\chi, n\right)}{\partial n}. \tag{A.20}$$

The three derived equations cannot be solved analytically. Instead, an estimate for the fitting parameters must be obtained numerically using a LS method. Using LS, the residual between the fitted curve and each datapoint of the dataset must be minimised. Minimising the residuals provides estimates for the fitting parameters. Once the estimates for K_χ, a, and n are obtained, the results can be employed to obtain estimates for μ and σ using Equations A.14 and A.17, respectively. The employed LS approach is discussed in more detail in the next subsection.

A.2.2 Estimates of the Fitting Parameters

An estimation of the model parameters can be obtained using LS. However, a classical LS method will lead to inaccurate estimations for higher stress values because each residual has an equal effect on the final estimation. For example, an increase of 10 in the residual for a fatigue life estimation of $N = 100$ has a similar effect as an increase of 10 for a fatigue life of $N = 10^6$. It is thus of interest to take into account the logarithmic scale of the fatigue life range during the estimation of the model parameters in order to reduce the influence of large fatigue life values. Therefore, it is proposed to fit the ψ-$2N$ function using a LSPR method, introduced by Tofallis (2008), which considers the percentage error rather than the absolute error.

LSPR is an adapted form of the weighted least squares method where the weights are equal to $\frac{1}{\hat{y}_i}$. In order to obtain values for the model fitting parameters, the residual between the experimental data and the estimations must be minimised. This is similar to minimising the sum of squared normalised deviations given as

$$E = \sum_{i=1}^{M} \left(\frac{\hat{y}_i - y_i}{\hat{y}_i}\right)^2, \tag{A.21}$$

where M is the total number of experimental datapoints, $\hat{y}_i$ is the fatigue life for the i$^{\text{th}}$ experimental datapoint, and y_i is the estimated fatigue life for the i$^{\text{th}}$ datapoint using Equation A.5. Minimising the residual will lead to retrieval of the model fitting parameters and thereby of the best-fit function to experimental fatigue life data.

Appendix B

Material Data: HexPly AS4/8552

This appendix provides additional information on the continuous unidirectional carbon fibre-reinforced epoxy prepreg plies (HexPly *AS4/8552* unidirectional prepreg plies (Hexcel, 2016)) used during the experimental campaign. Only information of direct interest to this study is provided here. For additional information on the material used and the curing cycle, the reader is referred to the information provided by Hexcel (2016).

An overview of the mechanical properties of the material is given in Table B.1. Note that only the properties of interest are provided here (i.e., those corresponding to dry conditions and room temperature (25°C)). In order to determine the lay-up of the manufactured laminate, more information was required in addition to the values provided by the manufacturer. The values for these additional properties (G_{12}, ν_{12}, and Y_c) were taken from Lopes et al. (2009).

Table B.1: Physical and mechanical properties at dry conditions and room temperature (25°C) of *AS4/8552* unidirectional carbon prepregs (Hexcel, 2016, Lopes et al., 2009)

Property	Unit	Value
Laminate density	kg/m^3	1580
E_1	GPa	141
E_2	GPa	10
G_{12}	GPa	4.9
ν_{12}	-	0.32
ν_{23}	-	0.487
X_t	MPa	2207
X_c	MPa	1531
Y_t	MPa	81
Y_c	MPa	200
S_{12}	MPa	115

The autoclave curing cycle employed during the experimental campaign is similar to the cycle recommended by the manufacturer Hexcel for monolithic parts (Hexcel, 2016). The curing cycle is also presented in Figure B.1.

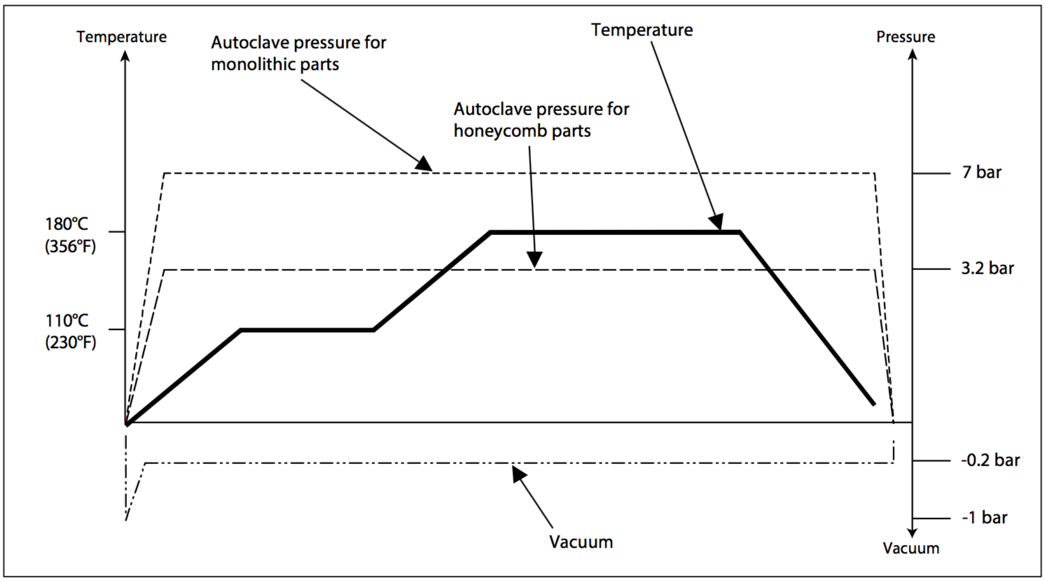

Figure B.1: Autoclave curing cycle for monolithic parts as recommended by Hexcel, reprinted from Hexcel (2016).

Appendix C

Test Data Results: Experimental Campaign

Fatigue life test values obtained from the conducted experimental campaign are presented in Tables C.1 to C.3. Fatigue life tests were conducted on a carbon-epoxy (AS4/8552) laminate with cross-ply lay-up of $[90/0/90]_{2S}$ at R-ratios of 0.1, -1, and χ = -0.60 and testing frequencies of $f = 10\,\mathrm{Hz}$, but also f = 5, 20, and 40 Hz. For each stress value, fatigue lives have been indicated, as well as the corresponding testing frequency and specimen number. The material properties from literature and autoclave cycle for the laminate have been included in Appendix B.

Table C.1: Experimental fatigue life test data for $[90/0/90]_{2S}$ at $R = 0.1$, resulting from the conducted experimental campaign. Run-outs have been indicated with (!).

R-ratio	$[90/0/90]_{2s}$			
0.1	$\sigma_{\max}$ [MPa]	N_f	f [Hz]	Specimen ID
	612.0	77	10	S16
	610.5	773	5	S05
	610.2	56	10	S12
	599.8	171,617	10	S09
	593.4	300	10	S14
	590.0	446,827	10	S15
	580.3	853,203 (!)	10	S17
	522.9	1,520,046 (!)	5	S06

Table C.2: Experimental fatigue life test data for $[90/0/90]_{2S}$ at $R = \chi$, resulting from the conducted experimental campaign. Run-outs have been indicated with (!).

R-ratio	$[90/0/90]_{2s}$			
χ	$\sigma_{\max}$ [MPa]	N_f	f [Hz]	Specimen ID
	606.5	2,891	10	S85
	603.6	5,792	10	S58
	603.4	3,204	10	S57
	547.4	41,733	10	S50
	546.4	200	10	S35
	546.4	16,267	10	S47
	546.4	38,249	10	S74
	546.4	45,214	10	S54
	484.0	215,077	10	S52
	483.3	73,327	10	S83
	483.3	133,400	10	S75
	483.3	148,183	10	S38
	482.0	73,427	10	S60
	420.8	1,013,785 (!)	10	S62

Table C.3: Experimental fatigue life test data for $[90/0/90]_{2S}$ at $R = -1.0$, resulting from the conducted experimental campaign. Run-outs have been indicated with (!).

R-ratio	$[90/0/90]_{2s}$			
-1	$\sigma_{\max}$ [MPa]	N_f	f [Hz]	Specimen ID
	390.0	7,885	10	S49
	390.0	9,223	10	S84
	390.0	15,433	10	S68
	382.4	14,262	10	S73
	382.2	57,274	10	S69
	381.8	50,838	10	S76
	374.7	13,388	10	S53
	372.5	59,045	10	S81
	361.6	74,299	10	S48
	357.3	33,558	10	S22
	356.1	34,940	10	S19
	346.8	1,028,232 (!)	10	S70
	345.7	35,898	10	S86
	345.7	72,843	10	S72
	329.1	145,997	10	S30
	218.1	2,225,742 (!)	10	S65
	380.6	6,039	5	S34
	367.6	19,044	5	S40
	365.3	20,542	5	S41
	366.4	27,932	20	S33
	362.5	80	40	S25
	360.3	75	40	S31

Appendix D

Test Data Results: Literature

Fatigue life test values obtained from literature are presented in Table D.2 and D.4 for laminates characterised by UTS>|UCS| and |UCS|>UTS, respectively. Moreover, in Table D.1 and D.3, the static strength values (UTS and UCS) have been included. In Table D.1 and D.2, data for the carbon-epoxy (T800H/3631) laminates with lay-up $[45/90/\text{-}45/0]_{2S}$ and $[0/60/\text{-}60]_{2S}$ has been included, for which testing was performed at 10 Hz. In addition, test data has been included for a carbon-epoxy (T800H/2500) laminate with a cross-ply lay-up of $[0/90]_{3S}$, also with a test frequency of 10 Hz. All data was presented by Kawai and Koizumi (2007). Note that some of the values have been adapted with respect to those given by Kawai and Koizumi (2007) due to found inconsistencies between the provided table and figures.

In Table D.3 and D.4, data for two laminates is presented, namely a carbon-epoxy (T800H/2500) laminate with lay-up $[\pm 60]_{3S}$, for which the data was presented by Kawai and Murata (2010), and a carbon-epoxy (T700/2592) laminate with lay-up $[45]_{16}$, for which the data was presented by Kawai and Itoh (2014). For the first laminate, testing was performed at both 2 and 10 Hz, while the testing frequency for the second laminate was 5 Hz. Note that for the latter laminate no actual values were published by Kawai and Itoh (2014) but that the presented values have been determined from the published figures.

Table D.1: Mean static strength test data (both tension and compression) for three laminates, as published by Kawai and Koizumi (2007).

	$[45/90/\text{-}45/0]_{2s}$	$[0/60/\text{-}60]_{2s}$	$[0/90]_{3s}$
UTS [MPa]	781.9	880.6	1414.1
UCS [MPa]	-532.4	-465.1	-618.0

Table D.2: Experimental fatigue life test data for three laminates, as published by Kawai and Koizumi (2007). Run-outs have been indicated with (!). Note that some fatigue lives do not correspond with those given by Kawai and Koizumi (2007) due to found discrepancies between values provided in Table 4 and the corresponding S-N curve plots in the corresponding article. The experimental data values were adjusted accordingly and are indicated in *italic* form.

R-ratio	$[45/90/\text{-}45/0]_{2s}$		$[0/60/\text{-}60]_{2s}$		$[0/90]_{3s}$	
	$\sigma_{\max}$ [MPa]	$2N_f$	$\sigma_{\max}$ [MPa]	$2N_f$	$\sigma_{\max}$ [MPa]	$2N_f$
0.1	625.5	2,128	748.5	1,818	1,060.6	6,614
	609.9	5,716	739.7	53,594	848.5	200,220
	586.5	15,414	730,9	142,964		
	563.0	14,696	704.5	250,840		
	532.9	225,080	678.0	2,000,000 (!)		
	508.3	146,602	660.4	1,008,260		
0.5	680.3	*2,920*	854.4	374	1,244.4	*260*
	664.6	5,612	836.5	3,442	1,202.0	498
	641.2	39,712	810.1	21,272	1,102.9	175,112
	625.5	52,604	792.5	411,480	1,060.6	255,160
	609.9	198,228	774.9	584,040		
	594.3	*716,200*	766.1	2,000,000 (!)		
χ	469.2	3,852	748.5	5,366	989.9	*130*
	430.1	6,856	704.5	3,236	777.8	7,782
	391.0	24,532	616.4	23,370	707.1	9,858
	351.9	*65,152*	528.3	61,986	636.3	29,692
	273.7	574,060	528.3	118,540	565.6	182,550
			440.3	1,225,840	530.3	774,300
-1	372.7	8,288	441.6	23,220	432.6	7,324
	346.1	12,234	418.6	59,000	389.3	368,480
	292.8	84,936	395.3	78,000	370.8	767,080
	266.2	259,500	395.3	78,000	370.8	595,380
	239.6	419,520	348.8	169,896		
	223.6	1,341,460	302.3	2,000,000 (!)		

Table D.3: Mean static strength test data (both tension and compression) for three laminates, as published by Kawai and Murata (2010) and Kawai and Itoh (2014).

	$[\pm 60]_{3S}$	$[45]_{16}$
UTS [MPa]	83.3	61.6
UCS [MPa]	-164.8	-151.6

Table D.4: Experimental fatigue life test data for three laminates, as published by Kawai and Murata (2010) for $[\pm 60]_{3S}$ and Kawai and Itoh (2014) for $[45]_{16}$. Run-outs have been indicated with (!). Note that some fatigue lives do not correspond with those given by Kawai and Murata (2010) due to found discrepancies between values provided in Table 3 and the corresponding S-N curve plots in the corresponding article. The experimental data values were adjusted accordingly and are indicated in *italic* form. For the $[45]_{16}$ lay-up, no exact values were provided, but these were derived from the published diagrams.

R-ratio	$[\pm 60]_{3S}$		$[45]_{16}$	
	$\sigma_{\max}$ [MPa]	$2N_f$	$\sigma_{\max}$ [MPa]	$2N_f$
0.1	73.4	2,560	46.	3,000
	69.0	7,350	44.5	9,800
	61.9	42,400	42.5	62,000
	58.0	229,676	37.0	220,000
	55.0	709,950	30.0	2,000,000 (!)
0.5	81.3	2,790	54.0	450
	79.6	4,330	51.5	800
	77.8	21,900	46.0	1,900
	76.0	*12,800*	40.0	2,000,000 (!)
	70.7	90,400		
-1	67.5	1,840	47.5	2,100
	64.1	3,630	40.0	12,000
	58.3	12,300	36.0	15,000
	55.8	17,800		
	53.3	19,700		
	48.0	169,179		
χ	61.6	445	99.0	750
	57.5	1,230	83.0	5,000
	53.7	4,060	75.0	50,000
	41.7	186,000	63.0	44,000
	33.3	200,000 (!)	58.0	110,000
			61.0	110,000
			50.0	200,000
			41.0	1,600,000
-3	123.6	8,610		
	115.4	67,400		
	107.2	137,000		
-5	140.1	255		
	136.0	2,930		
	131.9	12,100		
	123.6	87,700		
-10			123.0	300
			117.0	600
			113.0	1,300
			111.0	300,000
			105.0	370,000
10	153.3	4,000	149.0	200
	151.7	394	142.0	570
	150.0	2,250	137.0	48,000
	148.4	40,000		
	145.1	64,000		